

University of Alberta

Synthesis of Porphyrin-based Multimeric Fluorescent Compounds and Studies Towards the Formation of *Cis-anti-cis* Linear Triquinane

by

Linghui Yu

A thesis submitted to the Faculty of Graduate Studies and Research
in partial fulfillment of the requirements for the degree of

Master of Science

Department of Chemistry

©Linghui Yu
Fall 2011
Edmonton, Alberta

Permission is hereby granted to the University of Alberta Libraries to reproduce single copies of this thesis and to lend or sell such copies for private, scholarly or scientific research purposes only. Where the thesis is converted to, or otherwise made available in digital form, the University of Alberta will advise potential users of the thesis of these terms.

The author reserves all other publication and other rights in association with the copyright in the thesis and, except as herein before provided, neither the thesis nor any substantial portion thereof may be printed or otherwise reproduced in any material form whatsoever without the author's prior written permission.

ABSTRACT

Prion diseases are life-threatening diseases found in many mammals, including humans, and there is still no effective vaccine, treatment or therapy. In Chapter 1, a concise and effective synthetic route was reported to synthesize a library of porphyrin-based multimeric fluorescent compounds with anticipated anti-prion activity, and nine molecules have been synthesized, purified and characterized by using different binding units. The anti-prion assay results of the porphyrin-based and arene-based (prepared by other people) multimeric compounds were discussed as well.

In Chapter 2, the studies toward the formation of linear triquinanes with natural *cis-anti-cis* configuration via pyran-2-one photochemistry were discussed. Linear triquinanes with unnatural *cis-syn* configuration were readily available from substituted pyran-2-ones in a concise route. Two steps of modification produced an enone, and reduction of the enone presented an opportunity to obtain the natural *cis-anti-cis* configuration. Different reduction conditions were tried, and Birch reduction is underway to reach the natural configuration.

ACKNOWLEDGEMENTS

I would first like to give special thanks to professor Frederick G. West for his outstanding mentorship, intellectual guidance and great patience.

Secondly, I would also like to thank all the group members for their help and the friendly environment of the group during my stay. In particular, thanks to Dr. Graham Murphy and Shaon Joy for their careful proofreading of my thesis.

Thirdly, many thanks to all the supporting staff in the department of chemistry for their great job and help. In addition, I would like to thank the Westaway group at the University of Alberta, especially Charles Mays III, for the work on the anti-prion assays and toxicity tests of the anti-prion compounds.

Lastly, I would like to thank my family and friends for their love, support and encouragement over the past years.

TABLE OF CONTENTS

CHAPTER 1

SYNTHESIS OF PORPHYRIN-BASED MULTIMERIC FLUORESCENT COMPOUNDS FOR SELECTIVE BINDING TO INFECTIOUS PRION PROTEIN

1.1	Introduction of the Prion Diseases	1
1.2	Challenges and Recent Progress in Prion Research	7
1.3	Significance and Goal of Our Research	10
1.4	Project Rationale	12
1.5	Synthesis of Porphyrin-based Multimeric Molecules	
	1.5.1 Using Quinolines as the Binding Units	17
	1.5.2 Using 9-Amino-acridine as the Binding Units	28
1.6	Preliminary Biological Evaluation of Porphyrin-Based Multivalent Prion Binders	
	1.6.1 Introduction of Experimental Designs & Evaluation Results for Porphyrins 3-4 and Mono-Binding Units 12-17	34
	1.6.2 Evaluation Results for Porphyrin-Based Multimeric Compounds 18-23 & Promising Results of Arene-Based Multimeric Compounds	39
1.7	Experimental	
	1.7.1 General Information	42
	1.7.2 Substrate Synthesis	43
1.8	References and Notes	56

CHAPTER 2

STUDIES TOWARDS THE FORMATION OF *CIS-ANTI-CIS* LINEAR TRIQUINANES VIA PYRAN-2-ONE PHOTOCHEMISTRY

2.1	Introduction of Polyquinanes and Linear Triquinanes	61
2.2	Reported Routes to Build Linear Triquinanes	65
2.3	Concise Route to Linear Triquinanes From Pyran-2-Ones	71

2.4	Research In The Modification of The Relative Configuration of Unnatural Linear Triquinane	
	2.4.1 Preparation of the Advanced Intermediate Octatriene 64	74
	2.4.2 Progress In The Modification of The Configuration of Unnatural Linear Triquinane	77
2.5	Experimental Details	
	2.5.1 General Information	80
	2.5.2 Substrate Synthesis	81
2.6	References and Notes	84

CHAPTER 3

CONCLUSIONS AND FUTURE PLANS

3.1	Conclusions of the Prion and Triquinane Projects	87
3.2	Future Directions of The Research Projects	
	3.2.1 Future Plan of the Prion Project	88
	3.2.2 Future Plan of the Triquinane Project	90
3.3	References	90

APPENDIXES

A	SELECTED NMR SPECTRA FROM CHAPTER 1.....	92
B	SELECTED NMR SPECTRA FROM CHAPTER 2	116
C	X-RAY CRYSTALLOGRAPHIC DATA FOR COMPOUND 83 (CHAPTER 2)	122

LIST OF FIGURES

Chapter 1

Figure 1.1	Microscopic view of spongy architecture in tissue section with prion diseases	4
Figure 1.2	Heterodimer model of prion replication	5
Figure 1.3	Fibril Model of Prion Replication	6
Figure 1.4	Generic structures of dimeric, trimeric or tetrameric compounds	11
Figure 1.5	Structures of selected scaffolds	13
Figure 1.6	Structures of linkers	14
Figure 1.7	Structures of binding units	14
Figure 1.8	Generalized structures of congo red-based dimeric products	15
Figure 1.9	Generalized structures of 1,3,5-trisubstituted arene-based trimeric products	15
Figure 1.10	Generalized structures of porphyrin-based tetrameric products	16
Figure 1.11	Generic multimeric fluorescent products	17
Figure 1.12	The target molecules with quinolines as binding units	18
Figure 1.13	Retrosynthetic analysis of the target molecules	19
Figure 1.14	Structures of four N-(6-Chloro-2-methoxy acridin-9-yl)-alkyl diamine compounds	29
Figure 1.15	The structure of the desired compound 29 and undesired tri-substituted product	32
Figure 1.16	Antiprion activity of N-(7-chloroquinolin-4-yl)-alkyl-diamines 12-17 ...	36
Figure 1.17	Antiprion activity of simple porphyrins 3-4	38
Figure 1.18	Antiprion activity of six porphyrin-based multimeric molecules 18-23 ...	40
Figure 1.19	Structures of arene-based trimeric compounds prepared by Shaon Joy ...	41

Chapter 2

Figure 2.1	Diquinane, tetraquinane and three classes of triquinanes	61
Figure 2.2	Linear triquinanes with natural <i>cis-anti-cis</i> and unnatural <i>cis-syn-cis</i> relative configurations	62
Figure 2.3	Five types of natural linear triquinanes	63
Figure 2.4	Structures of coriolin, hirsutic acid, capnellene and one type of capnellanol	64
Figure 2.5	X-ray ORTEP representation of 83 at 20% probability level	78
Chapter 3		
Figure 3.1	Structures of mono-binding units 1-5	88
Figure 3.2	Structures of 2-methylquinoline-diamines 1 , 2-phenylquinoxaline-diamine 2 , acridine-diamines 3-4	89

LIST OF SCHEMES

Chapter 1

Scheme 1.1	Synthesis of <i>meso</i> -tetrasubstituted phenyl porphyrins	20
Scheme 1.2	Saponification of porphyrin 3 to get its corresponding acid 4	21
Scheme 1.3	General method for preparation of N-(7-chloroquinolin-4-yl)-alkyl diamines	21
Scheme 1.4	Amide bond formation reaction to form one of the target molecules ...	23
Scheme 1.5	The reaction to prepare N-(6-Chloro-2-methoxy acridin-9-yl)-alkyl diamine compounds	29

Chapter 2

Scheme 2.1	The biosynthetic pathway to form (+)-hirsutene 6	64
Scheme 2.2	Intramolecular 1,3-diyI trapping reactions to synthesize hirsutene	65
Scheme 2.3	Intramolecular meta-cycloaddition/cyclopropane cleavage pathway	66
Scheme 2.4	Radical initiated tandem polyolefinic cyclization pathways	67
Scheme 2.5	Diels-Alder/Paterno-Buchi reaction/reductive fragmentation pathway	68
Scheme 2.6	Diels-Alder reaction/1,2-acyl shift/reductive cleavage pathway	69
Scheme 2.7	Palladium catalyzed intramolecular cyclopentane pathway	70
Scheme 2.8	Tandem oxy-Cope-transannular reactions	70
Scheme 2.9	Concise route developed by a previous group member from pyran-2-ones to linear triquinanes with <i>cis-syn</i> configuration through a sequence of [4+4] cycloaddition/thermal decarboxylation/MeLi-mediated rearrangement	71
Scheme 2.10	Proposed mechanism for the formation of linear triquinane	72
Scheme 2.11	Preparation of furan 74 from aldehyde 72	75
Scheme 2.12	Preparation of furan 74 from acid 75	75

Scheme 2.13	Preparation of 63 from furan 74 and pyran 78	76
Scheme 2.14	Preparation of cyclooctatriene 64	76
Scheme 2.15	Attempts to reduce enone 65 by L-selectride	77
Scheme 2.16	Hydrogenation of compound 65	78
Scheme 2.17	Dehydration of compound 83	79
Scheme 2.18	Hydrogenation of compound 84	80

Chapter 3

Scheme 3.1	Synthesis of arene-based trimesic compounds by using acridine or others as the binding units	89
Scheme 3.2	Birch reduction and methylation at α -position	90

LIST OF TABLES

Chapter 1

Table 1.1	Classification of TSEs discovered in different hosts	3
Table 1.2	A list of prepared N-(7-chloroquinolin-4-yl)-alkyl-diamine products 12-17	22
Table 1.3	Structures and yields of six tetrameric porphyrin products	25
Table 1.4	Reactions of amide bond formation to get to the second series of target molecules	30

Chapter 2

Table 2.1	Scope of MeLi-mediated reaction to form triquinanes	73
Table 2.2	Triquinane formations from branched substrates	74
Table 2.3	Attempts to reduce enone 84 with SmI ₂ -mediated reaction conditions	79

LIST OF CHARTS

Chapter 1		
Chart 1.1	UV-Vis absorbance spectrum of compound 18	27
Chart 1.2	Fluorescence analysis of compound 18	28
Chart 1.3	UV-Vis absorbance spectrum of compound 30	33
Chart 1.4	Fluorescence analysis of compound 30	34
Chart 1.5	Densitometric analysis of Western blots from experiments of compounds 12-17 at various concentrations	37
Chart 1.6	Densitometric analysis of Western blots from experiments of compounds 3, 4 at various concentrations	38
Chart 1.7	Densitometric analysis of Western blots from experiments of porphyrin-based multimeric compounds 18-23 at various concentrations	40

LIST OF ABBREVIATIONS

Ac	acetyl
AIBN	2,2-azobisisobutyronitrile
Ar	aryl
app	apparent (spectral)
aq	aqueous
BORSM	based on recovered starting material
Bn	benzyl
br	Broad (spectral)
<i>n</i> -Bu	<i>n</i> -butyl
<i>t</i> -Bu	<i>tert</i> -butyl
°C	Degrees Celsius
calcd.	calculated
cat.	catalytic
COSY	homonuclear correlation spectroscopy
Conc.	concentrated
CSA	camphor-10-sulfonic acid
d	day(s); doublet (spectral)
DBU	1,8-diazabicyclo[5.4.0]undec-7-ene
DCC	1,3-dicyclohexylcarbodiimide
DCM	dichloromethane
DDQ	2,3-dichloro-5,6-dicyanobenzoquinone
dd	doublet of doublets (spectral)
ddd	doublet of doublet of doublets (spectral)
dddd	doublet of doublet of doublet of doublets (spectral)
Dibal-H	Diisobutylaluminum hydride
DMAP	4- <i>N,N</i> -dimethylaminopyridine
DME	1,2-dimethoxyethane

DMF	<i>N,N</i> -dimethylformamide
DMSO	dimethyl sulfoxide
dr	diastereomeric ratio
ee	enantiomeric
EI	electron impact (mass spectrometry)
equiv	equivalents
ESI	electrospray ionization (mass spectrometry)
EtOAc	ethyl acetate
g	gram(s)
h	hour(s)
HMQC	heteronuclear multiple bond coherence
HMBC	heteronuclear multiple quantum coherence
h ν	photochemical irradiation
HRMS	high resolution mass spectrum
Hz	herz
<i>J</i>	coupling constant (in NMR)
L	liter(s)
M	moles per liter
m	multiplet (spectral)
Me	methyl
MHz	megahertz
min	minute(s)
mL	milliliter(s)
mmol	milimole(s)
mol	mole(s)
m.p.	melting point
Ms	methanesulfonyl
m/z	mass to charge ratio (in mass spectrometry)
nm	nanometers (light)

NMR	nuclear magnetic resonance
Nu	nucleophile
Ph	phenyl
PK	proteinase K
piv	pivaloyl
ppm	parts per million (in NMR)
pyr	pyridine
R _f	retention factor (in chromatography)
r.t.	room temperature
s	singlet (NMR); second(s)
SDS-PAGE	sodium dodecyl sulfate polyacrylamide gel electrophoresis
t	triplet (spectral)
TEOA	triethyl orthoacetate
THF	tetrahydrofuran
TLC	thin layer chromatography
TMS	trimethylsilyl

CHAPTER 1

SYNTHESIS OF PORPHYRIN-BASED MULTIMERIC FLUORESCENT COMPOUNDS FOR SELECTIVE BINDING TO INFECTIOUS PRION PROTEIN

1.1 Introduction of the Prion Diseases

The spread of transmissible spongiform encephalopathies (TSEs)¹ is of great concern, not only because during one major outbreak it can result in huge economic losses in the cattle industry,² but also because it is a life-threatening disease that can be transmitted to humans.³ TSEs can cause degenerative tissue damage of brain and other components of the central nervous system of animals and humans. Currently they are untreatable and ultimately fatal, as the process of impairment of the central nervous system is irreversible.^{1c, 3}

According to the most widely accepted hypothesis, TSEs are transmitted by prions⁴ and thus TSEs are also known as prion diseases. The name ‘prion’, derived from both the words “proteinaceous” and “infectious”,⁵ was proposed by Dr. Stanley B. Prusiner in 1982, who received the Nobel Prize in Physiology or Medicine in 1997 for his work in prion research.⁶ Prion is the theoretical infectious unit that is mainly composed of mis-folded protein, usually labeled as PrP^{Sc}.⁷ In the term PrP^{Sc}, ‘Sc’ signifies ‘scrapie’, which is a type of prion disease found in sheep.⁸ PrP^C is the normal endogenous form of PrP^{Sc} and it has an extensive existence in healthy humans and animals. In PrP^C, ‘C’ means ‘cellular’ or ‘common’.⁸ PrP^C has mainly an α -helical structure, and its three dimensional (3D) structure is well defined. In contrast, PrP^{Sc} has a high portion of β -sheets and its exact 3D structure is still unknown.⁹ With high percentage of β -sheets, PrP^{Sc} can aggregate to form highly compact amyloid fibers, which can accumulate at its ends to form insoluble

plaques.⁹

A number of prion diseases have been found in many different types of mammals. For example, mad cow disease, also known as bovine spongiform encephalopathy, is the prion disorder most widely known to the public. This neurodegenerative disorder was first observed in England in 1986, and it remains the worst affected country. It was estimated that hundreds of thousands of cattle in the United Kingdom have been infected and millions were destroyed to minimize the spread of this disease.² Many cases were discovered and reported in other nations as well, such as Ireland, Portugal, France, Japan, Canada, United States and so on.¹⁰ The spread of mad cow disease has become a big global health concern, which requires extensive international cooperation to prevent the epidemic effectively. So far, prion diseases have been found in a variety of mammals, and **Table 1.1** provides detailed information for TSEs discovered in different species.¹¹ In general, the incubation time of the prion diseases is quite long. For example, the period of incubation in cattle affected by mad cow diseases usually varies from three to eight years. However, once the symptoms of amyloid plaque formation and spongiform change appear, the disorders can develop very rapidly, resulting in death.

Host	Diseases	Abbr.	Prions
Humans	Kuru	-	Kuru prion
	Creutzfeldt-Jakob disease	CJD	CJD prion
	Variant Creutzfeldt-Jakob disease	vCJD	vCJD prion
	Fatal familial insomnia	FFI	FFI prion
	Gerstmann-Straussler-Sheinker syndrome	GSS	GSS prion
Cattle	Bovine spongiform encephalopathy	BSE	BSE prion
Cats	Feline spongiform encephalopathy	FSE	FSE prion
Mink	Transmissible mink encephalopathy	TME	TME prion
Sheep and goats	Scrapie	-	Scrapie prion
Elk, deer	Chronic wasting disease	CDW	CWD prion
Nyala, greater kudu	Exotic ungulate encephalopathy	EUE	EUE prion

Table 1.1 Classification of TSEs discovered in different hosts.¹¹

More worrisomely, the cross-species spread of the mad cow disease can occur quite easily to humans through the food chain. Consumption of contaminated bovine products can result in a fatal human TSE, called new variant Creutzfeldt-Jakob disease (vCJD).¹² By October 2009, 280 cases of vCJD have been diagnosed and reported across the world.¹³ What is more, there is an unknown number with infection, as the incubation period can span up to decades without any symptom. This has led to another concern of secondary transmission of vCJD by blood transfusion.¹⁴ By October 2009, this disorder had already killed 210 individuals worldwide, and most of the victims were located in the United Kingdom.¹³ Besides vCJD, there are four other fatal prion diseases found in humans, which are Kuru, Fatal familial insomnia, Gerstmann-Straussler-Sheinker syndrome and Creutzfeldt-Jakob disease (CJD).¹⁵

Prions aggregate extracellularly within the central nervous system to form amyloid plaque. The formation of amyloid plaque can cause cell death and great damage to

the normal brain or spinal cord tissue structures. The disruption in the tissues slowly results in the formation of many ‘holes’, and the tissues gradually shape into spongy architecture (**Figure 1.1**).¹⁶ The spongy architecture of the prion diseases gives them a common name: transmissible ‘spongiform’ encephalopathy. Besides amyloid plaque and spongy architecture formation, the prion diseases also share other similarities, such as neuronal loss and astrogliosis in different mammals.¹⁷ Clinical signs of TSEs include behavior and personality changes, loss of memory, balance and coordination dysfunction. Loss of the ability to move and talk can also occur at later stages of the diseases for humans, due to damage to the brain and other components of the central nervous system.¹⁸

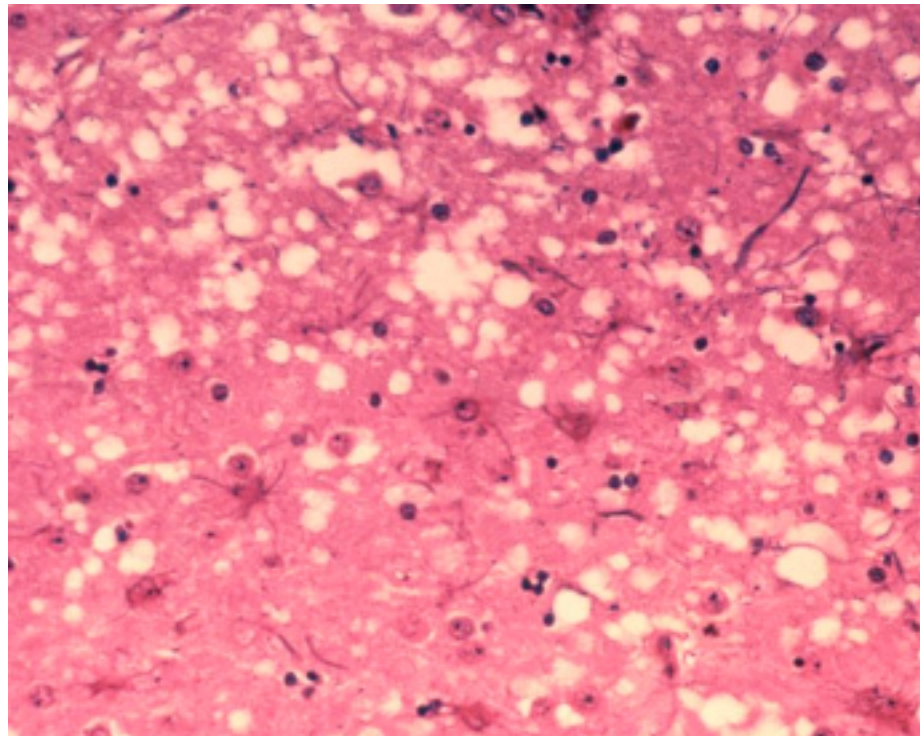


Figure 1.1 Microscopic view of spongy architecture in tissue section with prion diseases.¹⁹ Unstained areas indicate loss of nervous tissue.

The mechanism of prion replication is still quite unclear, and a few models have been proposed to explain it. One model, named as the heterodimer model, is illustrated as in **Figure 1.2**.²⁰ In this hypothesis, it is assumed that the PrP^{Sc} has the ability to change the conformation of PrP^C, and convert it to the infectious form. One molecule of PrP^{Sc}

interacts with one molecule of PrP^{C} , and PrP^{Sc} works as the catalyst. After the conversion is done, both PrP^{Sc} molecules separate to alter more PrP^{C} to its infectious isoform. Thus, according to this hypothesis, the rate of PrP^{C} to PrP^{Sc} conversion increases exponentially as the disease progresses, which consists with the finding that the disease progresses very rapidly at the later phase. However, this model does not fully explain why the incubation period is so long if the amount of PrP^{Sc} increase is also exponential during early stages. On the other hand, it is possible that in spite of exponential increase, accumulated PrP^{Sc} might have to reach a certain level (threshold) to cause disease symptoms.

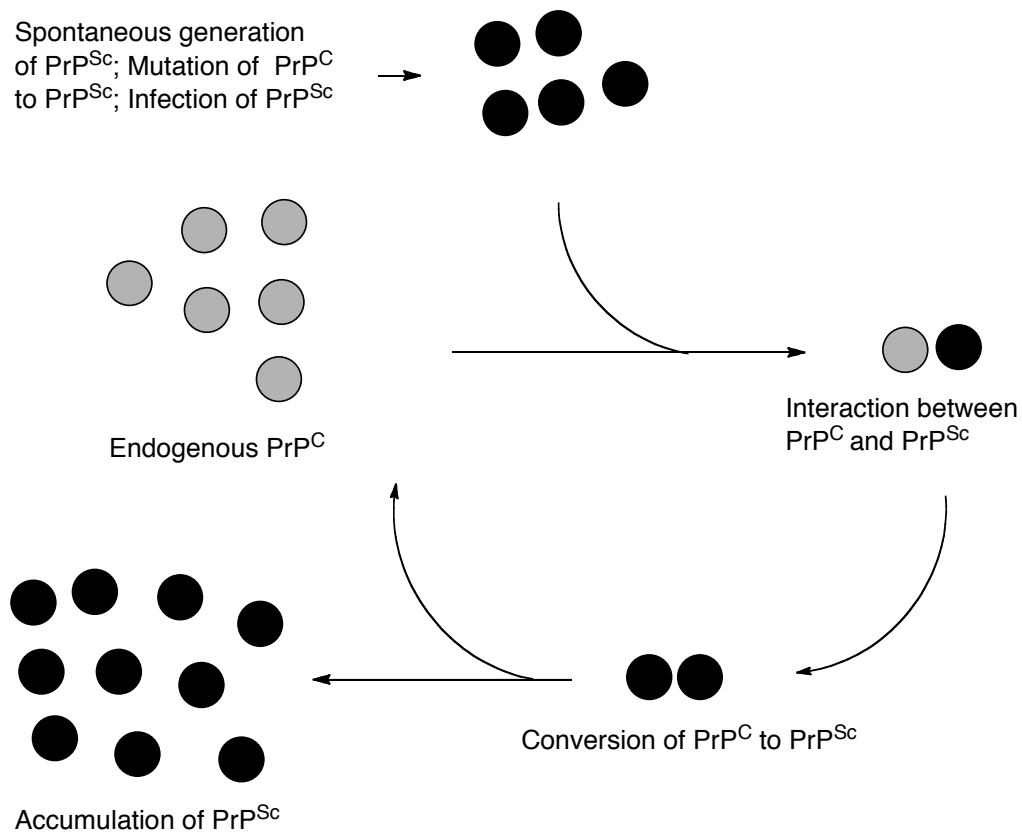


Figure 1.2 Heterodimer model of prion replication.²⁰ In the cycle, interaction of PrP^{Sc} (dark circle) with PrP^{C} (light circle) causes conformational changes in PrP^{C} , resulting in the conversion of PrP^{C} to PrP^{Sc} .

An alternative prion replication model, known as the fibril model, is introduced as in **Figure 1.3**. This model suggests that PrP^{Sc} only exists in the aggregate form of

‘fibrils’, rather than PrP^{Sc} monomers. The replication cycle is initiated by either infection of fibrils from external sources or nucleation of PrP^C. Since nucleation is rare, the cycles are likely to start with infection of fibrils in most cases. In the replication cycle, the end of fibril binds with PrP^C and converts it to its misfolded form. As the fibrils grow, they can later break into multiple new seeds to initiate more replication cycles, and thus the quantity of fibrils also increases in a manner of exponential growth.²¹

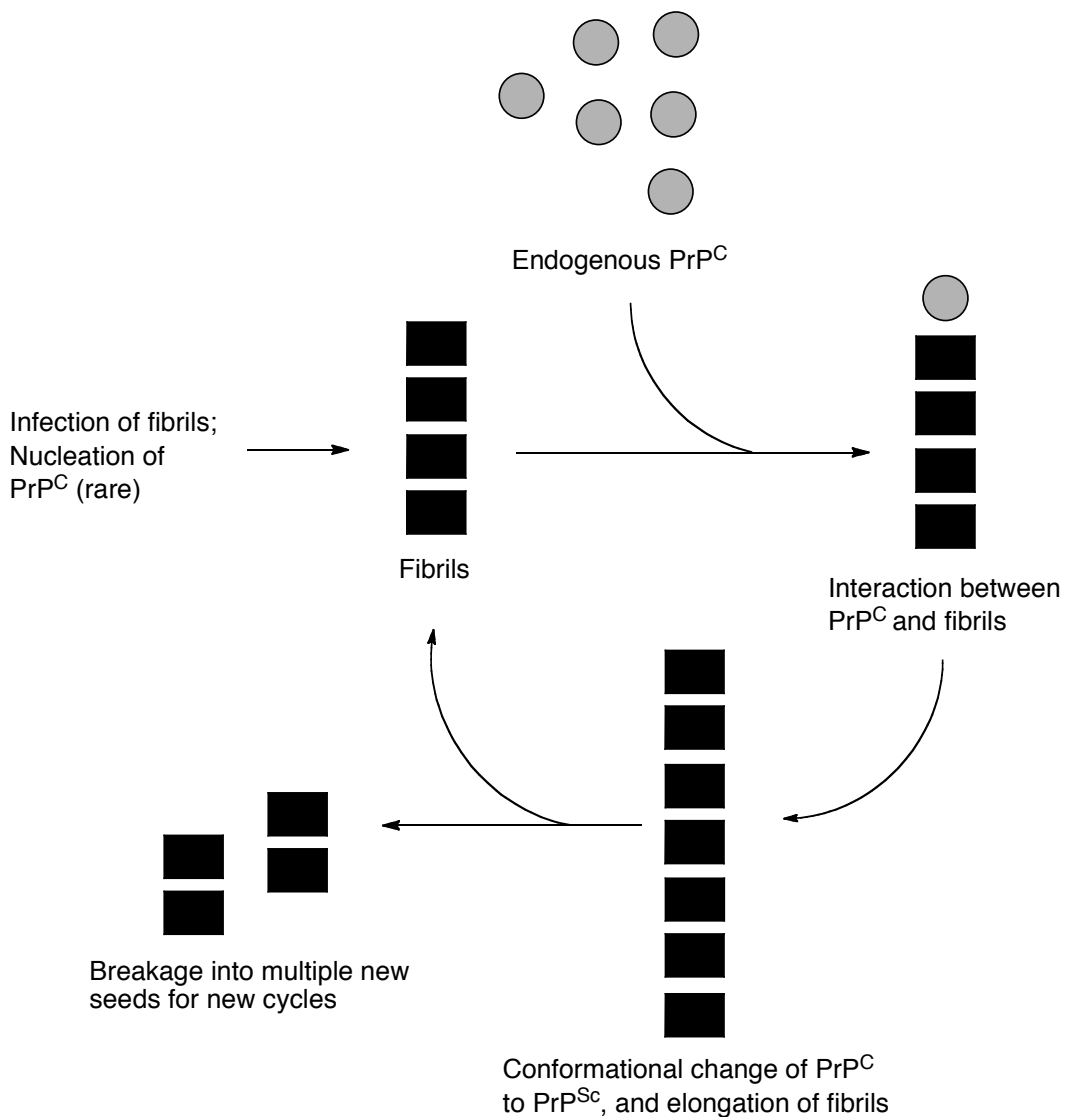


Figure 1.3 Fibril Model of Prion Replication.^{21a, b} In this model, PrP^{Sc} only exists in the form of fibrils. Interaction of fibrils (dark squares) with PrP^C (light circle) causes conformational changes in PrP^C, resulting in the conversion of PrP^C to PrP^{Sc} and the growth of the fibrils.

The main cause of transmission of prion diseases is through infection, for example, direct contact with affected particles, such as oral digestion of infected food, blood transfusion, or by contact with other body fluids.²² Another cause of these diseases is considered as familial or genetic, as a mutation of the prion protein *PRNP* gene is found in all inherited cases.¹⁶ The spontaneous occurrence of TSEs in humans is also discovered where no gene mutation or obvious exposure to external prion resources is identified, but it is very rare.²³

The tightly packed prion structure is extremely stable, and it is resistant to many common biological, chemical or physical denaturing methods, such as protease, boiling, irradiating and so on.²⁴ As a result, the established methods to combat microbial infection are not effective towards prions at all. This makes disposal of the contaminated animal particles very difficult, as prion protein can linger in the environment in the infective form for a very long time.²⁵

Unfortunately, there is still no effective vaccine, treatment or therapy for the universally fatal disease. The only existing way that we can minimize the danger and cost is to take precautions against the disease to prevent the spread. The common practice includes isolation, killing, burning of the affected animals, and deep burying of the remains of these animals beneath the ground. Also, feeding the cattle with cooked meat or bone meal of slaughtered cattle is strictly banned now, which was once a very common but unsafe practice in the European cattle industry.²⁶

In conclusion, the prion diseases are life-threatening diseases across many species, including humans, and there is still no effective vaccine, treatment or therapy. We hope that our effort and work for this prion project can help making new progress toward this great challenge.

1.2 Challenges and Recent Progresses in Prion Research

The prion diseases are a big mystery, and they have drawn a lot of attention from scientists worldwide. However, not much progress has been made so far towards their

treatment, not only because the TSEs have only been identified in very recent decades, but also because the research is highly challenging. A few challenges are as follows:

1. The precise mechanism of conversion of PrP^C to PrP^{Sc} is poorly understood, and the 3D structure of PrP^{Sc} is also unknown. No monomer of PrP^{Sc} has ever been isolated, and the aggregation of PrP^{Sc} makes the effort to reveal its 3D structure even more difficult;
2. The incubation period of TSEs in animals and humans is generally very long, ranging from a few months to many years. Thus projects in prion research are often costly and span long time frames;
3. Prion diseases are hard to diagnose in the early stages, due to the fact that no immune response can be triggered by prion. However, when the symptoms appear, the diseases develop very rapidly until death occurs;
4. The prion is primarily composed of protein that has highly compact and stable structure. Therefore, the prion protein is resistant to most established denaturing methods that are effective for common viruses or bacteria. In addition, the development of new denaturing methods specifically for the prion protein is also very difficult;
5. The understanding of transmission of the diseases is still very limited, even though direct contact with prion particles is generally considered as the main pathway.

Mostly, if not entirely, these reasons make the treatment of the prion diseases still a great global challenge.

Recent research into diagnosis, vaccination, or possible cures for prion diseases suggests a few interesting and promising options towards the treatment of the illness.²⁷ The main strategies include, but are not limited to, the prevention of the conversion of PrP^C to PrP^{Sc}, clearance of the aggregation of misfolded proteins and so on, and these can be achieved by targeting of PrP^C, PrP^{Sc} or the intermediate in the process of conversion by anti-prion compounds or antibodies. Discussion for research progress will focus on mainly four areas, which are genetic techniques, immunomodulation, immunotherapeutics and discovery of anti-prion compounds

Experiments of transgenic techniques by several groups show interesting results.

One effective approach developed by the Collinge group to inhibit further development of the prion diseases in infected mice is to knockout neuronal PrP^C through transgenic techniques at the early or mid stage of incubation period.²⁸ The result of these experiments also validates the hypothesis that the presence of PrP^C is necessary for the propagation and development of the prion diseases. However, the research is still at the experimental level, and it is not directly applicable to humans. Aguzzi and collaborators reported another experiment using transgenic techniques to produce dimeric protein PrP-Fc2, which is a fusion protein of PrP^C and immunoglobulin Fcγ.²⁹ PrP-Fc2 cannot be converted to the disease-related isoform, and they have higher affinity towards PrP^{Sc} than endogenous PrP^C. Consequently, PrP-Fc2 is competitive to block the interaction of PrP^C and PrP^{Sc} in transgenic mice of wild-type *Prnp* background, and thus prolong the incubation time.

Studies by different groups on immunomodulation of the prion diseases also led to some interesting discoveries which suggested possible ways to develop effective vaccines and therapeutics for the diseases.^{27, 30} Methods of immunomodulation that are found to be able to prolong incubation time slightly or modestly include:

1. Active immunization with prion peptide prior to infection;³¹
2. Passive immunization with monoclonal antibodies;³²
3. Immunostimulations by cytidyl-guanyl oligodeoxynucleotide 1826 (CpG 1826) alone or with complete Freund's adjuvant (CFA);³³
4. A combination of immunosuppression and anti-inflammatory agent treatment.³⁴

Some progress has been made in immunotherapeutics as well. Anti-prion antibodies with specificity and high affinity have been discovered through *in vitro* screening and animal model testing, which are able to reduce infectivity and inhibit PrP^{Sc} accumulation.^{27a} These antibodies can mainly be divided into several sub-categories as monoclonals, polyclonals, and single chain variable fragments, which include V5B2, 6H10, 6H4, D13/D18 (Fab), SAF34/SAF61, 110/31C6/44B1/72, Sha31, 3S9/2H9, 8B4/8H4, ICSM18/35, 6D11, 15B3.

In addition, a few small molecules were found to have certain promising affinity towards the PrP^{Sc} or were able to prolong the incubation period after thousands of synthetic or natural compounds were screened by different research groups in cell-based models or

animal models.^{27a} These anti-prion compounds can mainly be divided into several types based on their structures:

1. Congo red (CR) and its analogues,³⁵ which is widely used as a dye for histopathological stain of amyloid deposits;
2. Suramin and its derivatives and analogues,³⁶ which share certain structural similarity as congo red;
3. The antimalarial compound quinacrine³⁷ and its related hetero-tricyclic molecules,³⁸ such as chlorpromazine and acridine;
4. Tetrapyrrole molecules, such as phthalocyanines and porphyrins;³⁹
5. Dendritic polyamines and other cationic polyamines;⁴⁰
6. Polysulphated polyanionic compounds, such as heparan sulphate and analogues,⁴¹ dextran sulfate;⁴²
7. Nuclease-resistant 2'-amino(deoxy)pyrimidine-modified RNA aptamers;⁴³
8. PrP-derived peptides,⁴⁴ which are able to break β -sheets;
9. Other small molecules and divalent metal ions,⁴⁵ such as curcumin, statins, zinc, manganese, copper and copper chelator.

Based on the previous discussion, progress at genetic technique, immunomodulation, immunotherapeutics and discovery of anti-prion compounds provide some promising results towards vaccines and treatment of prion diseases. However, most of them are at preclinical levels, and the results are unpredictable from *in vitro* to *in vivo* system or from animal models to humans.

1.3 Significance and Goal of Our Research

Although some small molecules have been discovered to have promising anti-prion properties, and they are effective in some cases in either prolonging incubation time or reducing severity of prion diseases in animal models, it remains unknown whether they will also be effective in humans. Thus, it is desirable to have additional more effective compounds available for future clinical trials to increase the probability of obtaining

therapeutically effective compounds in humans. In particular, compounds with higher PrP^{Sc} binding affinity than those currently available ones should be developed, because they can more effectively prevent the conversion of PrP^C to its mis-folded isoform.

As a synthetic chemistry group, our strategy was to take advantage of these existing small molecules, which are known to have promising features, to make multimeric molecules with multi-binding units of improved binding affinity towards PrP^{Sc}. Specifically, the main objective of this project was to synthesize a library of multimeric (dimeric, trimeric or tetrameric) compounds with two, three or four effective binding units (**Figure 1.4**). Based on the knowledge that infectious prion particles consist of small oligomeric aggregates of PrP^{Sc}, the binding affinities of the newly synthesized compounds are expected to increase significantly through multivalent interactions, and some of them may be effective in halting the conversion of PrP^C to PrP^{Sc}.³⁹

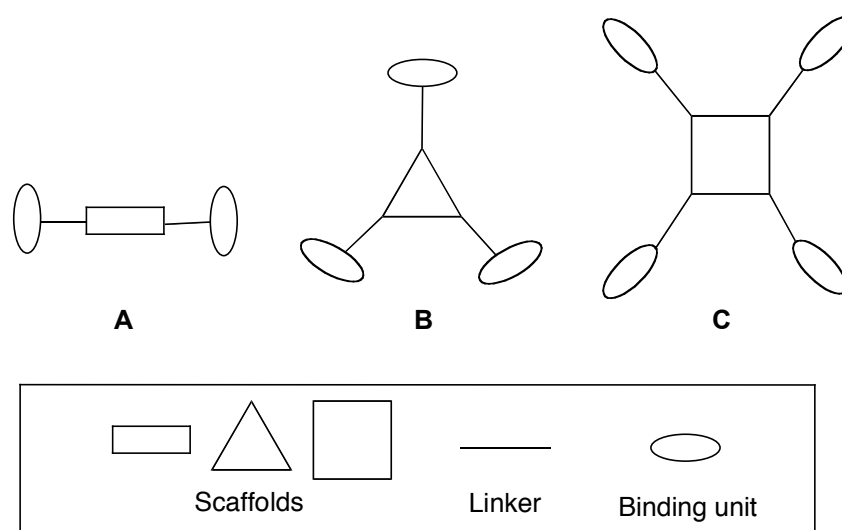


Figure 1.4 Generic structures of dimeric (A), trimeric (B) or tetrameric (C) compounds.

Besides their anticipated higher binding affinity and stronger anti-prion functions, the multimeric compounds might offer two additional benefits, including determination of the 3D structure of PrP^{Sc} and early detection and location of prion *in vivo*. The 3D structure of PrP^{Sc} is still quite unclear, and because PrP^{Sc} tends to aggregate to form insoluble plaque, the structure has been more difficult to be revealed. With the help of multimeric compounds that have high affinity towards PrP^{Sc}, there is a possibility of obtaining the

crystal structure of PrP^{Sc} bound with one multimeric anti-prion compound. If the crystal can indeed be obtained, the 3D structure of PrP^{Sc} may be revealed by X-ray crystallography. Although such an event is improbable, the potential importance of the outcome makes it a worthwhile effort. In addition, there is another probability to characterize the anti-prion compound stabilized PrP^{Sc} oligomers by NMR methods. Revealing the structure of PrP^{Sc} can not only help to improve the understanding of the mechanism of PrP^C to PrP^{Sc} conversion, but also help to design and develop new effective drugs specifically by targeting the potential binding sites/cavities in the structure.

The second potential benefit is that the availability of multimeric fluorescent compounds may facilitate early detection and location of the prion *in vivo*. Although some monomeric anti-prion compounds, such as acridine, are fluorescent and can be activated to give off fluorescent signals *in vivo* by binding to prion, their relatively weak binding affinity results in poor resolution between the target protein and background signal due to nonspecific binding. However, multimeric fluorescent compounds may provide much better resolution and potentially stronger fluorescent signals due to their higher binding affinity towards PrP^{Sc}. Our plan was to synthesize and find new multimeric fluorescent compounds with high affinity towards PrP^{Sc} by utilizing these monomeric fluorescent compounds as binding sites. If these compounds can concentrate in the area where there is a high concentration of PrP^{Sc}, they will help early detection and location of the prion *in vivo*. Early diagnosis of prion diseases is crucial for effective treatment before extensive damage to the central nerve system has occurred.

1.4 Project Rationale

This initial pilot study was carried out to synthesize a library of multimeric compounds that may have the capability to effectively bind to PrP^{Sc}. Multimeric compounds would be generated by adding two or more monomeric anti-prion binding units to a scaffold molecule, which is capable of accepting two to four monomeric binding units.

Disubstituted congo red, trisubstituted trimesic acid and tetrasubstituted

porphyrins were selected as scaffolds for the three categories of multimeric compounds for mainly two reasons (**Figure 1.5**). One reason is that they are able to provide a rigid and flat platform so that the binding units can be extended to different directions. The other reason is that they are multimeric molecules and this allows them to link to several monomeric binding units, and thus generating a structure with anticipated enhanced PrP^{Sc} binding affinity. In addition, porphyrins are fluorescent compounds, and the target molecules may be fluorescent as well if a porphyrin molecule is used as the scaffold.⁴⁶

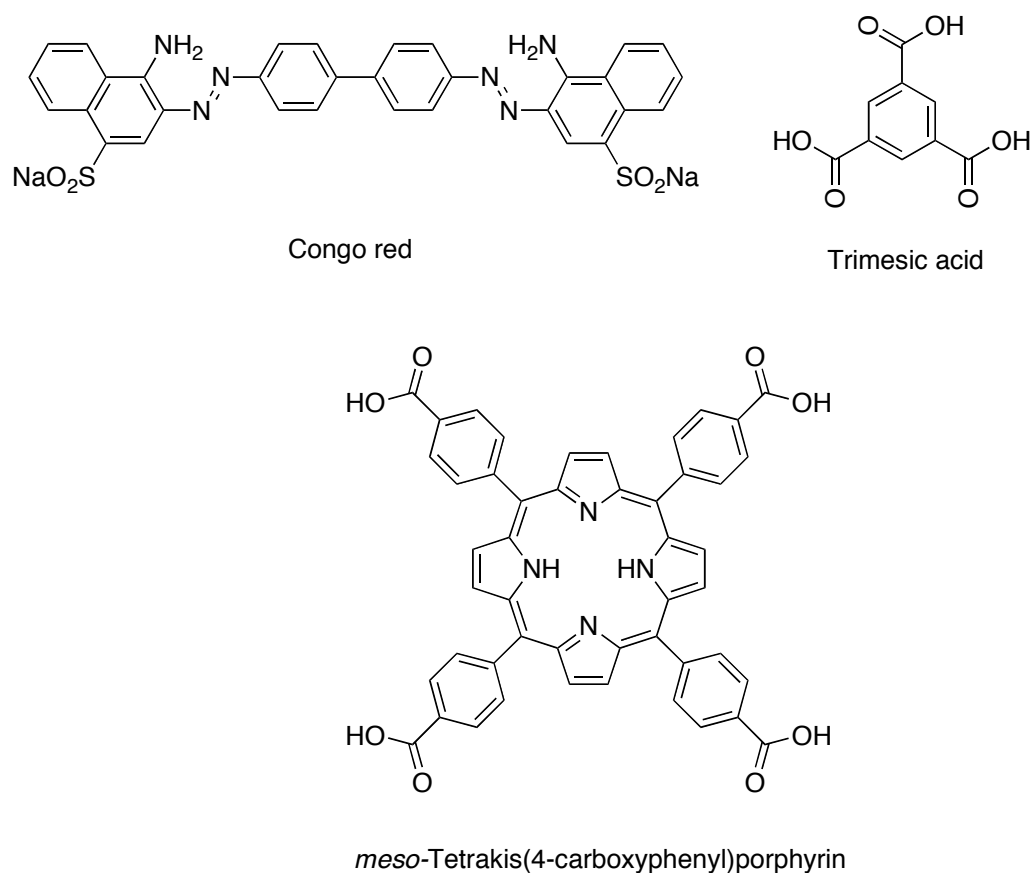


Figure 1.5 Structures of selected scaffolds.

Diamines were selected as linkers to connect to the scaffold through amide bond formation or palladium catalyzed coupling reactions (**Figure 1.6**). These diamines were chosen as linkers, because they have different rigidity and length. By building target molecules that have linkers with various lengths, it was hoped that some members of the library would have the right length to simultaneously complex with several binding sites in PrP^{Sc} oligomers, and thus show enhanced affinity.

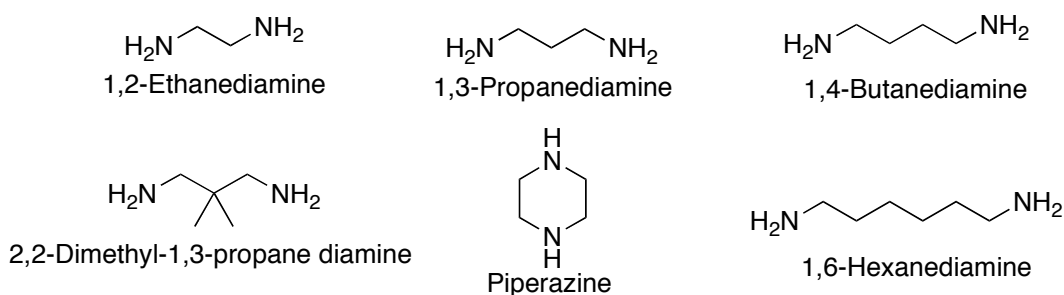


Figure 1.6 Structures of linkers.

Chloroquinoline⁴⁷ and methoxyacridine³⁸ were selected as the binding units, because they already show binding affinity towards PrP^{Sc} and are known to have anti-prion activity. It was hoped that the binding affinity of target molecules would be significantly enhanced through multivalent interaction between these known anti-prion binding units and PrP^{Sc} aggregates (**Figure 1.7**). In addition, some acridines display fluorescence, and the target molecules may be fluorescent if acridines are used as the binding units. With these multimeric target molecules in hand, they were to be evaluated for anti-prion activity by the Westaway group at the Centre for Prions and Protein Folding Diseases at the University of Alberta.

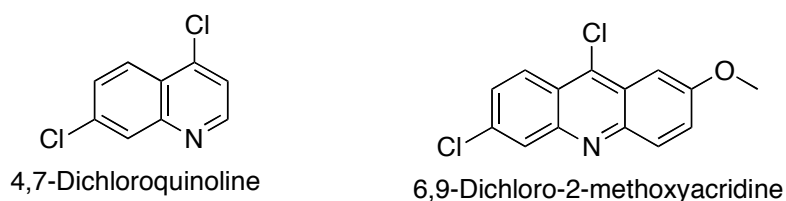


Figure 1.7 Structures of binding units.

Based on which scaffold is used, target molecules can be classified into three types. The first type of anticipated products are azo dye-based dimeric compounds as in **Figure 1.8**, mainly congo red and its derivatives. These targets were the focus of Dr. Lei Li.

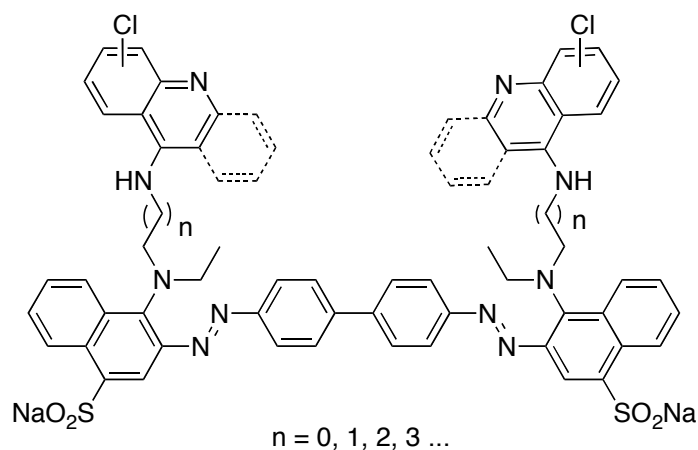


Figure 1.8 Generalized structures of congo red-based dimeric products.

The second type of target multimeric products is a series of 1,3,5-trisubstituted arene-based compounds, which are symmetrical molecules with three binding units (**Figure 1.9**). Shaon Joy synthesized and purified this type of target molecules.

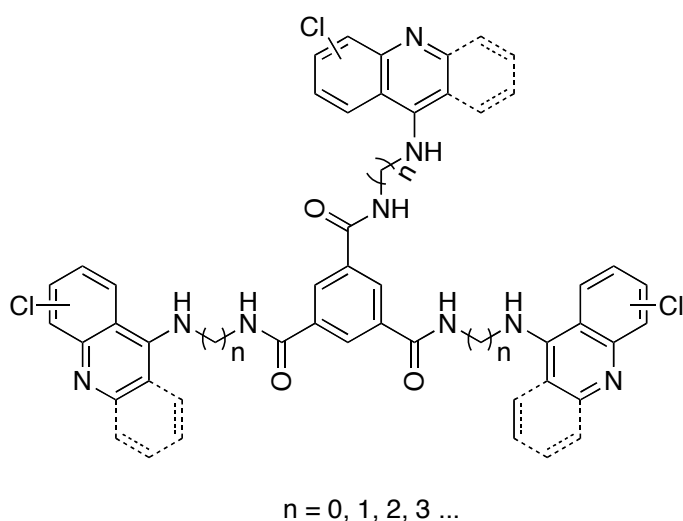


Figure 1.9 Generalized structures of 1,3,5-trisubstituted arene-based trimeric products.

The third type of anticipated products are porphyrin-based multimeric molecules as in **Figure 1.10**. As discussed earlier, their flat tetrameric structure makes them suitable scaffold for organic synthesis. The synthesis, purification and characterization of these compounds are the subject of this chapter.

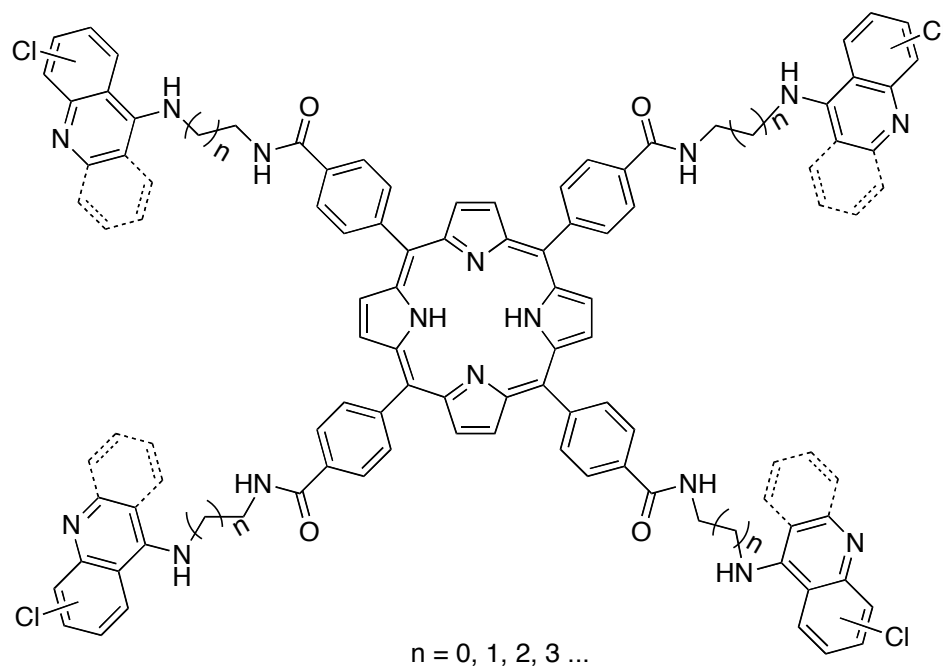


Figure 1.10 Generalized structures of porphyrin-based tetrameric products.

Besides exploring the efficient synthetic routes towards the three types of multimeric compounds, there is another plan to make fluorescent compounds when the routes of synthesis are well established. To achieve this, one pathway is to replace one of the binding units with a fluorophore, as illustrated by icon **A** in **Figure 1.11**. One example of the fluorophore is the cyanine dye Cy5, which can avoid quenching by azo dye, porphyrins or the acridine binder, because it emits longer wavelength.⁴⁸ Besides this, there are two other pathways to prepare fluorescent compounds. Simple installation of fluorescent binding units or usage of fluorescent scaffolds may achieve this goal as well, as exemplified by icon **B** and **C**. When both binding units and scaffold are fluorescent, the target molecule as icon **D** might be fluorescent as well, although the potential for internal quenching must be taken into account.

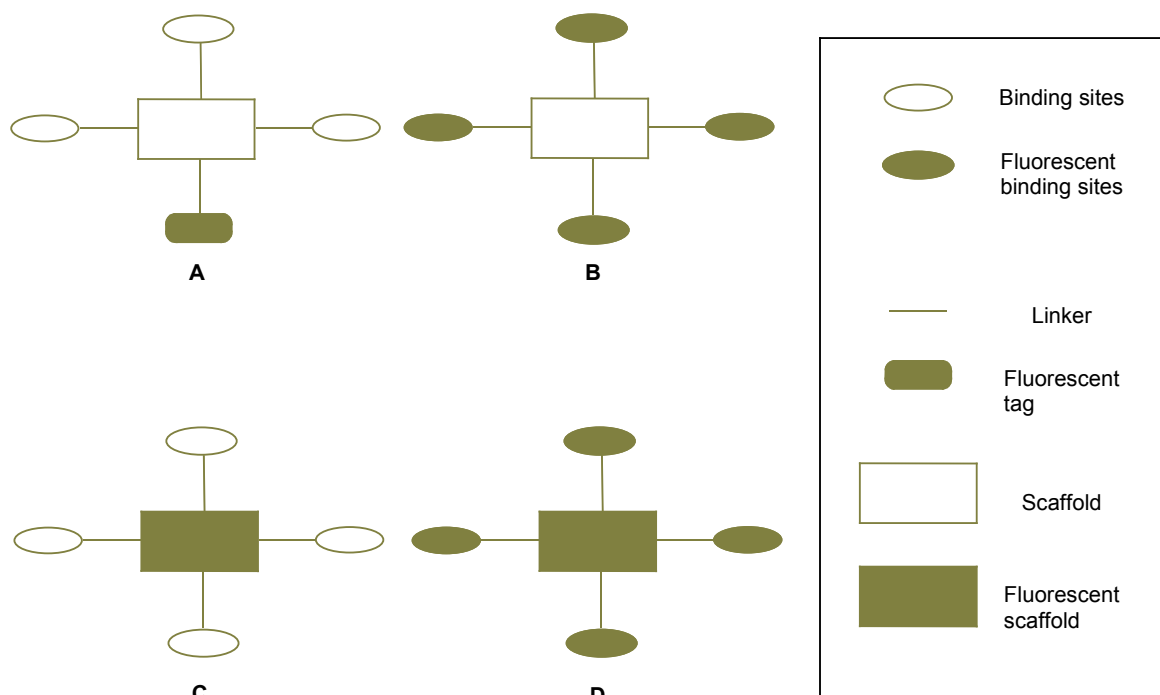


Figure 1.11 Generic multimeric fluorescent products.

The properties of ideal candidate molecules that may be clinically useful to treat prion diseases are highlighted in the following box:

1. The compounds show strong anti-prion activity;
2. They are fluorescent. Although this property is not necessary for compounds to be a drug candidate, fluorescent compounds provide additional benefits;
3. They can go across cell membrane easily;
4. They are able to go across blood-brain barrier;
5. They are resistant to digestion and are stable *in vivo*;
6. They are not toxic towards normal cells in humans or animals.

1.5 Synthesis of Porphyrin-Based Multimeric Molecules

1.5.1 Using Quinolines as the Binding Units

The porphyrin-based multimeric molecules are the target molecules that may have enhanced affinity towards PrP^{Sc} . An effective synthetic route needed to be explored and established for us to readily access a library of these compounds. In the initial attempts, the quinolines were employed as the binding units as in **Figure 1.12**, and other small molecules would be used later as the binding units once the synthetic routes have been well established.

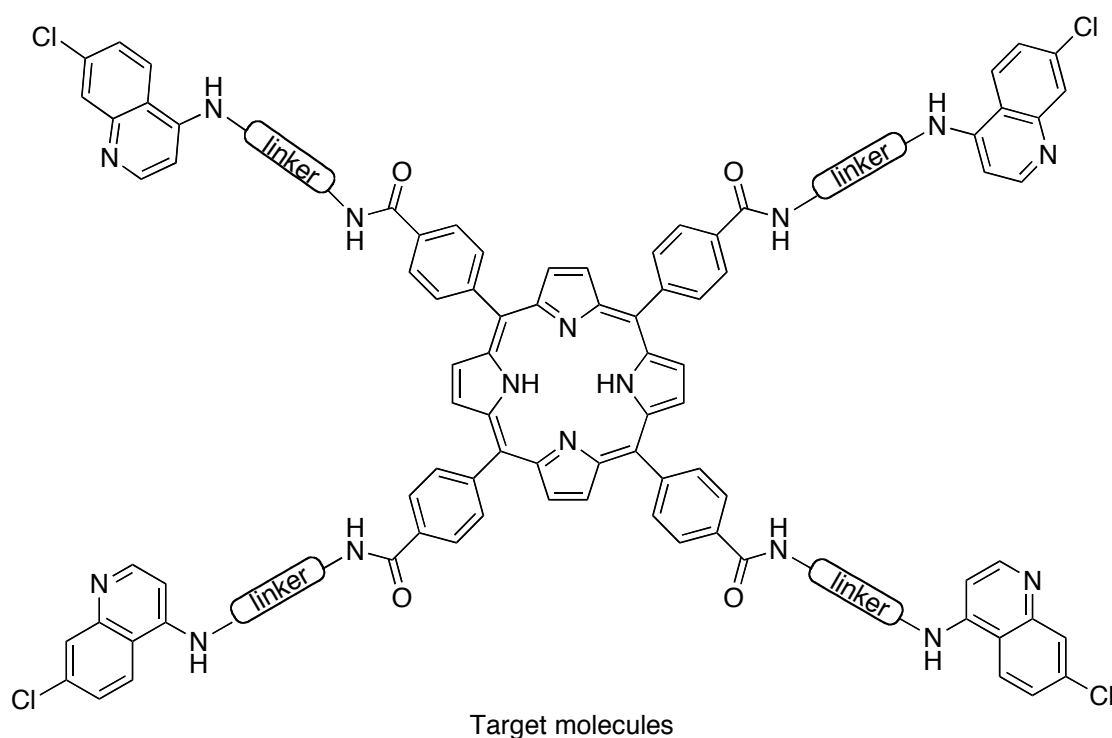


Figure 1.12 The target molecules with quinolines as binding units.

In the retrosynthetic analysis, the key steps to build these molecules mainly include assembling the porphyrin molecules and formation of the amide bond linkages. As in **Figure 1.13**, two alternative synthetic routes **A** and **B** were proposed, differing only in the order of steps. Since the synthesis of amide bond has already been well established and widely applied,⁴⁹ we envisioned using this step last. As a result of this decision, the porphyrin would be assembled using a relatively simple carboxybenzaldehyde building block. With the choice of route **A**, route **B** was held in reserve as a contingency plan in case the first approach was not satisfactory.

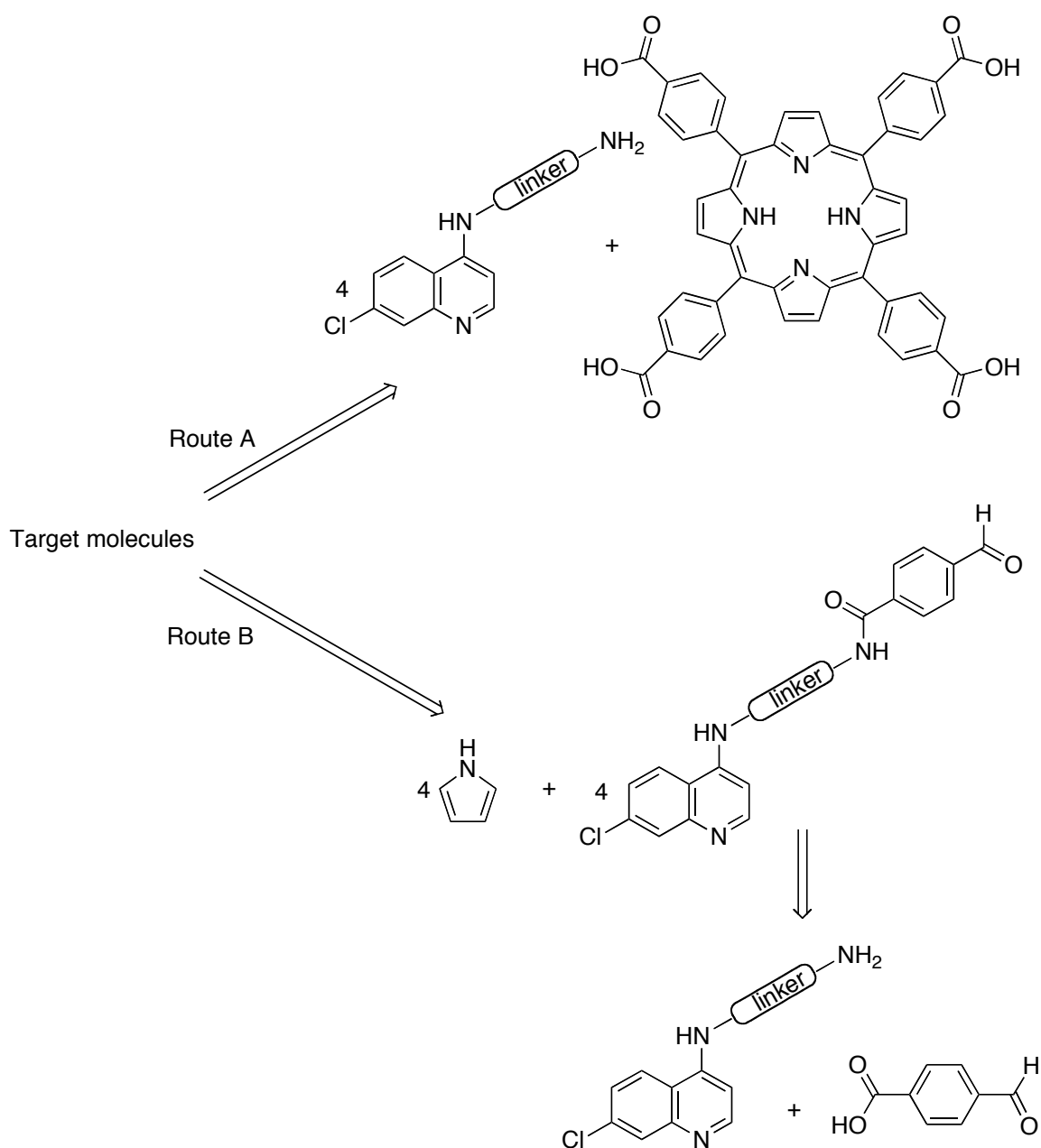
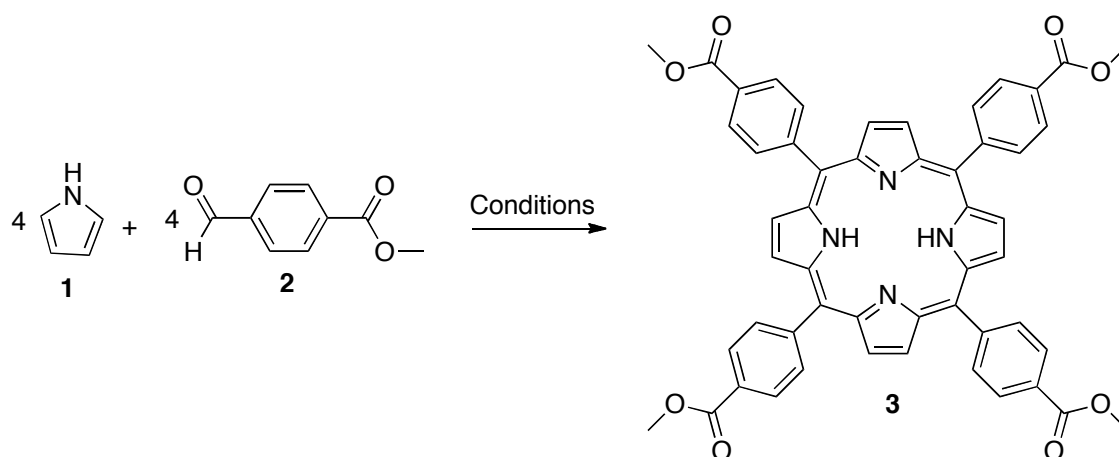


Figure 1.13 Retrosynthetic analysis of the target molecules.

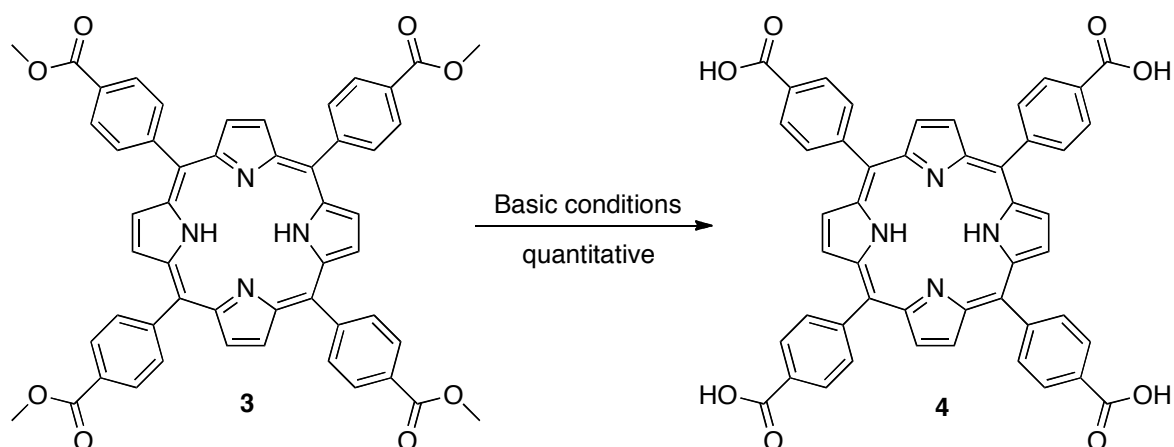
As in the synthetic route **A**, the first step is to make the central porphyrin molecule from pyrrole **1** and simple benzaldehyde **2**. Under the condition of Lewis acid $\text{BF}_3 \cdot \text{OEt}_2$, the benzaldehyde **2** was consumed completely before oxidant DDQ or *p*-chloranil was added.⁵⁰ In a single pot reaction, porphyrin **3** is obtained in a low 21% yield. The yield can be significantly improved to 56% by using $\text{BF}_3 \cdot \text{OEt}_2$ and TFA as the cocatalysts, with subsequent addition of *p*-chloranil as the oxidant (**Scheme 1.1**).⁵¹



Entry	Reaction conditions	Yields
1	0.1 equiv. $\text{BF}_3 \cdot \text{OEt}_2$, 1 equiv. TEOA, CH_2Cl_2 , r.t. 4~5 h; 0.8 equiv. DDQ, r.t, 1 h	21%
2	0.03 equiv. $\text{BF}_3 \cdot \text{OEt}_2$, 1.5 equiv. TFA, CH_2Cl_2 , r.t. 3 h; 1 equiv. p-chloranil, r.t, 1 h	56%

Scheme 1.1 Synthesis of *meso*-tetrasubstituted phenyl porphyrins.

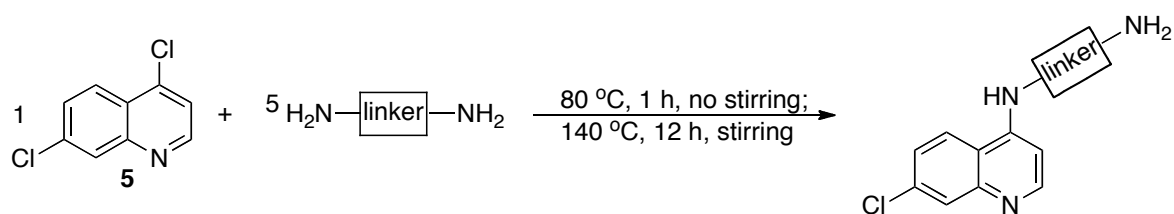
After the porphyrin **3** was prepared and purified, saponification of this compound could be readily achieved as in **Scheme 1.2** under the basic reaction conditions and a high temperature. Saponification of the four attached ester functional groups in porphyrin **3** went to completion, and the corresponding acid **4** was obtained in quantitative yields. The acid was then used as the scaffold to connect four binding units through amide bond formation.



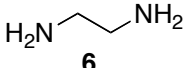
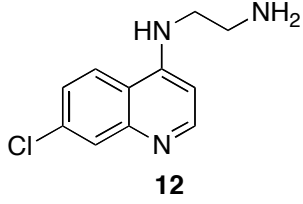
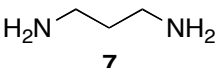
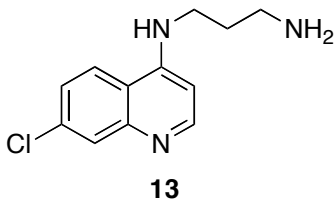
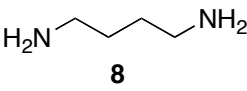
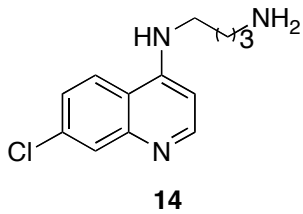
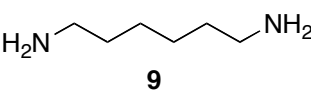
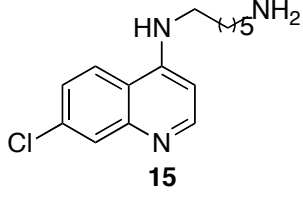
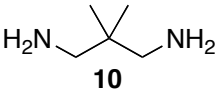
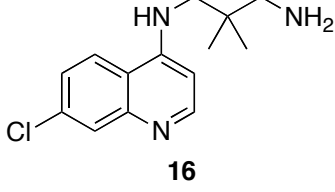
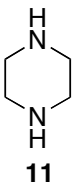
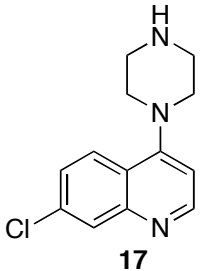
Entry	Conditions
1	4 wt% KOH solution, THF (v/v 3:4), 70-80 °C, 12h; 1N HCl solution
2	10 wt% NaOH solution, CH ₂ Cl ₂ , EtOH (v/v/v 1:1:1), 70-80 °C, 12h; 1N HCl solution

Scheme 1.2 Saponification of porphyrin **3** to get its corresponding acid **4**.

Diamines were utilized as linkers to connect the quinoline binding units and the porphyrin scaffold **4**. Before the last step of amide bond formation, synthesis of N-(7-chloroquinolin-4-yl)-alkyl-diamine compounds **12-17** was accomplished by heating the mixture of excess diamine and quinoline for a few hours, in a 5:1 molar ratio without any solvent as in **Scheme 1.3**.⁵² Six different products were obtained with a range of yields, depending upon diamines used (**Table 1.2**).



Scheme 1.3 General method for preparation of N-(7-chloroquinolin-4-yl)-alkyl-diamines.

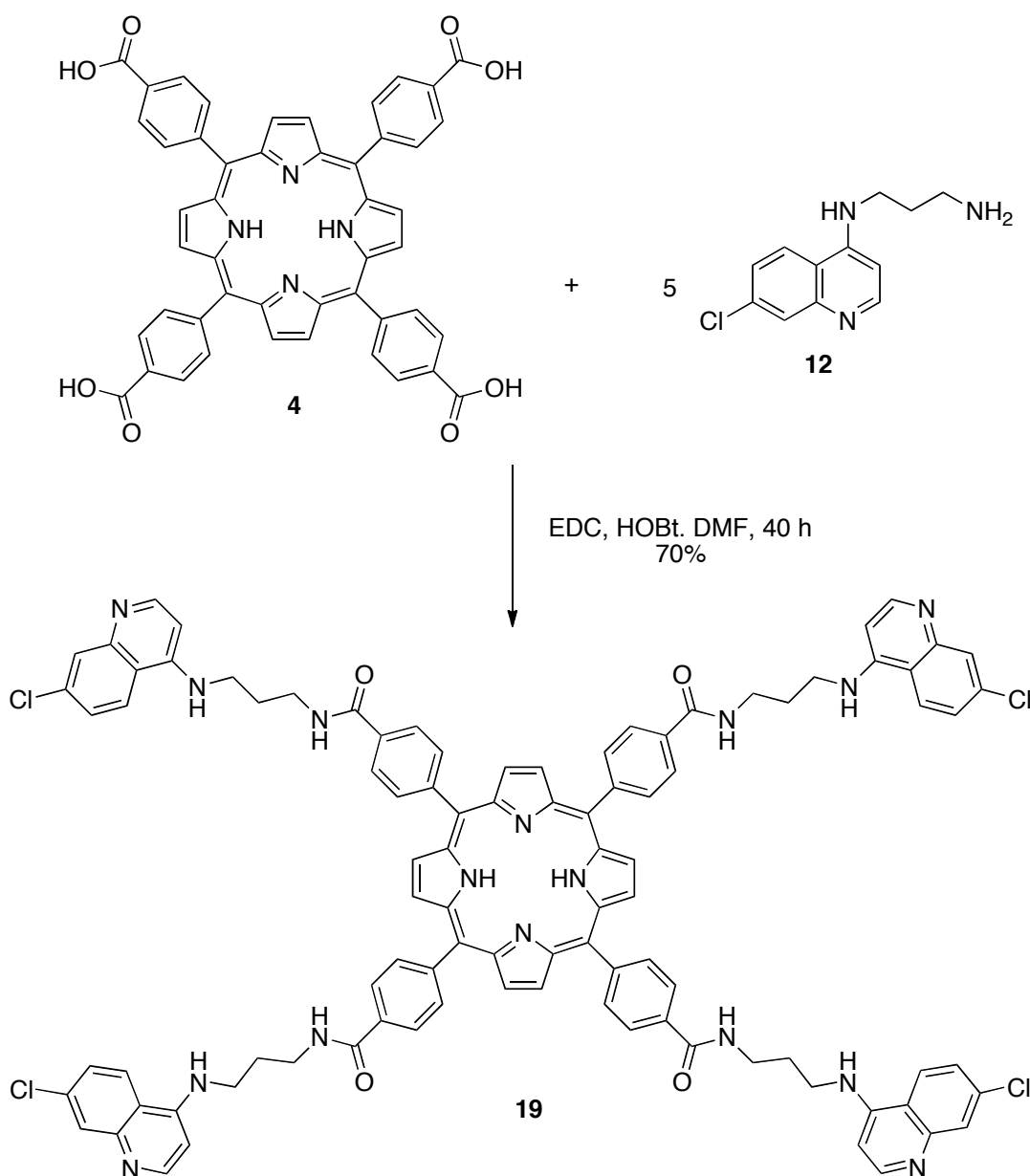
Entry	Diamines	Products	Yields
1	 6	 12	53%
2	 7	 13	88%
3	 8	 14	32%
4	 9	 15	25%
5	 10	 16	79%
6	 11	 17	52% ¹

1. Part of compound **17** is provided by Shaon Joy.

Table 1.2 A list of prepared N-(7-chloroquinolin-4-yl)-alkyl-diamine products **12-17**.

With both the porphyrin **4** and the products **12-17** in hand, the target multimeric molecules could be obtained through the amide bond formation as in **Scheme 1.4** using a

5:1 ratio of N-(7-chloroquinolin-4-yl)alkyldiamine and porphyrin. The diamine partner was used in excess to minimize the occurrence of incomplete conversion to the desired tetraamide. The amide bond formation reaction worked smoothly in this case as well, and the porphyrin-based tetra-substituted target molecule **19** was obtained in the yield of 70%.⁵³

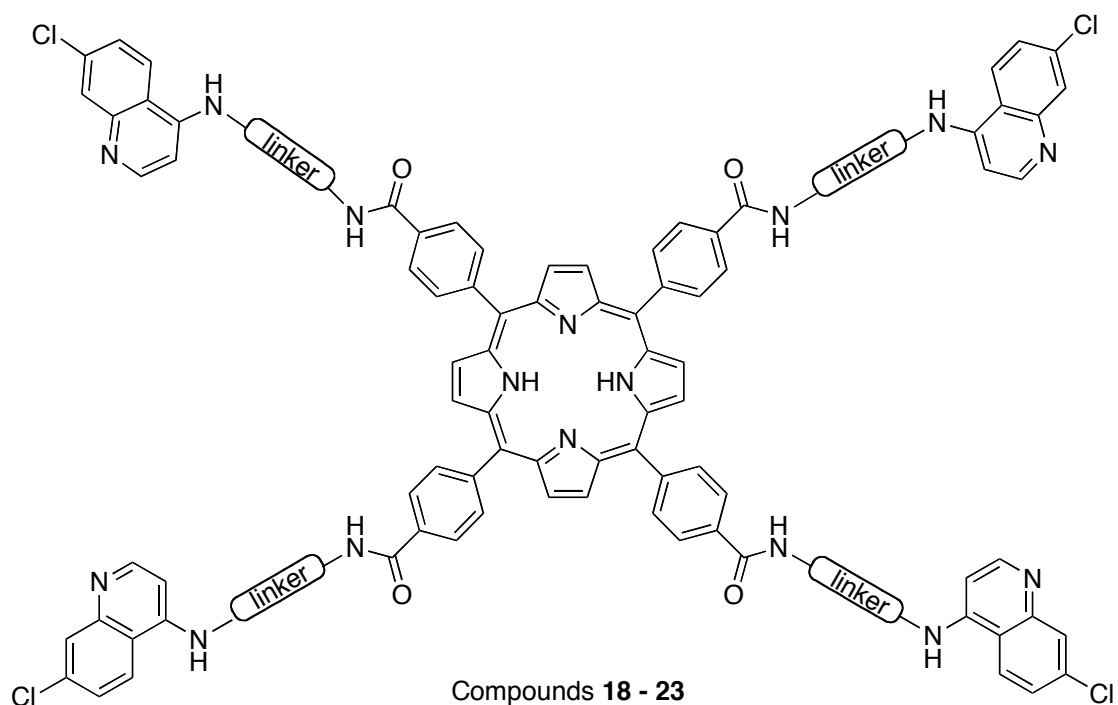


Scheme 1.4 Amide bond formation reaction to form one of the target molecules.

Therefore, a short and effective synthetic route has been established to make porphyrin-based tetrameric compounds, which comprises of four steps in total from

commercially available starting materials. This synthetic route includes a sequence of assembling porphyrin rings, saponification, synthesis of N-(7-chloroquinolin-4-yl)-alkyl-diamine compounds, and amide bond formation.

Besides compound **19**, five other tetrameric compounds **18**, **20-23** as listed in **Table 1.3** were also prepared with this synthetic route by employing different diamines and moderate to good yields have been obtained. They share linear or cyclic carbon chains with different length and rigidity, as the length and rigidity of the chains may also play an important role in enhancing the binding affinity towards PrP^{Sc}.



Entry	Linkers	Products	Yields
1		18	82%
2		19	70%
3		20	70%
4		21	69%
5		22	65%
6		23	79%

Table 1.3 Structures and yields of six tetrameric porphyrin products.

These newly synthesized multimeric compounds are very polar compounds and all of them show poor solubility in most commonly used solvents in the lab, such as hexane, EtOAc, acetone, DCM, toluene, Et₂O, THF. In general, these compounds are moderately soluble in DMF and DMSO at the room temperature, as the color change of

DMF or DMSO solution can be easily detected by eye when the brightly colored porphyrin derivatives undergo dissolution. Most of them also show very slight solubility in methanol as well. These properties of the compounds give rise to a few problems for purification and characterization.

Many purification methods were tried to purify these porphyrin-based multimeric compounds, including flash chromatography, preparative reverse-phase thin layer chromatography, and recrystallization in different solvent systems. However, these common purification methods were not successful for them.

Flash chromatography was not applicable to purify any of the six compounds, because the compounds are very polar and their R_f values on TLC are all close to zero even when a polar solvent system of 20% MeOH in DCM was used as the eluent.

The reverse-phase chromatography was also tried in small scale using reverse-phase TLC plates. The sample of compound **18** was loaded on the reverse-phase TLC, separation occurred when polar eluent solvent systems was used. The gel of each band of separation was removed to recover the compounds on it. However, no expected product was isolated and identified in this way. Furthermore, the efficiency is quite low, due to the weak solubility of compounds in the eluent solvent as well as the solvent used to load the compounds on the plates.

Recrystallization in two-solvent system, for example DMF and Et₂O, was tried to purify compounds **18**, **19** and **22**, but in all cases only precipitates rather than crystals of the products were obtained.

Eventually, trituration was found to provide the best option for obtaining the desired compounds free of soluble starting materials and impurities. As a result, the impurities could be removed, but some products were lost as well. Also, solvents such as water, MeOH and DMF are difficult to be removed completely from these purified polar macromolecules, and trace amounts of toluene were also sometimes present when it was used in the trituration, due to π -stacking. However, the presence of traces of solvents was considered to be tolerable, since sample preparation for biological testing would entail preparation of dilute DMSO solutions.

Similar problems also exist for the characterizations of these compounds due to

their poor solubility in most solvents. It is difficult to find the right solvent or solvent system besides DMF and DMSO to dissolve these compounds for the analytical methods of UV, fluorescence analysis and HRMS. Eventually, MeOH or a combination of MeCN, H₂O or MeOH provides a solution to the problems. However, only qualitative results of fluorescence analysis have been obtained. All ¹H NMR spectra (*d*-DMSO) of the compounds have a shielded proton peak around -3 ppm (2H), which locates in the center of the porphyrin. The purity of these compounds has also been confirmed by their ¹H NMR spectra, although solvent peaks (mostly water) do exist in most samples.

UV-Visible absorbance spectra of all the six molecules shows a significant Soret band around 415-418 nm, which is a common feature of porphyrin molecules (**Chart 1.1**). Broad Q bands around 550 nm were also observed in these samples, but the intensity was found to be much weaker if compared with that of Soret bands.⁵⁴ Besides the Soret and Q bands, peaks around 220, 230 and 330 nm were also observed, and these absorbances were attributed to the quinoline moieties.

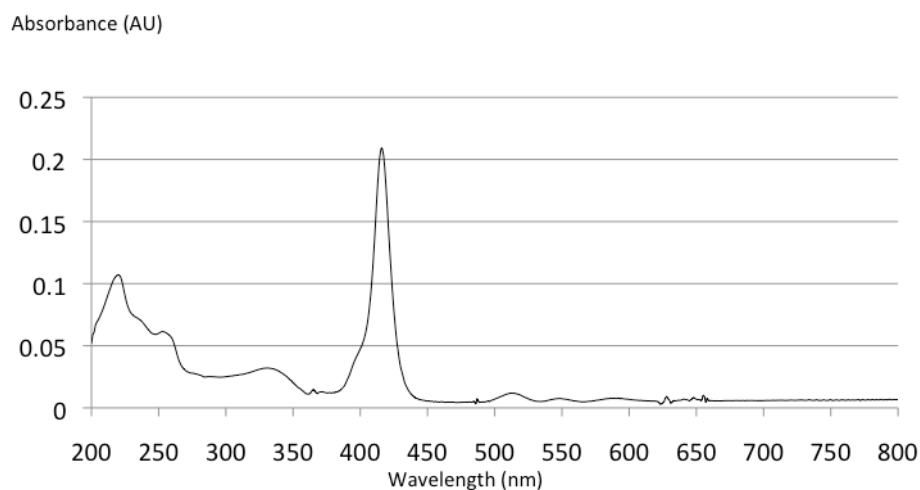


Chart 1.1 UV-Vis absorbance spectrum of compound **18**.

Fluorescence analysis was also carried out for all the products, as porphyrins are expected to be fluorescent compounds. In general, after the excitation scans, wavelength of 425 nm was used for emission scan. Wavelengths of emission around 648 and 715 nm were observed in all products, which is consistent with that of the starting porphyrin

material **3** and **4** (**Chart 1.2**). Therefore, all six of the products are fluorescent compounds. This characteristic could be very useful, if these molecules were also found to have high affinity towards PrP^{Sc}, because fluorescent compounds that bind effectively to PrP^{Sc} could be used to detect and locate infectious prion particles *in vivo*.

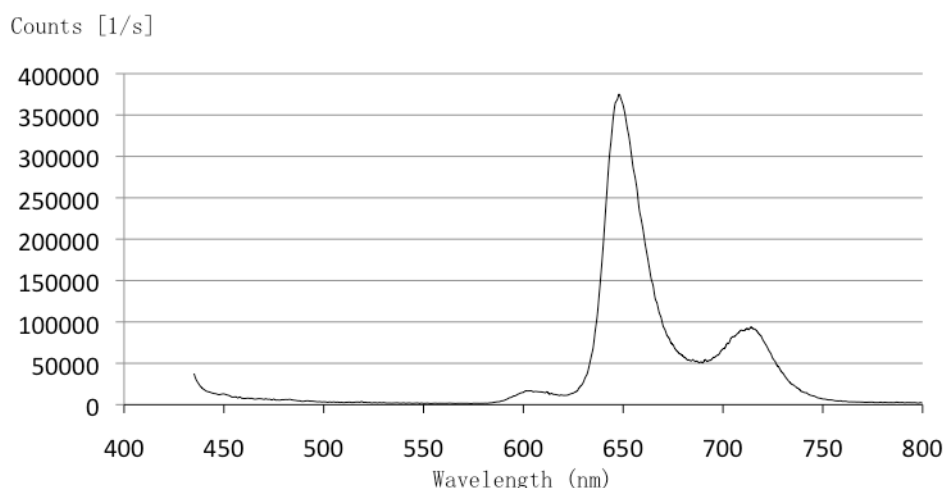


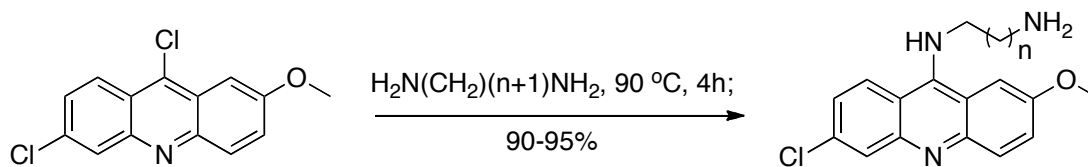
Chart 1.2 Fluorescence analysis of compound **18**. When excited by light of 425 nm, emission of 648 and 715 nm were observed.

Therefore, the porphyrin-based multimeric compounds by using quinolines as the binding units have been synthesized and purified, and the results have been confirmed by the characterization methods of IR, UV, fluorescence analysis, HRMS, ¹H NMR and ¹³C NMR.

1.5.2 Using 9-Amino-acridine as the Binding Units

Besides quinolines, 9-amino-acridines are also well known anti-prion compounds that show promising affinity towards PrP^{Sc}.³⁸ Therefore, it was considered desirable to make a second series of porphyrine-based tetrameric compounds by using 9-amino-acridine as the binding units. These compounds were prepared by following the synthetic route and purification methods described in the previous section.

The N-(6-chloro-2-methoxyacridin-9-yl)-alkyl-diamine compounds could be prepared through the reaction of direct coupling of the corresponding 6-chloroacridine and diamine with excellent yield as shown in **Scheme 1.5**.⁵⁵



Scheme 1.5 The reaction to prepare N-(6-chloro-2-methoxyacridin-9-yl)-alkyl diamine compounds.

Four starting materials of N-(6-Chloro-2-methoxyacridin-9-yl)-alkyl diamine compounds **25-28** listed in **Figure 1.14** were prepared and provided to me by following literature procedures by another group member, Dr. Kendre Dhananjay, as he has extra amount of these materials besides his own usage.⁵⁶

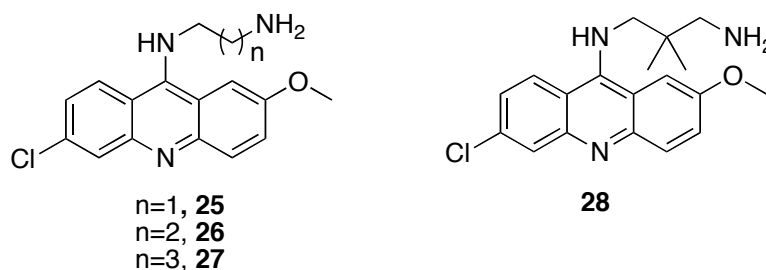
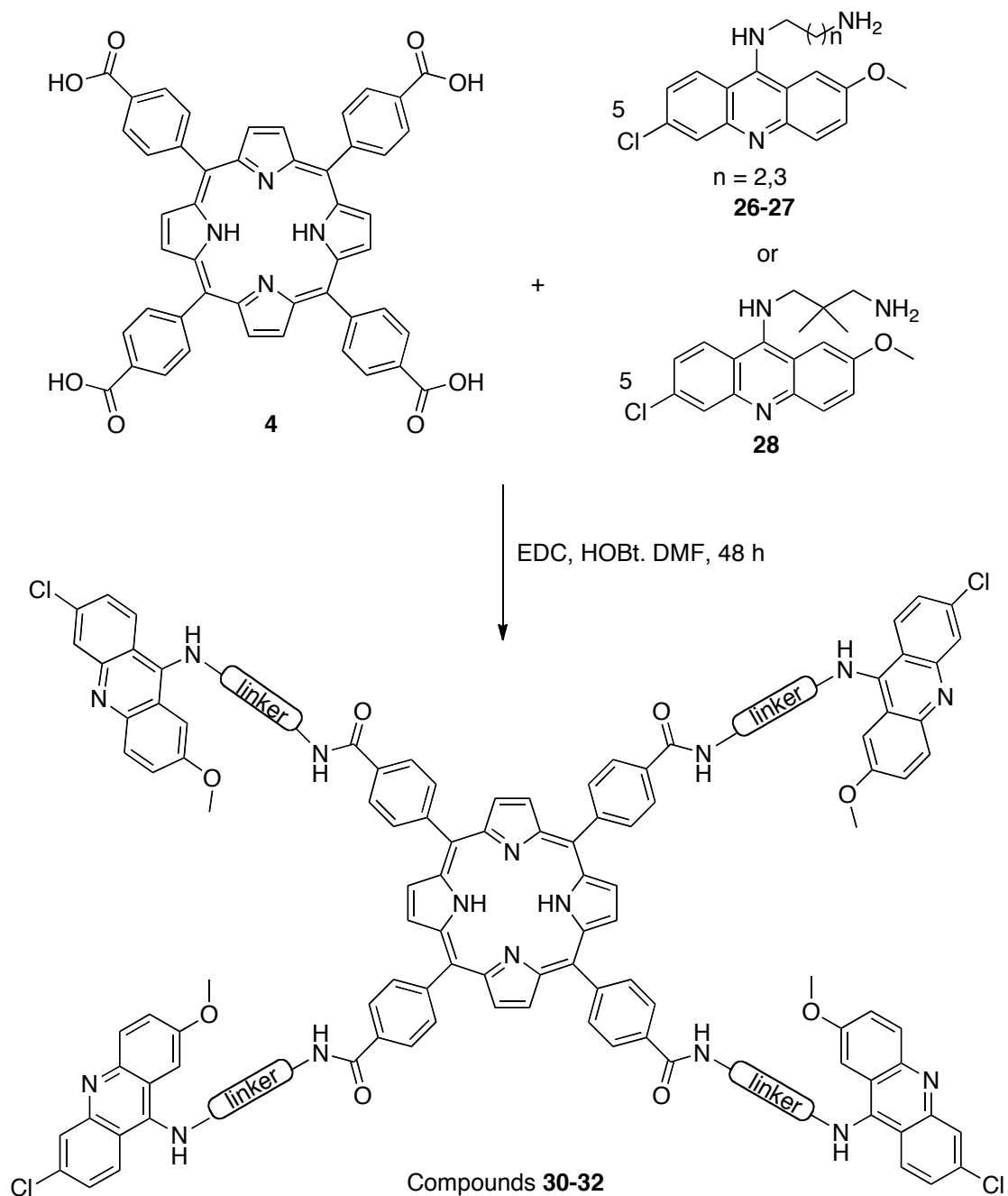


Figure 1.14 Structures of four N-(6-Chloro-2-methoxyacridin-9-yl)-alkyl diamine compounds.

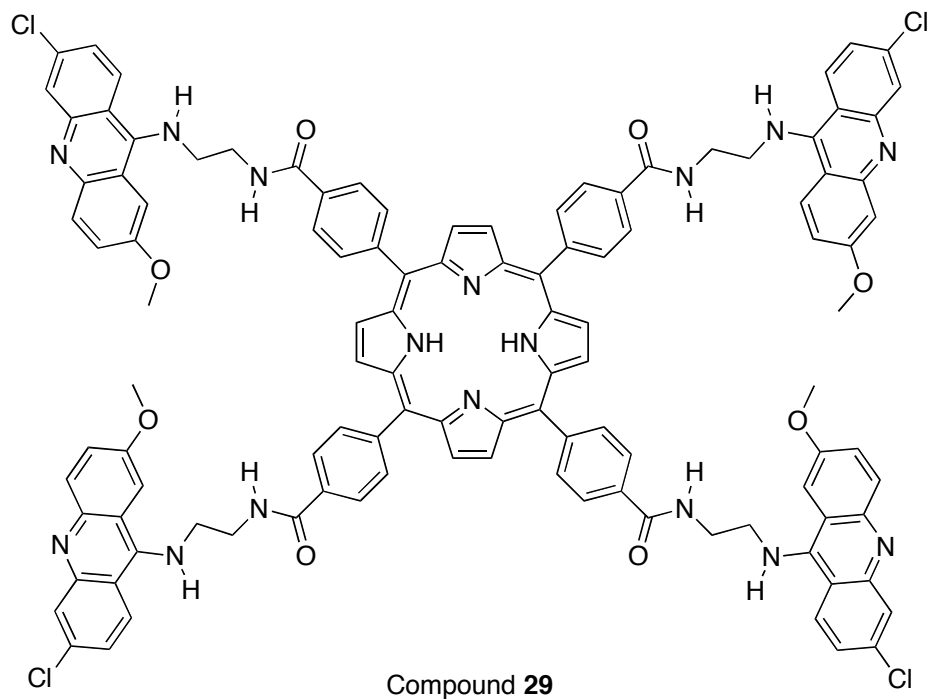
The last step of amide bond formation as in **Table 1.4** also worked well in the case of three N-(6-chloro-2-methoxyacridin-9-yl)-alkyl-diamine compounds **26-28** to furnish the second series of target molecules, and different products have been obtained in good or moderate yields.



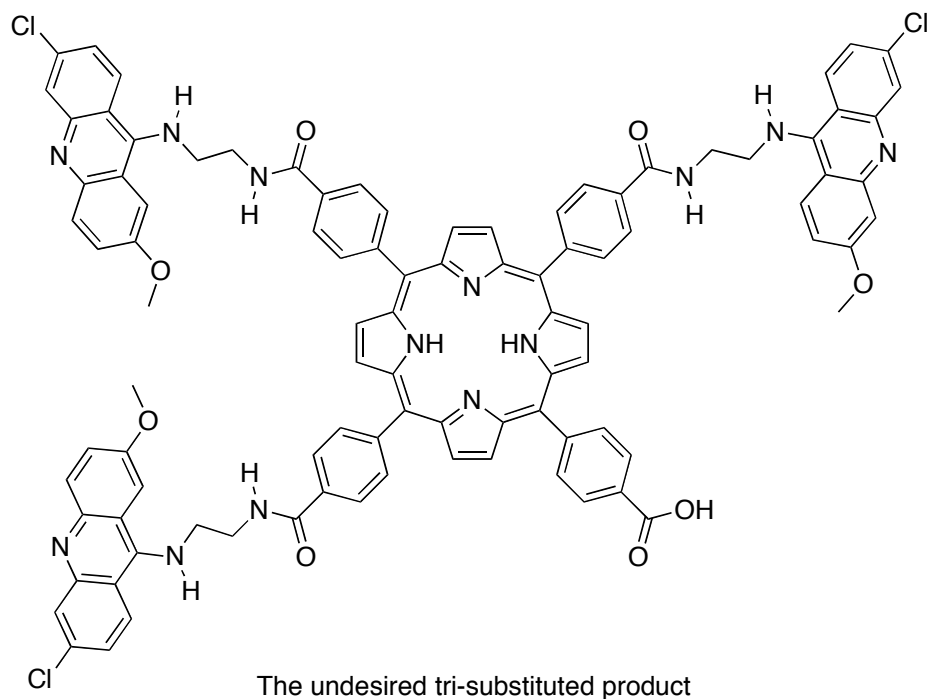
Entry	Linkers	Related products	Yields
1	$\text{H}_2\text{N}-\text{CH}_2-\text{CH}_2-\text{CH}_2-\text{NH}_2$	30	75 %
2	$\text{H}_2\text{N}-\text{CH}_2-\text{CH}_2-\text{CH}_2-\text{CH}_2-\text{NH}_2$	31	57 %
3	$\text{H}_2\text{N}-\text{CH}_2-\text{C}(\text{CH}_3)_2-\text{CH}_2-\text{NH}_2$	32	54 %

Table 1.4 Reactions of amide bond formation to get to the second series of target molecules

In the case of compound **25**, however, the reaction did not go to completion, and a mixture of mono-, di- and tri-substituted compounds besides the desired tetra-substituted product **29** were obtained in an overall yield of 76%. In another attempt, the reaction did not go to completion either, although an excess amount of the starting material **25** (10 equiv.) was used and the reaction time was extended to 4 days. In both reactions, the undesired mono-, di- and tri-substituted compounds were identified by both low- and high-resolution mass spectrometry (LRMS & HRMS), and the peak of tri-substituted product was always the most significant peak among the undesired products (**Figure 1.15**). The products in the mixture cannot be separated from each other, because they are all very polar compounds with weak solubility in most solvents. Compound **25** has a shorter 1,2-ethanediamine linker than those of compounds **26-28**. The shorter linkers may increase the effect of π -stacking, and thus decrease the solubility of the products of compound **25**. This may explain the lower reactivity of compound **25** in the amide bond formation reaction, as once some of the undesired products precipitates, they will not react further more.



HRMS (MALDI) calculated for $C_{112}H_{87}Cl_4N_{16}O_8$ ($[MH]^+$) 1923.5641, found 1923.5641



HRMS (MALDI) calculated for $C_{96}H_{73}Cl_3N_{13}O_8$ ($[MH]^+$) 1640.4765, found 1640.4772

Figure 1.15 The structures of the desired compound **29** and undesired tri-substituted product.

The polarity of the products **30-32** was found to be very similar as the

quinoline-binded compounds in **Section 1.5.1**, as they are also very polar compounds that cannot be purified by flash chromatography. The solubility of these 9-aminoacridine-linked compounds is even weaker than the quinoline-linked products. They only show slight solubility in DMF and DMSO at the room temperature, and they can be dissolved in methanol very slightly as well. Similarly, these compounds were purified by trituration to remove soluble impurities. They are characterized by the analytical methods of IR, UV, fluorescence analysis, HRMS and ^1H NMR. However, the signals in ^{13}C NMR spectra were very weak for the three compounds due to their weak solubility, and many sp^2 carbons were missing for compounds **30** and **31** in their ^{13}C NMR spectra.

UV-Visible absorbance spectra of the three samples shows a significant Soret band around 416-418 nm and a weak broad Q band between 500 and 650 nm (**Chart 1.3**). In addition, strong peaks around 225, 270 nm were also observed, which may be the characteristic peaks of 9-amino-acridine moieties.

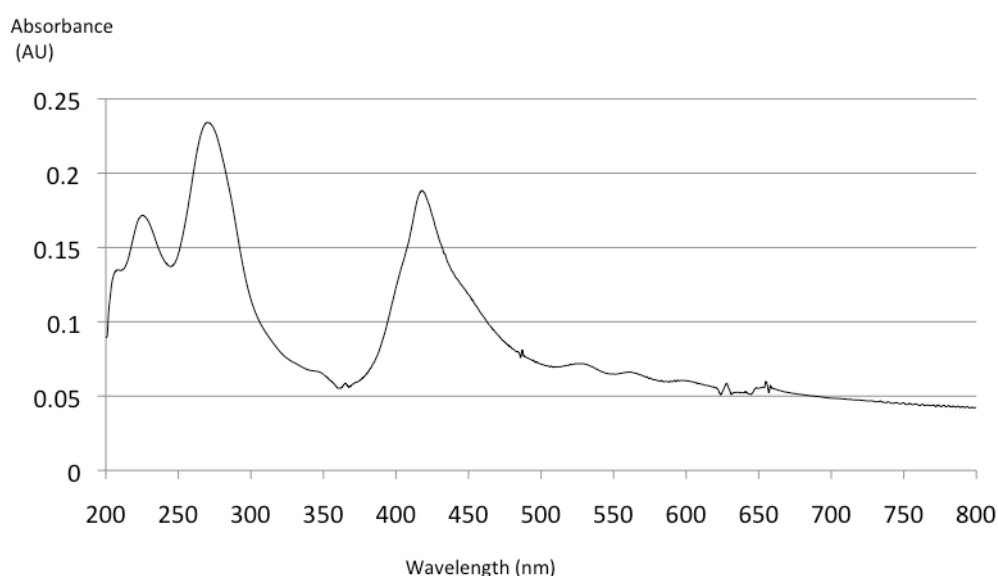


Chart 1.3 UV-Visible absorbance spectrum of compound **30**.

Furthermore, these compounds were found to be fluorescent as well. When they were excited at 430 nm, emission at wavelengths of around 475, 650, 720 nm was observed (**Chart 1.4**). Besides the porphyrin emission of 650 and 720 nm, emission of 475

nm is from the 9-amino-acridine moieties.

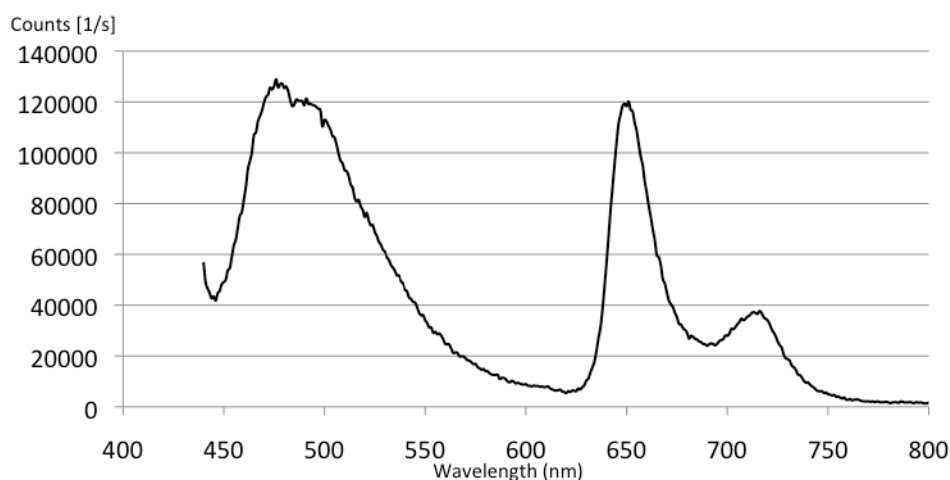


Chart 1.4 Fluorescence analysis of compound **30**. When the compound is excited by light of 430 nm, emission of wavelength of 470 nm, 650 nm and 715 nm were observed.

1.6 Preliminary Biological Evaluation of Porphyrin-Based Multivalent Prion Binders

1.6.1 Introduction of Experimental Designs & Evaluation Results for Porphyrins 3-4 and Mono-Binding Units 12-17

After the compounds were synthesized and purified, the samples were prepared in DMSO in the concentration of 1 mM or 0.5 mM. They were sent to our collaborator, the Westaway group, for anti-prion assays. The starting materials **3-4** and **12-17** used to build porphyrin-based multimeric compounds were also submitted for the assay for the purpose of comparison and analysis.

The anti-prion assay is based on Scrapie-infected Mouse Brain (SMB) cells *in vitro*.⁵⁷ The SMB cells were treated with different concentrations of putative anti-prion compounds for six days. Treated cells were digested by Proteinase K (PK) to remove the proteins except the proteinase resistant PrP^{Sc}. Western blotting analysis was performed to quantify PrP^{Sc} levels after treatment with compounds.⁵⁸ A sample from untreated cells was

also included in the analysis to serve as a control. The more effective an anti-prion compound is, the less amount of PrP^{Sc} will be left in the sample after the six-day treatment. In the western blotting analysis, the three bands of un-, mono-, di-glycosylated PrP^{Sc} proteins are detected between 16 and 36 kilodaltons (kDa). There is a reference band where no treatment of putative anti-prion compounds but blank DMSO solution is applied for the purpose of comparison. The band color intensity in the film indicates the amount of PrP^{Sc} left. Densitometric analysis of the results of western blots gives a semi-quantitative evaluation of the effectiveness of the anticipated anti-prion compounds.

The results of the mono-binding units **12-17** show that these compounds exhibit anti-prion activity more or less at the concentration of 5 μ M (**Figure 1.16** and **Chart 1.5**). At this concentration, compound **16** is very effective in completely clearing the amount of PrP^{Sc}, and compounds **13** and **15** are also quite effective in reducing the amount of PrP^{Sc} by more than 50%. Although the other three compounds are not as effective as compounds **13**, **15** and **16**, they still show positive effect in lowering the levels of PrP^{Sc} by from 20% to 40%.

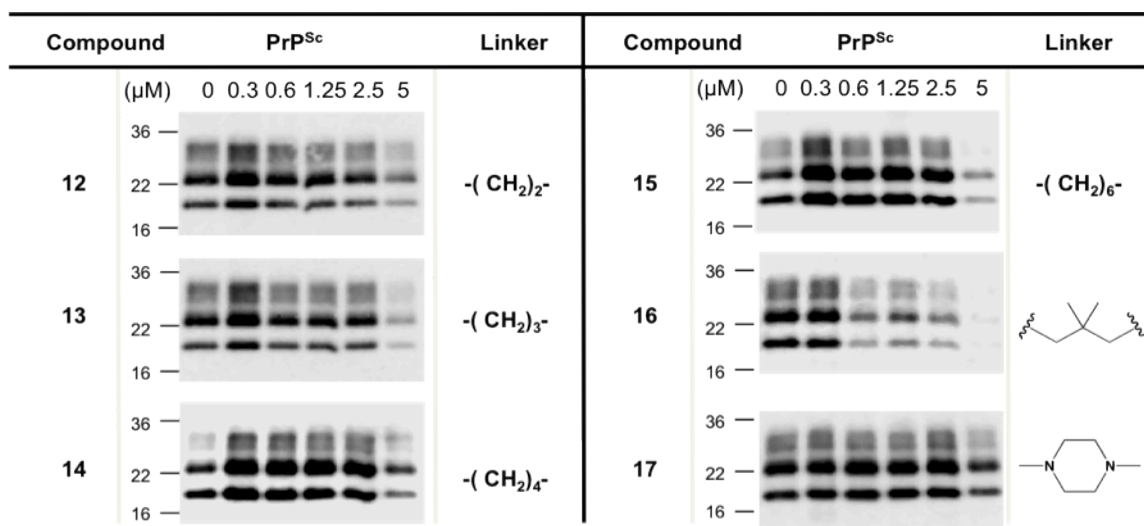
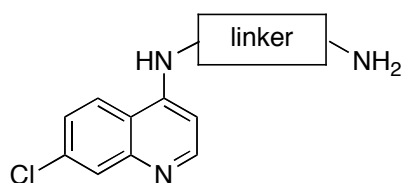


Figure 1.16 Antiprion activity of N-(7-chloroquinolin-4-yl)-alkyl-diamines **12-17**.⁵⁹ Western blotting analysis of SMB cells was utilized to measure the anti-prion activity of the N-(7-chloroquinolin-4-yl)-alkyl-diamine compounds at concentrations of 0, 0.3, 0.6, 1.25, 2.5, or 5 μM after the 6-day treatment. Three bands in the film between 16 and 36 kDa are the un-, mono-, di-glycosylated PrP^{Sc} proteins that resist to PK digestion. The band intensity indicates the amount of PrP^{Sc} in the assay after the treatment of different compounds. The bands in the first column from left are the reference bands from untreated cells. As an example, compound **16** is able to clear PrP^{Sc} efficiently at the concentration of 5 μM .

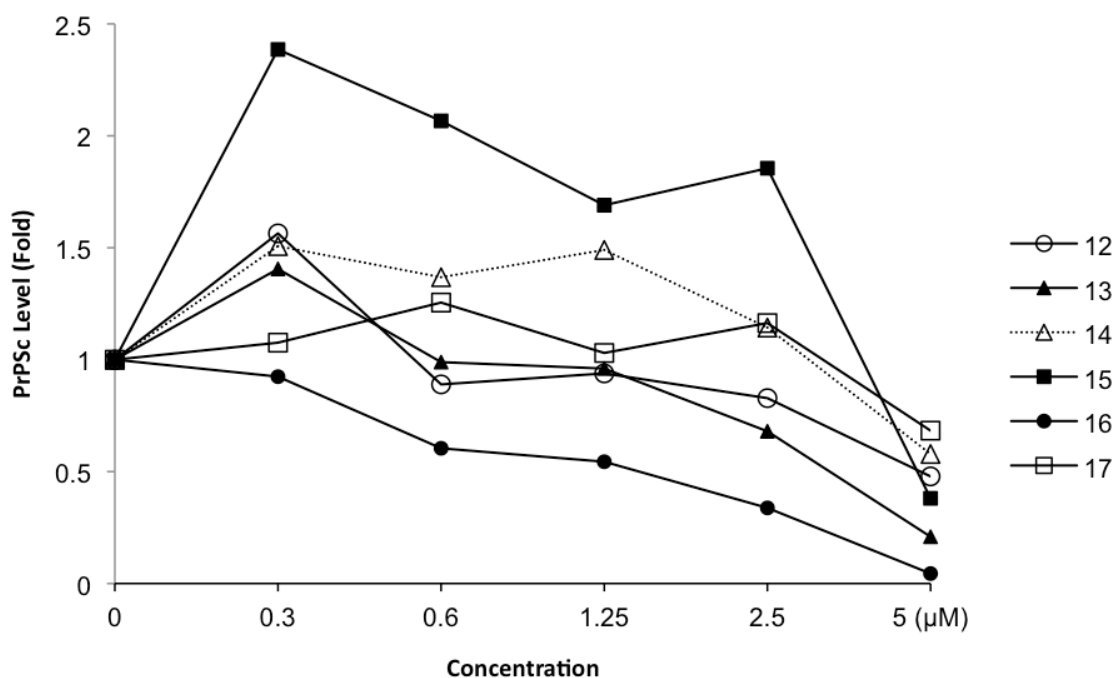


Chart 1.5 Densitometric analysis of Western blots from experiments of compounds **12-17** at various concentrations.⁵⁹ This is used to estimate the response of PrP^{Sc} propagation to various concentrations of N-(7-chloroquinolin-4-yl)-alkyl-diamines. When there is no treatment, the PrP^{Sc} level will be at 1. With complete clearance of PrP^{Sc}, PrP^{Sc} level will drop to 0. Increasing of the amount of PrP^{Sc} will result in the increase in PrP^{Sc} level in this chart. It shows that compound **16** is the most effective one in inhibiting the propagation of PrP^{Sc} under different concentrations.

Based on the outcome of the assays, the porphyrins **3** and **4** basically exhibited little anti-prion activity at all concentrations, with an exception of the compound **4** at 5 µM, where it shows slight inhibition by reducing 10% of PrP^{Sc} amount (**Figure 1.17** and **Chart 1.6**).

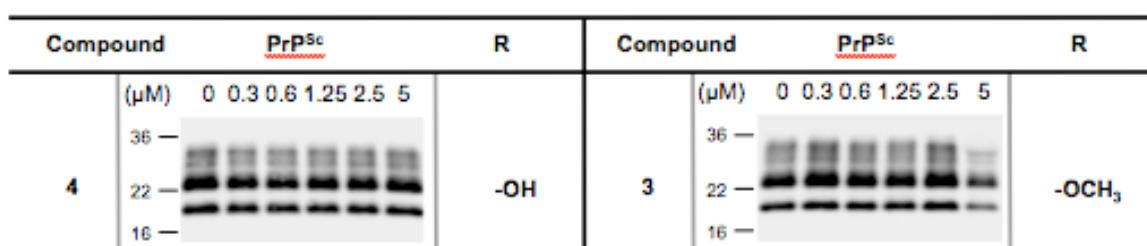
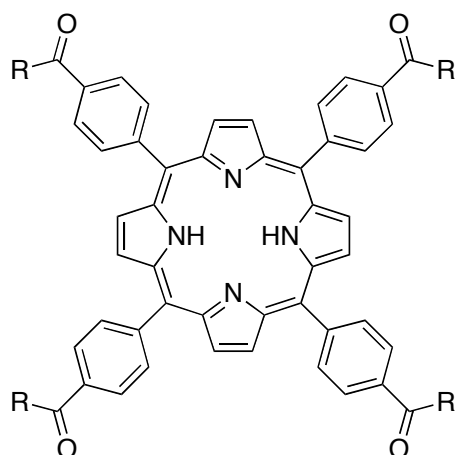


Figure 1.17 Antiprion activity of simple porphyrins 3-4.⁵⁹ Western blotting analysis of SMB cells was utilized to measure the anti-prion activity of the compounds at concentrations of 0, 0.3, 0.6, 1.25, 2.5, or 5 μ M, and the results show that both compounds are ineffective in inhibiting the propagation of PrP^{Sc}.

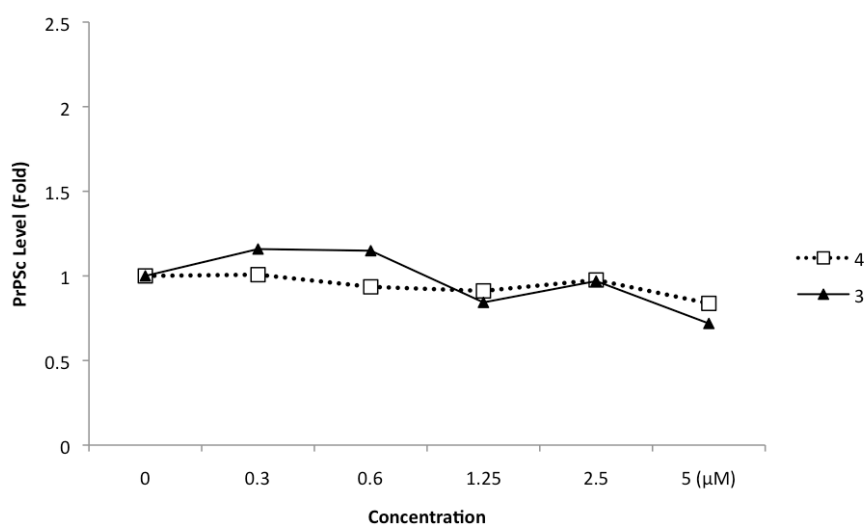
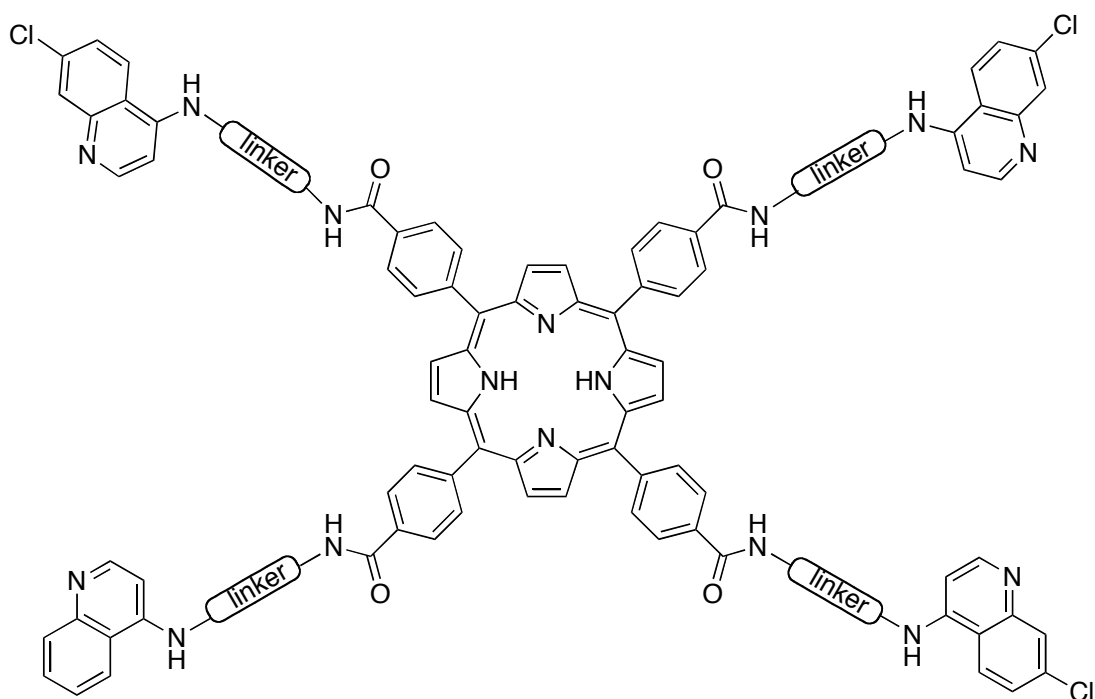


Chart 1.6 Densitometric analysis of Western blots from experiments of compounds 3, 4 at various concentrations.⁵⁹

1.6.2 Evaluation Results for Porphyrin-Based Multimeric Compounds 18-23 & Promising Results of Arene-Based Multimeric Compounds

Anti-prion assays of the porphyrin-based multimeric compounds showed that unfortunately no significant reduction in the levels of PrP^{Sc} was observed in most cases (**Figure 1.18** and **Chart 1.7**). Only compounds **22** and **23** show slight anti-prion activity by reducing the amount of PrP^{Sc} by less than 40% or 50% at high concentrations. In some cases, however, the amounts of PrP^{Sc} increase slightly or significantly when the SMB cells were treated with different concentrations of the six porphyrin-based multimeric products. This suggests that this type of macromolecules may play a role in *accelerating* the growth of PrP^{Sc} sometimes rather than inhibiting it, which is exactly the opposite of our expectation. Despite the presence of four units, these multimeric compounds were less effective than the simple monomeric quinoline diamine fragments in suppressing the formation of PrP^{Sc}. It may be that the extended porphyrin scaffold does not permit effective binding by all of the individual quinolines. Observation of *enhanced* production of PrP^{Sc} in one case also raises the possibility that two conflicting mechanisms may be largely cancelling each other out.



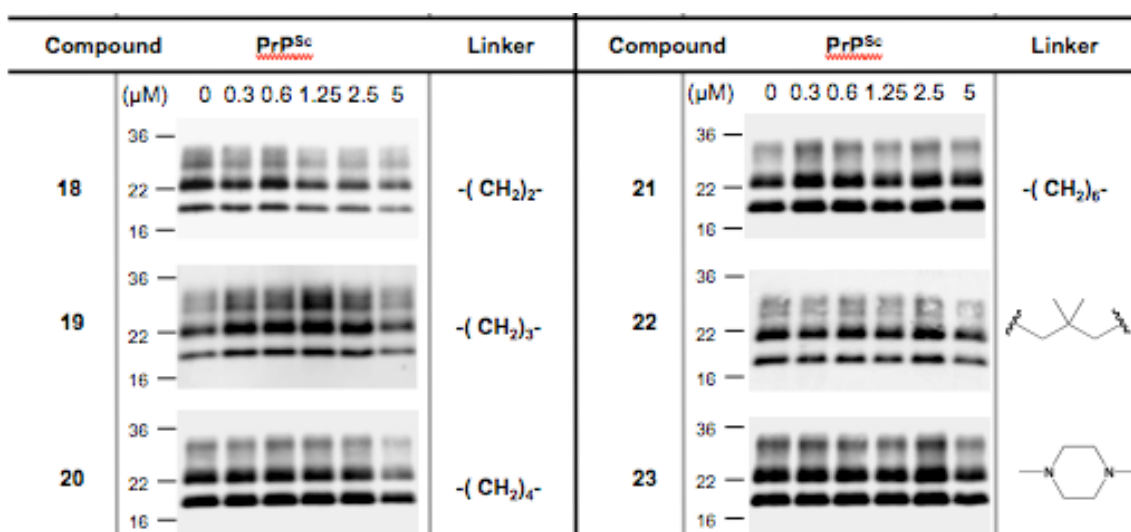


Figure 1.18 Antiprion activity of six porphyrin-based multimeric molecules **18-23**.⁵⁹ Western blotting analysis was utilized to measure the anti-prion activity of the compounds as listed, and the results show that none of them is very effective in inhibiting the propagation of PrP^{Sc}.

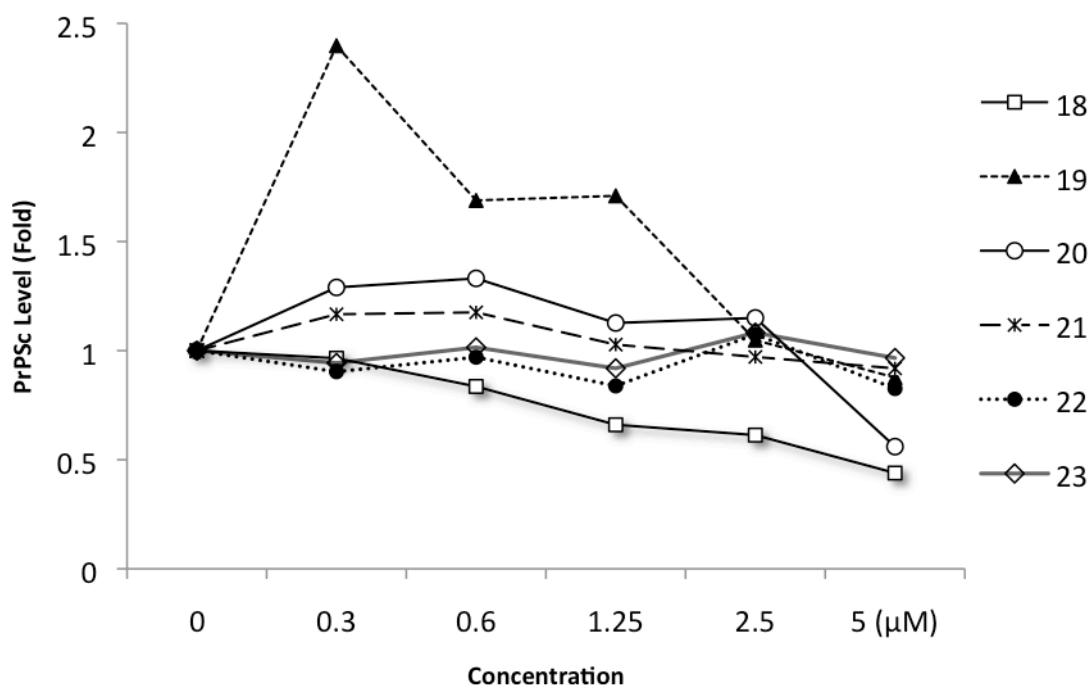


Chart 1.7 Densitometric analysis of Western blots from experiments of porphyrin-based multimeric compounds **18-23** at various concentrations.⁵⁹

The corresponding acridine-containing multimeric porphyrin compounds **30-32** and the acridine diamine building blocks **25-28** have not yet been subjected to the same assays as the quinoline series. However, the results described above suggest that these compounds will be unlikely to display favorable activity. Even though the porphyrin-based multimeric fluorescent compounds do not have significantly enhanced anti-prion activity, they still may have the potential application in diagnosis if they can bind effectively to the prion particles. Therefore, it is desirable to have the affinity test of these fluorescent compounds.

Although results for the six porphyrin-based tetrameric molecules are unexpected, the outcomes for smaller sized arene-based trimeric compounds are very interesting and promising (**Figure 1.19**). These molecules, prepared by Shaon Joy, show strong anti-prion activity *in vitro* and are very efficient in the clearance of PrP^{Sc} at concentrations of 1.25 μ M or greater. They show stronger anti-prion activity than quinacrine in the anti-prion assay, which is a drug under full clinical trial in the United Kingdom, the United States and Japan for the treatment of the human-based Creutzfeldt-Jakob disease.^{37, 60} Therefore, the results of arene-based compounds are very exciting and promising. Toxicity tests of both the porphyrin-based and arene-based multimeric compounds show that all these compounds are not toxic towards normal mouse brain cells at the concentration of 5 μ M or below, which are the concentrations used in the treatment.⁶¹

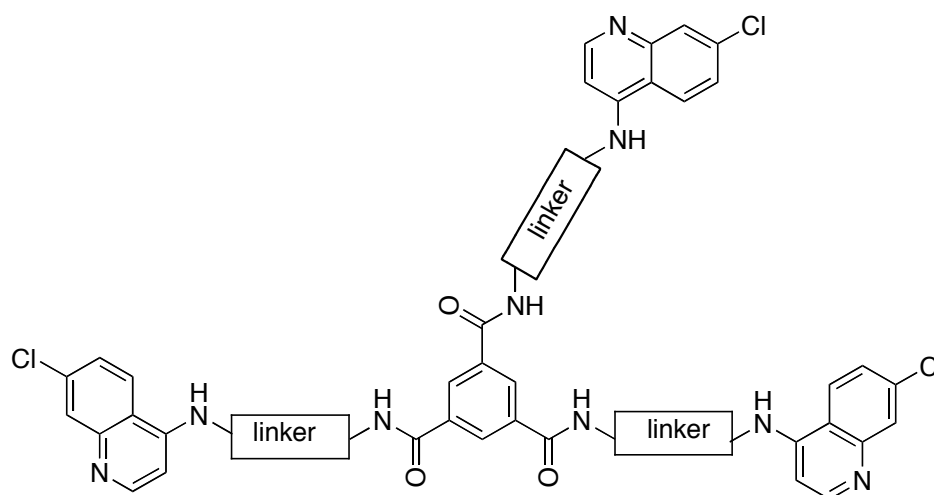


Figure 1.19 Structures of arene-based trimeric compounds prepared by Shaon Joy. Linker = $-\text{CH}_2\text{CH}_2-$, $-\text{CH}_2\text{CH}_2\text{CH}_2-$, or $-\text{CH}_2\text{C}(\text{CH}_3)_2\text{CH}_2-$.

Based on the experimental results, the size of the scaffold and the length of the linkers both play an important role in determining multimeric compounds' binding affinity towards PrP^{Sc}. It seems that compounds with small-sized scaffolds such as benzene rings are more effective than those with large porphyrin scaffolds, although the results of porphyrin-based multimeric compounds with acridine as the binding units have not been obtained yet. Compounds with a linker of 1,2-ethanediamine or 1,3-propanediamine in arene-based multimeric compounds show stronger affinity towards PrP^{Sc} than its analogues, which suggests that such linkers in arene-based compounds can better fix the space of aggregate of the PrP^{Sc} fibrils. Further study is still in progress.

(For further discussion of the conclusions and future directions of this research project, see **Chapter 3.**)

1.7 Experimental Details

1.7.1 General Information

Reactions were conducted in oven-dried (110 °C) or flame-dried glassware under a positive argon atmosphere unless otherwise noted. Transfer of anhydrous solvents, reagents or mixtures was accomplished with oven-dried syringes or *via* cannulae. Solvents were distilled before use: dichloromethane over calcium hydride; tetrahydrofuran and diethyl ether over sodium benzophenone ketyl; toluene over sodium metal. Thin layer chromatography (TLC) was performed on 0.25 mm thick precoated silica gel plates (Merck Fertigplatten Kieselgel 60F254). Flash chromatography columns were packed with 230-240 mesh silica gel.

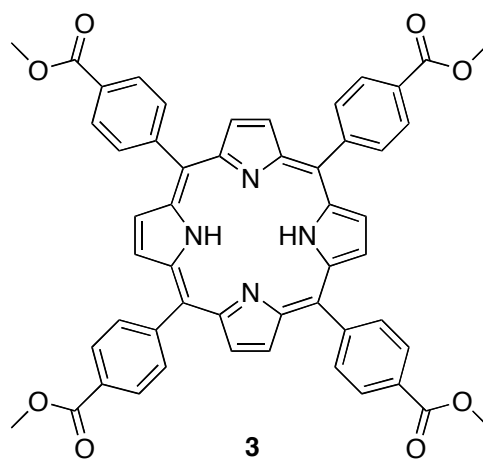
Proton nuclear magnetic resonance spectra (¹H NMR) were recorded at 300, 400 MHz or 500 MHz, and the chemical shifts are reported on the δ scale (ppm) relative to the tetramethylsilane (0 ppm). Coupling constants (*J*) are reported in Hz. Second order splitting patterns are indicated. Splitting patterns are designated as s, singlet; d, doublet; t,

triplet; q, quartet; m, multiplet; br, broad; dd, doublet of doublets, dt, doublet of triplets, etc. Carbon nuclear magnetic resonance spectra (^{13}C NMR) were recorded at 100 MHz or 125 MHz and are reported in ppm relative to the centerline of the triplet from deuteriochloroform at 77.23 ppm. Infrared (IR) spectra were measured with a Magna 750 FT-IR infrared spectrophotometer. Ultraviolet-visible (UV-Vis) absorption spectra were measured with a Hewlett Packard 8453 UV-VIS Spectrophotometer between 200-900 nm. Fluorescence analysis was carried on Photon Technology International (PTI) MP1 Fluorescence Syetem. Mass spectra were determined on a Agilent 6220 oaTOF electrospray positive ion mode spectrometer (ESI) or a Bruker Daltonics Apex-Qe FTICR MS high resolution MALDI spectrometer.

All reagents and catalysts were purchased from Aldrich or Sigma or Strem and were used without further purification unless otherwise stated.

1.7.2 Substrate Synthesis

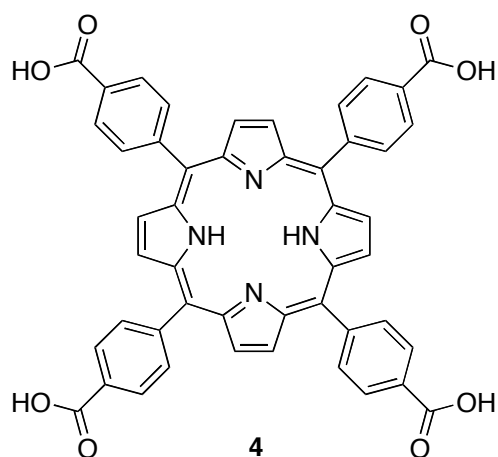
Preparation of *meso*-tetrakis [4-(methoxycarbonyl)phenyl]porphyrin **3**.



Freshly distilled pyrrole (694 μL , 10.0 mmol) was added to a solution of methyl-4-formyl-benzoate (1.64 g, 10.0 mmol) in 1.00 L dry dichloromethane in a 3 L 3-neck round-bottom flask, which had been purged with argon. The mixture was stirred for 5 minutes, and the reaction vessel was shielded with aluminum foil to avoid ambient

lighting. Trifluoroacetic acid (1.11 mL, 15.0 mmol) was added to the reaction mixture, and then $\text{BF}_3 \cdot \text{OEt}_2$ (37 μL , 0.30 mmol) was added. The reaction was stirred under argon for 2.5 h before *p*-chloranil (2.46 g, 10.0 mmol) was added to the solution. The flask was immersed into a preheated 45 °C water bath, and the solution was stirred at reflux for another 1 h. After cooling to room temperature, solvent was removed with a rotary evaporator. The crude product was purified via flash chromatography (silica gel, $\text{Et}_2\text{O}/\text{DCM}$ 1:19) to yield **3** (1.19 g, 56%) as purple solid: m.p. > 300 °C; $R_f = 0.53$ (1:19 $\text{Et}_2\text{O}/\text{DCM}$); IR (microscope) 3319, 3120, 2951, 2843, 1722 cm^{-1} ; UV-Vis absorbance peaks 229, 420, 451 nm; fluorescence analysis: when excited at 425 nm, wavelength of emission detected at 640, 715 nm; ^1H NMR (400 MHz, CDCl_3) δ 8.82 (s, 8H), 8.45 (d, $J = 8.1$ Hz, 8H), 8.30 (d, $J = 8.1$ Hz, 8H), 4.12 (s, 12H), -2.80 (s, 2H); ^{13}C NMR (125 MHz, CDCl_3) δ 167.2, 146.6, 134.5, 131.3, 129.8, 128.0, 119.4, 52.5 (1 sp^2 carbon missing); HRMS (ESI) calculated for $\text{C}_{52}\text{H}_{39}\text{O}_8\text{N}_4$ ($[\text{M} \cdot \text{H}]^+$) 847.2762, found 847.2759.

Preparation of *meso*-tetrakis[(4-carboxy)phenyl]porphyrin **4**.

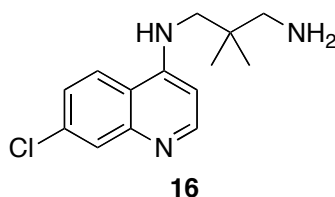


Compound **3** (166 mg, 0.20 mmol) was dissolved in 10 mL DCM, and the solution was added to a mixture of ethanol/water (1:1 v/v, 20 mL) containing NaOH (1.00 g, 25.0 mmol) in a 100 mL round-bottom flask. The mixture was stirred at reflux under argon at the temperature around 70 – 80 °C for 24 h. After cooling to room temperature, ethanol and DCM were removed with a rotary evaporator. 1N HCl was added dropwise to the aqueous

solution until no more green precipitate formed (pH = 1 by pH paper). The precipitate was collected by vacuum filtration and washed with DI water several times. The compound **4** was dried under high-pressure vacuum for 8 h to afford the desired compound (155 mg, quantitative yield) as a green powder: m.p. > 300 °C; IR (microscope) 3170, 3036, 1720, 1682, 1606 cm⁻¹; UV-Vis absorbance peaks 230, 415 nm; fluorescence analysis: when excited at 450 nm, wavelength of emission detected at 648, 715 nm; ¹H NMR (400 MHz, CDCl₃) δ 8.85 (s, 8H), 8.45 (d, *J* = 8.1 Hz, 8H), 8.30 (d, *J* = 8.1 Hz, 8H), -2.80 (s, 2H), (4 COOH protons missing); ¹³C NMR (125 MHz, CDCl₃) δ 167.4, 145.4, 134.5, 131.6, 130.5, 127.9, 119.3 (1 sp² carbon missing); HRMS (ESI) calculated for C₄₈H₂₇O₈N₄ ([M-H]⁻) 789.1991, found 789.1990; C₄₈H₂₇O₈N₄ ([M-2H]⁻²) 394.0959, found 394.0966.

One example for the direct coupling of 4,7-dichloroquinoline and diamines.

Preparation of N-(7-chloroquinolin-4-yl)-propane-2,2-dimethyl-1,3-diamine **16**.



4,7-Dichlororoquinoline (198 mg, 1.00 mmol) was mixed with propane-2,2-dimethyl-1,3-diamine (610 mg, 5.00 mmol) in a 10 mL round-bottom flask, and it was heated at 80 °C for 1 hour without stirring to make a paste. The temperature was then raised to 140 °C with stirring. After 12 hours, the reaction mixture was cooled to the room temperature, and a 1M NaOH solution (5 mL) was added to the solution. The organic product was extracted by EtOAc (5×10 mL), washed with DI water (2×5 mL) and dried over MgSO₄. Compound **16** was obtained by flash chromatography (15% MeOH/DCM) as a pale yellow solid (208 mg, 79%): m.p. 128-130 °C; R_f = 0.52 (20% MeOH/DCM); IR (DCM, cast film) 3474, 3315, 3081, 2958 cm⁻¹; ¹H NMR (400 MHz, CDCl₃) δ 8.48 (d, *J* = 5.6 Hz, 1H), 8.46 (br s, 1H), 7.91 (d, *J* = 2.1 Hz, 1H), 7.72 (d, *J* = 8.8 Hz, 1H), 7.29 (dd, *J* = 8.8, 2.1 Hz, 1H), 6.27 (d, *J* = 5.6 Hz, 1H), 3.18 (s, 2H), 2.87 (s, 2H), 1.56 (br s, 2H), 1.08

(s, 6H); ^{13}C NMR (125 MHz, *d*-DMSO) δ 151.9, 150.8, 149.1, 133.3, 127.5, 124.0, 123.9, 117.4, 98.6, 37.5, 35.6, 24.6, 24.4; HRMS (ESI) calculated for $\text{C}_{14}\text{H}_{19}\text{ClN}_3$ ($[\text{M}\cdot\text{H}]^+$) 264.1262, found 264.1259.

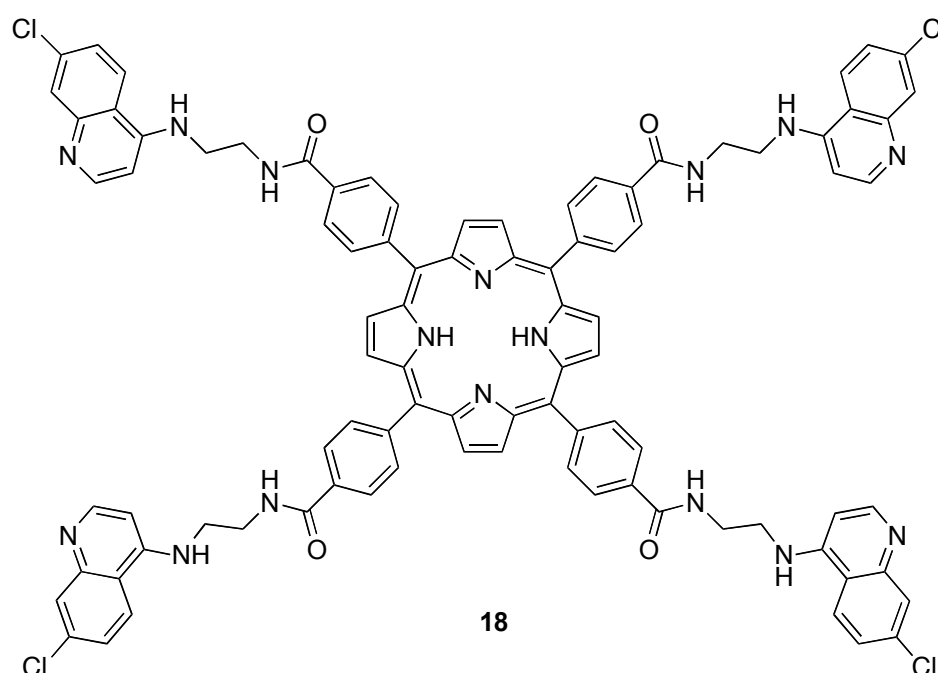
The preparation of other N-(7-chloroquinolin-4-yl)-alkyl diamine compounds **12-15** and **17** were carried out by following the literature procedures (the same as described above), which are reported compounds in the supplementary information of the literature.⁵²

Reactions for the amide bond formation.

Representative Example:

Preparation of

meso-tetrakis[(N-(7-chloroquinolin-4-yl)-ethane-1,2-diaminecarbonyl)phenyl]porphyrin **18**.

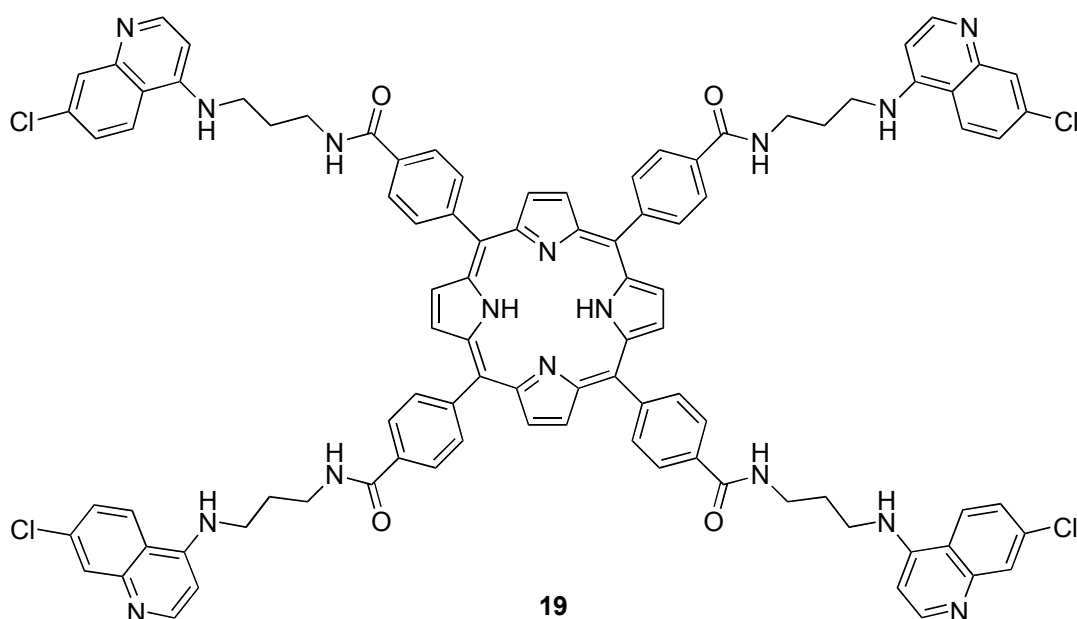


A mixture of compound **4** (29.5 mg, 0.0373 mmol), compound **12** (41.2 mg, 0.186 mmol), HOBt (25.2 mg, 0.186 mmol), and EDC (35.8 mg, 0.186 mmol) in DMF (2 mL) in a 10 mL round-bottom flask was stirred at room temperature under argon atmosphere for 40 h. After

the reaction was complete, the solution in the round-bottom flask was transferred to a 25 ml test tube by a pipet. Et₂O (20 mL) was added to the test tube to dilute DMF solution, and dark red precipitate formed. The mixed solvent was removed by pipet carefully, and the residue in the test tube was washed successively with DI water, DCM, acetone and MeOH several times. The solid was dried under high-pressure vacuum for 8 h to afford the desired compound **18** (49.0 mg, 82%) as a dark red solid: m.p. > 300 °C; IR (microscope) 3308, 3059, 2940, 1930, 1815, 1628, 1606, 1577, 1539 cm⁻¹; UV-Vis absorbance peaks 220, 253, 331, 416 nm; fluorescence analysis: when excited at 425 nm, wavelength of emission detected at 648, 715 nm; ¹H NMR (400 MHz, *d*-DMSO) δ 9.13 (t, *J* = 5.6 Hz, 4H), 8.84 (s, 8H), 8.47 (d, *J* = 5.2 Hz, 4H), 8.31 (m, 16H), 8.29 (d, *J* = 8.8 Hz, 4H), 7.81 (d, *J* = 2.2 Hz, 4H), 7.62 (t, *J* = 5.2 Hz, 4H), 7.49 (dd, *J* = 8.8, 2.2 Hz, 4H), 6.73 (d, *J* = 5.2 Hz, 4H), 3.72 (td, *J* = 9.2, 5.2 Hz, 8H), 3.61 (td, *J* = 9.2, 5.2 Hz, 8H), -2.93 (s, 2H); ¹³C NMR (125 MHz, *d*-DMSO) δ 166.7, 152.5, 148.3, 144.7, 143.9, 135.3, 134.1, 133.8, 131.6, 125.8, 125.3, 124.7, 124.1, 119.4, 116.7, 98.7, 42.5, 38.0 (1 sp² carbon missing); HRMS (MALDI) calculated for C₉₂H₇₁Cl₄N₁₆O₄ ([M•H]⁺) 1603.4593, found 1603.4604.

Preparation of

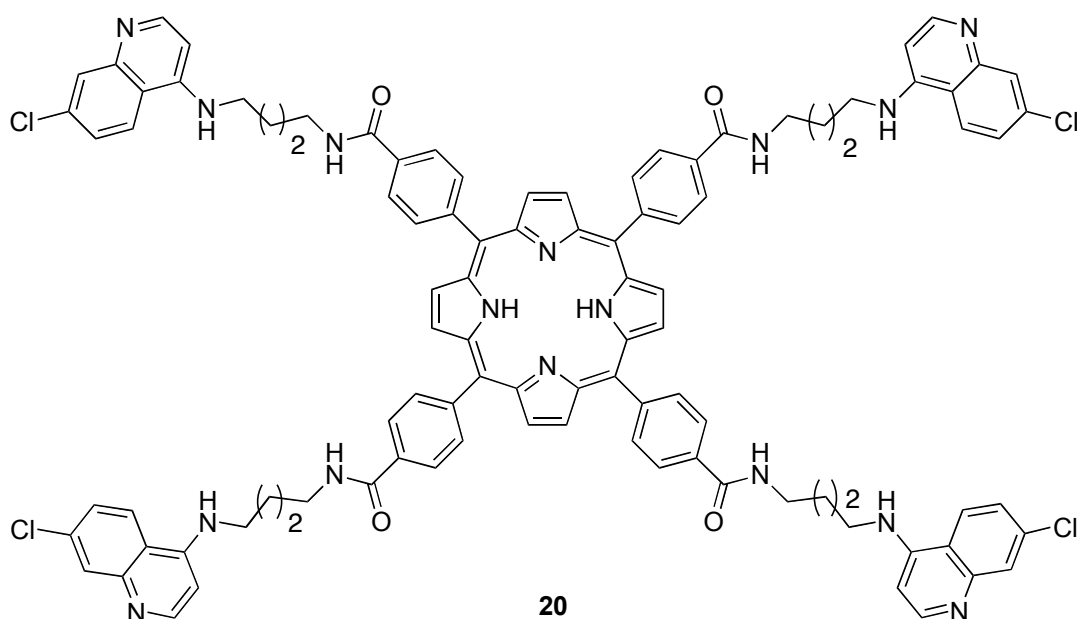
***meso*-tetrakis[(*N*-(7-chloroquinolin-4-yl)-propane-1,3-diaminecarbonyl)phenyl]porphyrin **19**.**



The procedure described above in the synthesis and purification of compound **18** was applied in this example to give **19** (92 mg, 70 %) as a dark red solid: m.p. > 300 °C; IR (microscope) 3315, 3066, 2936, 1928, 1810, 1633, 1610, 1581, 1547, 1500 cm⁻¹; UV-Vis absorbance peaks 217, 253, 330, 416 nm; fluorescence analysis: when excited at 425 nm, wavelength of emission detected at 648, 715 nm; ¹H NMR (400 MHz, *d*-DMSO) δ 8.96 (t, *J* = 5.6 Hz, 4H), 8.84 (s, 8H), 8.48 (d, *J* = 5.8 Hz, 4H), 8.41 (d, *J* = 9.0 Hz, 4H), 8.30 (m, 16H), 7.94 (t, *J* = 5.1 Hz, 4H), 7.84 (d, *J* = 1.5 Hz, 4H), 7.56 (dd, *J* = 9.0, 1.5 Hz, 4H), 6.68 (d, *J* = 5.8 Hz, 4H), 3.57 (td, *J* = 8.8, 5.6 Hz, 8H), 3.47 (td, *J* = 8.8, 5.6 Hz, 8H), 2.01 (m, 8H), -2.93 (s, 2H); ¹³C NMR (125 MHz, *d*-DMSO) δ 166.3, 152.5, 147.8, 144.2, 143.8, 135.5, 134.1, 134.0, 131.3, 125.8, 125.3, 124.8, 123.6, 119.4, 116.6, 98.7, 40.6, 37.3, 27.7 (1 sp² carbon missing); HRMS (MALDI) calculated for C₉₆H₇₉Cl₄N₁₆O₄ ([M•H]⁺) 1659.5219, found 1659.5201.

Preparation of

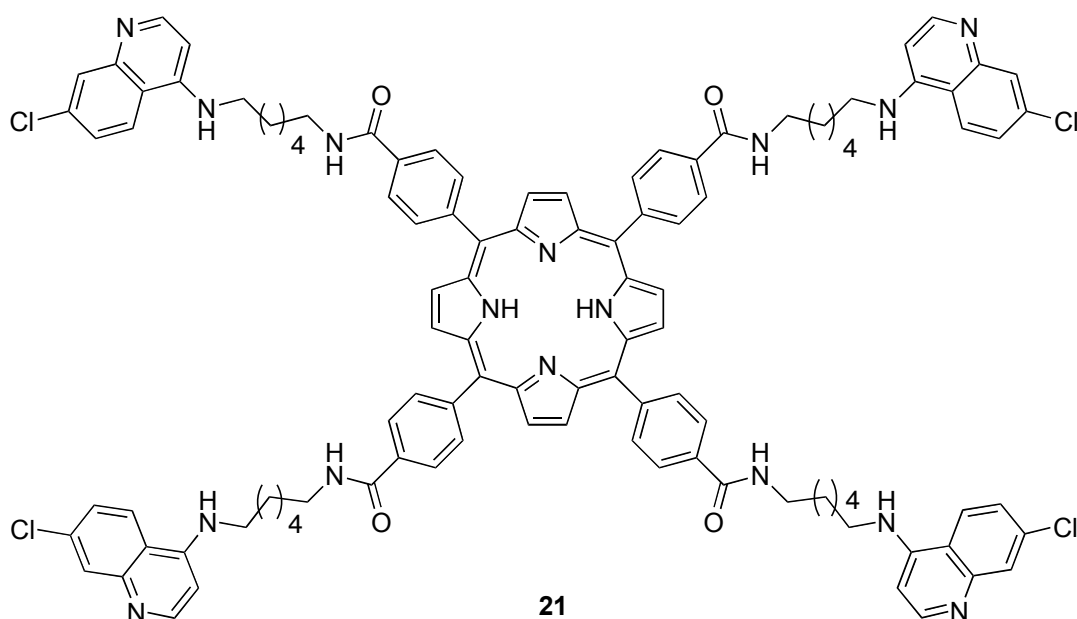
meso-tetrakis[(N-(7-chloroquinolin-4-yl)-butane-1,4-diaminecarbonyl)phenyl]porphyrin **20.**



The procedure described in the synthesis and purification of compound **18** was applied in this example to give **20** (77 mg, 70 %) as a dark red solid: m.p. > 300 °C; IR (microscope) 3312, 3062, 2941, 2867, 1716, 1628, 1605, 1576, 1531 cm⁻¹; UV-Vis absorbance peaks 219, 253, 331, 416 nm; fluorescence analysis: when excited at 400 nm, wavelength of emission detected at 648, 715 nm; ¹H NMR (400 MHz, *d*-DMSO) δ 8.85 (t, *J* = 5.6 Hz, 4H), 8.83 (s, 8H), 8.41 (d, *J* = 5.6 Hz, 4H), 8.32 (d, *J* = 8.8 Hz, 4H), 8.28 (m, 16H), 7.77 (s, 4H), 7.45 (d, *J* = 8.8 Hz, 4H), 6.56 (d, *J* = 5.2 Hz, 4H), 3.50 (*J* = 9.2, 5.2 Hz, 8H), 1.40 (td, *J* = 9.2, 5.2 Hz, 8H), 1.80 (m, 16H), -2.94 (s, 2H); ¹³C NMR (125 MHz, *d*-DMSO) δ 166.1, 152.6, 147.5, 144.0, 143.7, 135.5, 134.2, 134.1, 131.1, 125.8, 125.2, 124.9, 123.4, 119.4, 116.5, 98.6, 42.5, 26.8, 25.5, 25.2 (1 sp² carbon missing); HRMS (MALDI) calculated for C₁₀₀H₈₇Cl₄N₁₆O₄ ([M•H]⁺) 1715.5845, found 1715.5860.

Preparation of

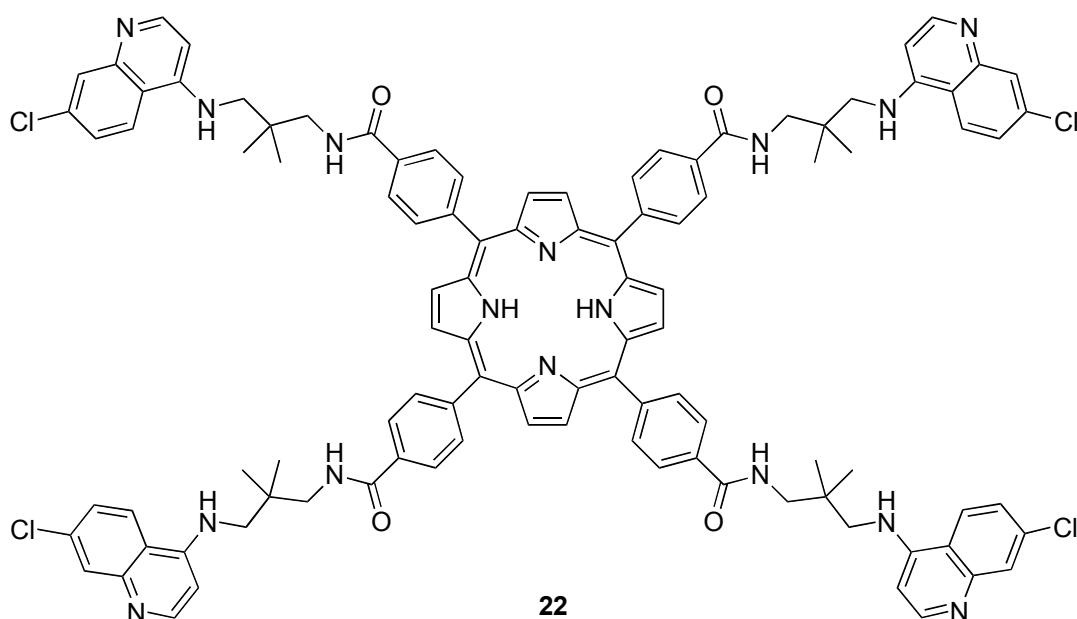
***meso*-tetrakis[*N*-(7-chloroquinolin-4-yl)-hexane-1,6-diaminecarbonyl]phenyl]porphyrin **21**.**



The procedure described in the synthesis and purification of compound **18** was applied in this example to give **21** (130 mg, 61 %) as a dark red solid: m.p. > 300 °C; IR (microscope) 3258, 3027, 2933, 2859, 1943, 1631, 1612, 1551 cm⁻¹; UV-Vis absorbance peaks 254, 330, 416 nm; fluorescence analysis: when excited at 425 nm, wavelength of emission detected at 648, 715 nm; ¹H NMR (400 MHz, *d*-DMSO) δ 8.86 (t, *J* = 5.6 Hz, 4H), 8.84 (s, 8H), 8.45 (d, *J* = 9.2 Hz, 4H), 8.43 (d, *J* = 6.4 Hz, 4H), 8.28 (m, 20H), 7.85 (d, *J* = 2.0 Hz, 4H), 7.55 (dd, *J* = 9.2, 2.0 Hz, 4H), 6.64 (d, *J* = 6.0 Hz, 4H), 3.41 (m, 16H), 1.73 (m, 8H), 1.67 (m, 8H), 1.47 (m, 16H), -2.95 (s, 2H); ¹³C NMR (125 MHz, *d*-DMSO) δ 166.1, 153.9, 145.0, 143.7, 141.3, 136.6, 134.3, 134.1, 131.4, 125.8, 125.4, 121.1, 119.4, 115.9, 98.5, 42.9, 30.6, 29.1, 27.6, 26.3, 26.2 (2 sp² carbons missing); HRMS (MALDI) calculated for C₁₀₈H₁₀₃Cl₄N₁₆O₄ ([M•H]⁺) 1827.7097, found 1827.7116.

Preparation of

***meso*-tetrakis[(*N*-(7-chloroquinolin-4-yl)-propane-2,2-dimethyl-1,3-diaminecarbonyl)phenyl]porphyrin **22**.**

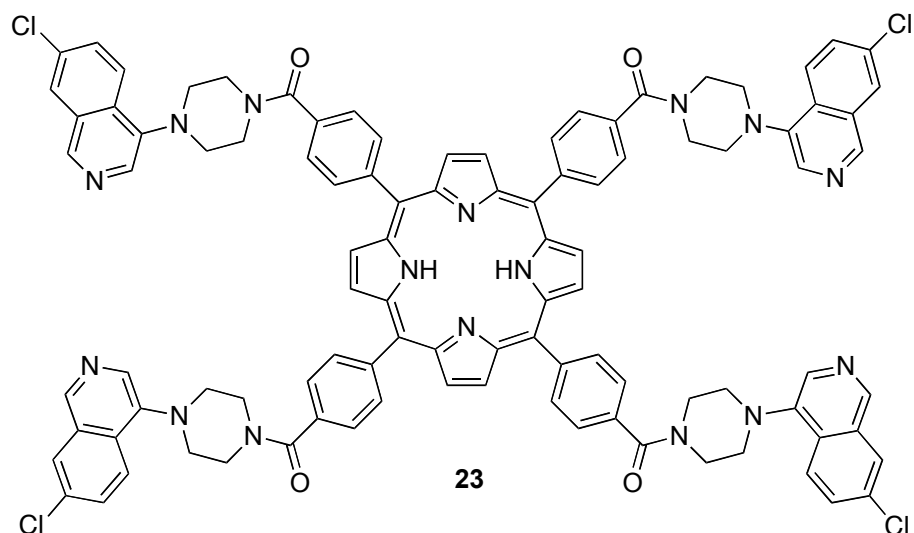


The procedure described in the synthesis and purification of compound **18** was applied in this example to give **22** (5 mg, 65 %) as a dark red solid: m.p. > 300 °C; IR (microscope) 3257, 3064, 2960, 2872, 1610, 1582, 1549, 1500 cm⁻¹; UV-Vis absorbance peaks 219, 254, 333, 416 nm; fluorescence analysis: when excited at 440 nm, wavelength of emission detected at 650, 715 nm; ¹H NMR (300 MHz, *d*-DMSO) δ 9.18 (t, *J* = 6.0 Hz, 4H), 8.88 (s, 8H), 8.50 (d, *J* = 8.1 Hz, 4H), 8.47 (d, *J* = 5.2 Hz, 4H), 8.37 (m, 16H), 8.22 (t, *J* = 6.0 Hz, 4H), 7.91 (dd, *J* = 8.4, 1.5 Hz, 4H), 7.88 (d, *J* = 1.5 Hz, 4H), 6.90 (d, *J* = 6.0 Hz, 4H), 3.52 (m, 8H), 3.47 (m, 8H), 1.11 (m, 24H), -2.90 (s, 2H); ¹³C NMR (125 MHz, *d*-DMSO) δ 167.9, 152.1, 149.8, 149.7, 144.0, 134.5, 134.1, 134.0, 133.9, 126.1, 125.7, 124.9, 123.9, 119.4, 116.9, 98.9, 49.1, 47.0, 23.7, 23.6 (1 sp² carbon missing); HRMS (MALDI) calculated for C₁₀₄H₉₅Cl₄N₁₆O₄ ([M•H]⁺) 1771.6471, found 1771.6486.

Preparation of

***meso*-tetrakis[(N-(7-chloroquinolin-4-yl)-1,4-piperazinecarbonyl)phenyl]porphyrin**

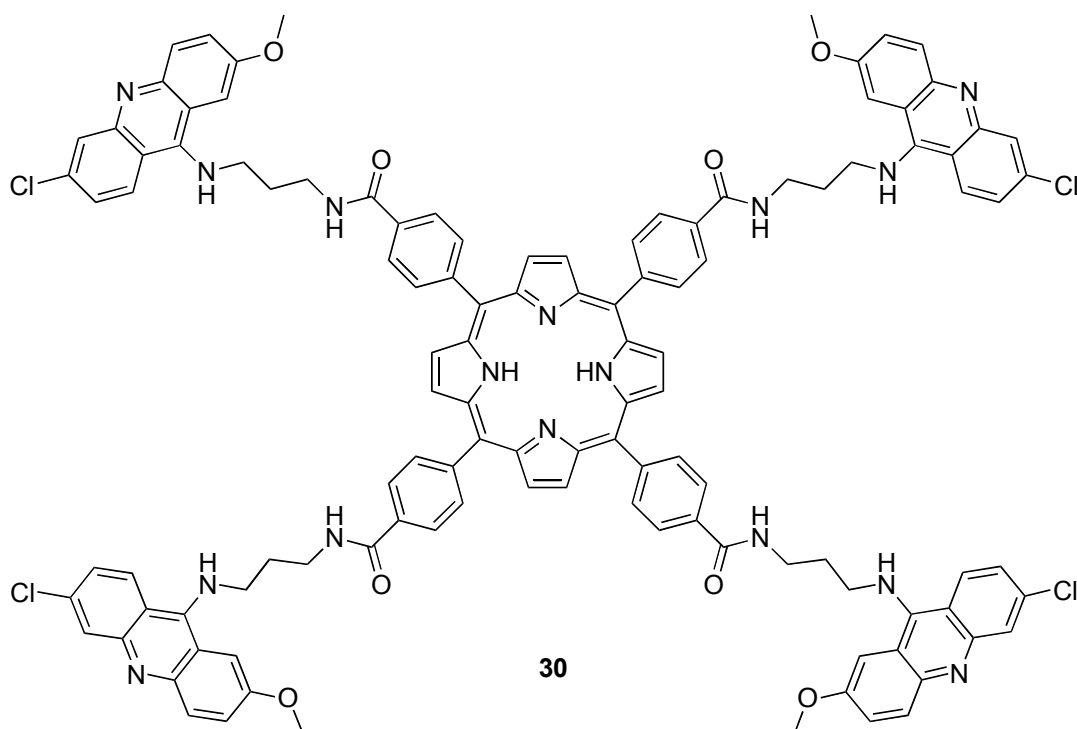
23.



The procedure described in the synthesis and purification of compound **18** was applied in this example to give **23** (15 mg, 79 %) as a dark red solid: m.p. > 300 °C; IR (microscope) 3318, 3030, 2893, 2822, 2095, 1636, 1577 cm⁻¹; UV-Vis absorbance peaks 226, 355, 415 nm; fluorescence analysis: when excited at 425 nm, wavelength of emission detected at 648, 715 nm; ¹H NMR (300 MHz, *d*-DMSO) δ 8.93 (s, 8H), 8.78 (d, *J* = 6.6 Hz, 4H), 8.35 (d, *J* = 7.8 Hz, 8H), 8.30 (d, *J* = 9.6 Hz, 4H), 8.07 (s, 4H), 7.96 (d, *J* = 7.8 Hz, 8H), 7.71 (d, *J* = 9.6 Hz, 4H), 7.24 (d, *J* = 6.6 Hz, 4H), 4.08 (m, 16H), 3.86 (m, 16H), -2.89 (s, 2H); ¹³C NMR (125 MHz, *d*-DMSO) δ 169.1, 156.0, 152.2, 149.6, 142.3, 135.4, 134.3, 134.1, 133.7, 128.1, 126.1, 125.9, 125.8, 121.4, 119.4, 109.8, 51.9, 51.7 (1 sp² carbon missing); HRMS (MALDI) calculated for C₁₀₀H₇₉Cl₄N₁₆O₄ ([M•H]⁺) 1707.5219, found 1707.5216.

Preparation of

***meso*-tetrakis[(N-(6-chloro-2-methoxyacridin-9-yl)propane-1,3-diaminecarbonyl)phenyl]porphyrin 30.**

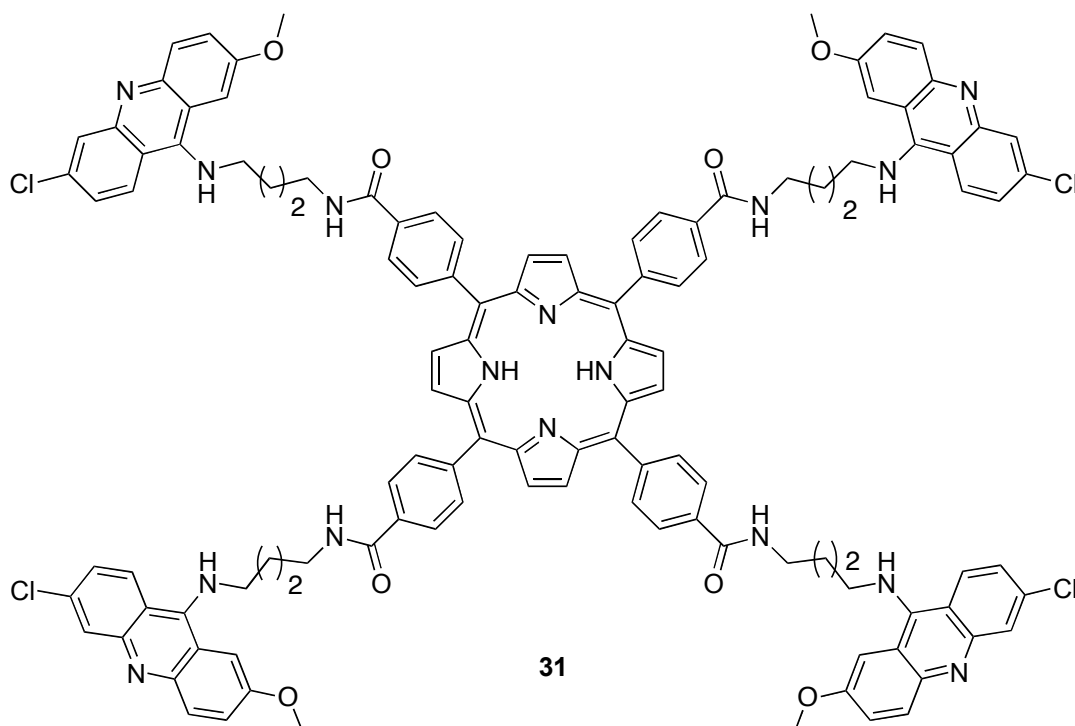


The procedure described in the synthesis and purification of compound **18** was applied in this example to give **30** (30 mg, 75 %) as a dark red solid: m.p. > 300 °C; IR (microscope) 3246, 3039, 2937, 2833, 1630, 1606, 1587, 1560 cm⁻¹; UV-Vis absorbance peaks 268, 342, 416 nm; Fluorescence analysis: when excited at 430 nm, wavelength detected at 480, 650, 720 nm; ¹H NMR (500 MHz, CDCl₃) δ 9.01 (s, 4H), 8.84 (s, 8H), 8.56 (d, *J* = 8.1 Hz, 4H), 8.28 (d, *J* = 8.1 Hz, 8H), 8.20 (d, *J* = 8.1 Hz, 8H), 8.12 (s, 4H), 7.98 (s, 4H), 7.90 (s, 4H), 7.85 (d, *J* = 8.1 Hz, 4H), 7.63 (d, *J* = 8.1 Hz, 4H), 7.47 (d, *J* = 8.1 Hz, 4H); 4.20 (br s, 8H), 4.01 (s, 12H), 3.57 (d, *J* = 5.5 Hz, 8H), 2.25 (br s, 8H), -2.93 (s, 2H); ¹³C NMR (125 MHz, *d*-DMSO) δ 166.2, 155.7, 143.8, 134.1, 133.7, 128.5, 126.6, 125.7, 123.0, 119.4, 56.2, 46.6, 36.8, 29.5 (11 sp² carbons missing); HRMS (MALDI) calculated for C₁₁₆H₉₅Cl₄N₁₆O₈ ([M•H]⁺) 1979.6267, found 1979.6266. HRMS (ESI) calculated for C₁₁₆H₉₈Cl₄N₁₆O₈ ([M•4H]⁴⁺) 495.6621, found 495.6625; calculated for C₁₁₆H₉₇Cl₄N₁₆O₈ ([M•3H]³⁺) 660.5471, found 660.5480; calculated for C₁₁₆H₉₆Cl₄N₁₆O₈ ([M•2H]²⁺) 990.3170, found 990.3161.

Preparation of

***meso*-tetrakis[*N*-(6-chloro-2-methoxyacridin-9-yl)-butane-1,4-diaminecarbonyl]phen**

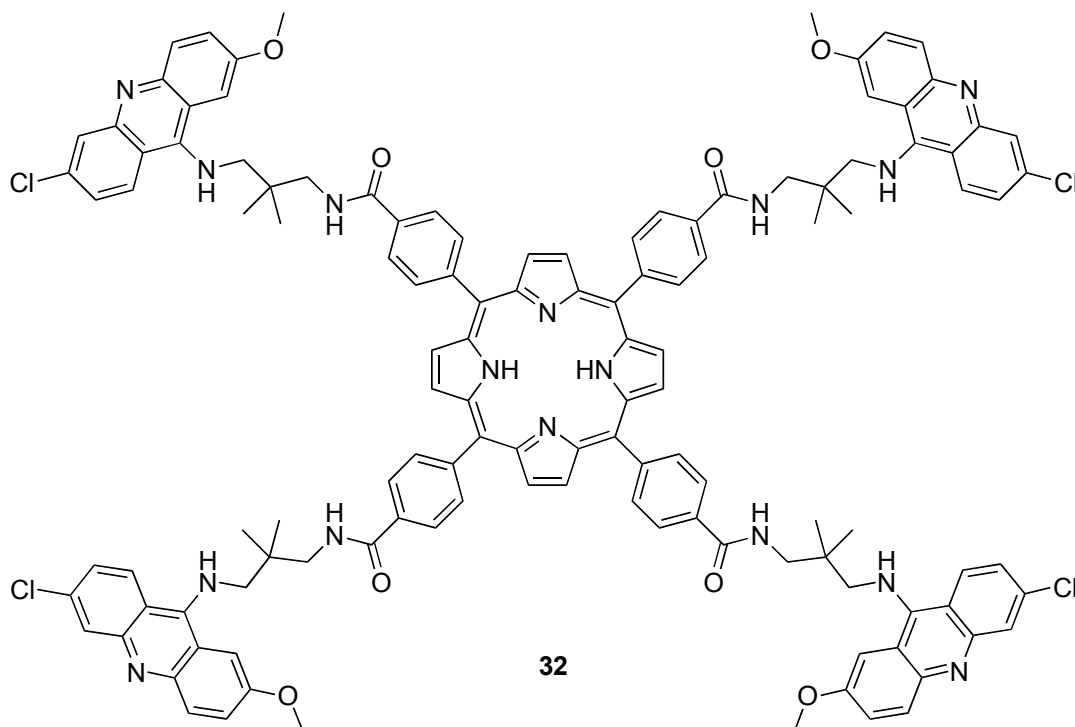
yl]porphyrin **31**.



The procedure described in the synthesis and purification of compound **18** was applied in this example to give **31** (23 mg, 57 %) as a dark red solid: m.p. > 300 °C; IR (microscope) 3242, 3030, 2936, 2869, 1629, 1586, 1561 cm^{-1} ; UV-Vis absorbance peaks 223, 275, 344, 416 nm; Fluorescence analysis: when excited at 430 nm, wavelength detected at 480, 648, 725 nm; ^1H NMR (500 MHz, CDCl_3) δ 8.88 (s, 4H), 8.83 (s, 8H), 8.57 (d, $J = 8.7$ Hz, 4H), 8.29 (d, $J = 8.0$ Hz, 8H), 8.24 (d, $J = 7.8$ Hz, 8H), 7.98 (s, 4H), 7.90 (s, 4H), 7.85 (d, $J = 9.1$ Hz, 4H), 7.65 (d, $J = 8.5$ Hz, 4H), 7.53 (d, $J = 8.5$ Hz, 4H), 7.32 (s, 4H), 4.19 (br s, 8H), 3.99 (s, 12H), 3.48 (d, $J = 5.5$ Hz, 8H), 2.05 (d, $J = 6.1$ Hz, 8H), 1.79 (t, $J = 6.9$ Hz, 8H), -2.93 (s, 2H); ^{13}C NMR (125 MHz, d -DMSO) δ 166.2, 155.8, 143.7, 138.7, 134.1, 127.0, 126.7, 125.8, 123.2, 120.8, 119.4, 117.5, 56.3, 48.4, 47.4, 26.6, 26.5 (9 sp^2 carbons missing); HRMS (ESI) calculated for $\text{C}_{120}\text{H}_{106}\text{Cl}_4\text{N}_{16}\text{O}_8$ ($[\text{M}\cdot 4\text{H}]^{4+}$) 509.6778, found 509.6783; calculated for $\text{C}_{120}\text{H}_{105}\text{Cl}_4\text{N}_{16}\text{O}_8$ ($[\text{M}\cdot 3\text{H}]^{3+}$) 679.2346, found 679.2348; calculated for $\text{C}_{120}\text{H}_{104}\text{Cl}_4\text{N}_{16}\text{O}_8$ ($[\text{M}\cdot 2\text{H}]^{2+}$) 1018.3483, found 1018.3467.

Preparation of

meso-tetrakis[(*N*-(6-chloro-2-methoxyacridin-9-yl)-propane-2,2-dimethyl-1,3-diamine carbonyl)phenyl]porphyrin **32**.



The procedure described in the synthesis and purification of compound **18** was applied in this example to give **32** (28 mg, 54 %) as a dark red solid: m.p. > 300 °C; IR (microscope) 3236, 3066, 2960, 2930, 2873, 1626, 1607, 1578, 1548 cm⁻¹; UV-Vis absorbance peaks 227, 282, 346, 417 nm; Fluorescence analysis: when excited at 430 nm, wavelength detected at 485, 652, 720 nm; ¹H NMR (500 MHz, CDCl₃) δ 9.42 (s, 4H), 8.88 (s, 8H), 8.65 (d, *J* = 6.6 Hz, 4H), 8.37 (br s, 16H), 8.23 (s, 4H), 8.06 (s, 4H), 7.95 (s, 4H), 7.92 (d, *J* = 9.3 Hz, 4H), 7.69 (d, *J* = 7.6 Hz, 4H), 7.55 (d, *J* = 7.2 Hz, 4H), 4.09 (s, 12H), 4.01 (br s, 8H), 3.49 (br s, 8H), 1.04 (s, 24H), -2.91 (s, 2H); ¹³C NMR (125 MHz, *d*-DMSO) δ 168.1, 160.0, 144.3, 140.9, 138.1, 135.7, 134.0, 133.1, 131.3, 128.1, 126.9, 123.3, 121.8, 119.3, 119.0, 118.5, 114.8, 110.5, 102.5, 56.1, 54.5, 48.6, 46.6, 23.8 (2 sp² carbons missing); HRMS (ESI) calculated for C₁₂₄H₁₁₅Cl₄N₁₆O₈ ([M•5H]⁵⁺) 419.1562, found 419.1567; C₁₂₄H₁₁₄Cl₄N₁₆O₈ ([M•4H]⁴⁺) 523.6934, found 523.6935; C₁₂₄H₁₁₃Cl₄N₁₆O₈ ([M•3H]³⁺) 697.9222, found 697.9212; C₁₂₄H₁₁₂Cl₄N₁₆O₈ ([M•2H]²⁺) 1046.3796, found 1046.3791.

1.8 References and Notes

1. (a) Watts, J.; Westaway, D., *Biochim. Biophys. Acta* **2007**, *1772*, 654-672; (b) Ronga, L.; Palladino, P.; Costantini, S.; Facchiano, A.; Ruvo, M.; Benedetti, E.; Ragone, R.; Rossi, F., *Curr. Protein and Pept. Sci.* **2007**, *8*, 83-90; (c) Aguzzi, A.; Calella, A. M., *Physiol. Rev.* **2009**, *89*, 1105-1152; (d) Vilette, D., *Vet. Res.* **2008**, *39*, 10-28.
2. Brown, D., The 'recipe for disaster' that killed 80 and left a £5bn bill. *The Daily Telegraph*, June 19, 2001.
3. Aguzzi, A., *Proc. Natl. Acad. Sci. USA* **2008**, *105*, 11-12.
4. (a) Simpson, J.; Weiner, E., In *Oxford English Dictionary*, 2nd ed.; Oxford University Press: Oxford, 1989; (b) DeArmond, S. J.; Bouzamondo, E., *Toxicology* **2002**, *2002*, 9-16.
5. Prusiner, S. B., *Proc. Natl. Acad. Sci. USA* **1998**, *95*, 13363-13383.
6. "The Nobel Prize in Physiology or Medicine 1997". Nobelprize.org. http://www.nobelprize.org/nobel_prizes/medicine/laureates/1997/NobelPrize. (last accessed Sep. 29, 2011).
7. Ryan, K. J.; Ray, C. G., In *Sherris Medical Microbiology* 4th ed.; McGraw Hill: 2004, pp. 624-628.
8. Priola, S. A.; Chesebro, B.; Caughey, B., *Science* **2003**, *300*, 917-919.
9. Pan, K.-M.; Baldwin, M.; Nguyen, J.; Gasset, M.; Serban, A.; Groth, D.; Mehlhorn, I.; Huang, Z.; Fletterick, R. J.; Cohen, F. E.; Prusiner, S. B., *Proc. Natl. Acad. Sci. USA* **1993**, *90*, 10962-10966.
10. (a) Becker, G. S., "Bovine Spongiform Encephalopathy and Canadian Beef Imports." CRS Report for Congress. March 11, 2005; (b) McNeil, D. G., Case of Mad Cow in Texas Is First to Originate in U.S. *New York Times*, June 30, 2005.
11. Ramasamy, I.; Law, M.; Collins, S.; Brook, F., *Lancet Infect. Dis.* **2003**, *3*, 214-222.
12. Jones, M.; Peden, A.; Prowse, C., *J. Pathol.* **2007**, *213*, 21-26.
13. Variant Creutzfeldt-Jakob Disease, Current Data (October 2009), The National Creutzfeldt-Jakob Disease Surveillance Unit (NCJDSU), University of Edinburgh. 2009.
14. Ironside, J. W., *Haemophilia* **2006**, *12*, 8-15.
15. (a) Collins, S.; McLean, C.; Masters, C., *J. Clin. Neurosci.* **2001**, *8*, 387-397; (b) Niimi,

- Y.; Iwasaki, Y.; Umemura, T.; , *Neuropathology* **2008**, *28* 645–651.
16. Goldmann, W., *Vet. Res.* **2008**, *39*, 30.
17. Belay, E. D., *Annu. Rev. Microbiol.* **1999**, *53*, 283-314.
18. Collinge, J., *Annu. Rev. Neurosci.* **2001**, *24*, 519-550.
19. Microscopic image of tissue section from Animal and Plant Health Inspection Service (APHIS), United States, Department of Agriculture (USDA).
20. Cohen, F. E.; Pan, K.-M.; Huang, Z.; Baldwin, M.; Fletterick, R. J.; Prusiner, S. B., *Science* **1994**, *264*, 530-531.
21. (a) Bamborouph, P.; Wille, H.; Telling, G. C.; Yehiely, F.; Prusiner, S. B.; Cohen, F. E., *Cold Spring Harb. Symp. Quant. Biol.*, 1996; Vol. 61, pp 495-509; (b) Tanaka, M.; Collins, S.; Toyama, B.; Weissman, J., *Nature* **2006**, *442*, 585-589; (c) Dobson, C., *Philos. Trans. R. Soc. Lond. B Biol. Sci.* **2001**, *356*, 133-145.
22. Brown, P.; Preece, M.; Brandel, J.; Sato, T.; McShane, L.; Zerr, I.; Fletcher, A.; Will, R.; Pocchiari, M.; Cashman, N.; d'Aignaux, J.; Cervenakova, L.; Fradkin, J.; Schonberger, L.; Collins, S., *Neurology* **2000**, *55*, 1075-1081.
23. Geissen, M.; Krasemann, S.; Matschke, J.; Glatzel, M., *Vaccine* **2007**, *25*, 5631-5636.
24. Li, J.; Browning, S.; Mahal, S.; Oelschlegel, A.; Weissmann, C., *Science* **2010**, *327*, 869-872.
25. Johnson, C.; Pedersen, J.; Chappell, R.; McKenzie, D.; Aiken, J., *PLoS Pathogens* **2007**, *3*, e93.
26. BSE: Disease control & eradication - Causes of BSE, Department for Environment, Food, and Rural Affairs, March 2007.
27. (a) Trevitt, C. R., *Brain* **2006**, *129*, 2241-2265; (b) He, J.; Zhang, Y.; Hong, T., *Sci. China Life Sci.* **2010**, *53*, 959-963.
28. Mallucci, G.; Dickinson, A.; Linehan, J.; Klöhn, P.-C.; Brandner, S.; Collinge, J., *Science* **2003**, *302*, 871-874.
29. Meier, P.; Genoud, N.; Prinz, M.; Maissen, M.; Rulicke, T.; Zurbriggen, A.; Raeber, A. J.; Aguzzi, A., *Cell* **2003**, *113*, 49-60.
30. (a) Sakaguchi, S.; Ishibashi, D.; Matsuda, H., *Expert Opin. Ther. Pat.* **2009**, *19*, 907-917; (b) Aguzzi, A.; Heppner, F. L.; Heikenwalder, M.; Prinz, M.; Mertz, K.; Seeger,

- H.; Glatzel, M., *Br. Med. Bull.* **2003**, *66*, 141-159.
31. Sigurdsson, E.; Brown, D.; Daniels, M.; Kascsak, R.; Kascsak, R.; Carp, R., *Am. J. Pathol.* **2002**, *161*, 7.
32. White, A.; Enever, P.; Tayebi, M.; Mushens, R.; Linehan, J.; Brandner, S., *Nature* **2003**, *422*, 3.
33. Sethi, S.; Lipford, G.; Wagner, H.; Kretzschmar, H., *Lancet* **2002**, *360*, 229-230.
34. (a) Outram, G.; Dickinson, A.; Fraser, H., *Nature* **1974**, *249*, 855-856; (b) Outram, G.; Dickinson, A.; Fraser, H., *Lancet* **1975**, *305*, 198-200.
35. (a) Sellarajah, S.; Lekishvili, T.; Bowring, C.; Thompsett, A. R.; Rudyk, H.; Birkett, C. R.; Brown, D. R.; Gilbert, I. H., *J. Med. Chem.* **2004**, *2004*, 5515-5534; (b) Frid, P.; Anisimov, S. V.; Popovic, N., *Brain Res. Rev.* **2007**, *53*, 135-160.
36. Gilch, S.; Winklhofer, K.; Groschup, M.; Nunziante, M.; Lucassen, R.; Spielhauer, C., *EMBO J.* **2001**, *20*, 3957-3966.
37. May, B. C. H.; Witkop, J.; Sherrill, J.; Anderson, M. O.; Madrid, P. B.; Zorn, J. A.; Prusiner, S. B.; Cohen, F. E.; Guy, R. K., *Bioorg. Med. Chem. Lett.* **2006**, *16*, 4913-4916.
38. Barret, A.; Tagliavini, F.; Forloni, G.; Bate, C.; Salmona, M.; Colombo, L.; De Luigi, A.; Limido, L.; Suardi, S.; Rossi, G.; Auvre, F.; Adjou, K. T.; Sales, N.; Williams, A.; Lasmezas, C.; Deslys, J. P., *J. Virol.* **2003**, *77*, 8462-8469.
39. Priola, S. A.; Raines, A.; Caughey, W. S., *Science* **2000**, *287*, 1503-1506.
40. Supattapone, S.; Nguyen, H.; Cohen, F.; Prusiner, S.; Scott, M., *Proc. Natl. Acad. Sci. USA* **1999**, *96*, 14529-14534.
41. Adjou, K.; Simoneau, S.; Sales, N.; Lamoury, F.; Dormont, D.; Papy-Garcia, D., *J. Gen. Virol.* **2003**, *84*, 2595-2603.
42. Caughey, B.; Raymond, G., *J. Virol.* **1993**, *67*, 643-650.
43. Rhie, A., *J. Biol. Chem.* **2003**, *278*, 39697-39705.
44. Lau, A. L.; Yam, A. Y.; Michelitsch, M. M. D.; Wang, X.; Gao, C.; Goodson, R. J.; Shimizu, R.; Timoteo, G.; Hall, J.; Medina-Selby, A.; Coit, D.; McCoin, C.; Phelps, B.; Wu, P.; Hu, C.; Chien, D.; Peretz, D., *Proc. Natl. Acad. Sci. USA* **2007**, *104*, 11551-11556.
45. Jackson, G. S., *Proc. Natl. Acad. Sci. USA* **2001**, *98*, 8531-8535.
46. (a) Milgrom, L. R., *The Colours of Life: An Introduction to the Chemistry of*

Porphyrins and Related Compounds. Oxford, 1997; (b) Yasuhiro, I.; Yuko, N.; Masahiko, I.; Masaharu, N.; Shigenobu, F., *Inorg. Chem.* **2000**, *39*, 4793-4801.

47. Klingenstein, R.; Melnyk, P.; Leliveld, S.; Ryckebusch, A.; Korth, C., *J. Med. Chem.* **2006**, *49*, 5300-5308.

48. Southwick, P. L.; Ernst, L. A.; Tauriello, E. W.; Parker, S. R.; Mujumdar, R. B.; Mujumdar, S. R.; Clever, H. A.; Waggoner, A. S., *Cytometry* **1990**, *11*, 418-430.

49. Valeur, E.; Bradley, M., *Chem. Soc. Rev.* **2009**, *38*, 606-631.

50. (a) Lindsey, J. S.; MacCrum, K. A.; Tyhonas, J. S.; Chuang, Y.-Y., *J. Org. Chem.* **1994**, *59*, 579-587; (b) Lindsey, J. S.; Schreiman, I. C.; Hsu, H. C.; Kearney, P. C.; Marguerettaz, A. M., *J. Org. Chem.* **1987**, *52*, 827-836.

51. Geier III, G. R.; Riggs, J. A.; Lindsey, J. S., *J. Porphyrins Phthalocyanines* **2001**, *5*, 681-690.

52. Musonda, C. C.; Little, S.; Yardly, V.; Chibale, K., *Bioorg. Med. Chem. Lett.* **2007**, *17*, 4733-4736.

53. Nishida, Y.; Tsurumi, T.; Sasaki, K.; Watanabe, K.; Dohi, H.; Kobayashi, K., *Org. Lett.* **2003**, *5*, 3775-3778.

54. (a) Smith, K. M., *Porphyrins and Metalloporphyrins*. Elsevier, Amsterdam, 1975 ed; (b) Sagun, E. I., *Chem. Phys.* **2002**, *275*, 211.

55. Chibale, K.; Haupt, H.; Kendrick, H.; Yardley, V.; Saravanamuthu, A.; Fairlamb, A. H.; Croft, S. L., *Bioorg. Med. Chem. Lett.* **2001**, *11*, 2655-2657.

56. Thanks Dr. Kendre Dhananjay for providing the starting materials, four N-(6-Chloro-2-methoxy-acridin-9-yl)-alkyldiamine compounds.

57. (a) Haig, D. A.; Clarke, M. C., *Nature* **1970**, *234*, 106-107; (b) Birkett, C. R.; Hennion, R. M.; Bembridge, D. A.; Clarke, M. C.; Chree, A.; Bruce, M. E.; Bostock, C. J., *EMBO J* **2001**, *20*, 3351-3358; (c) Rubenstein, R.; Carp, R. I.; Callahan, S., *J. gen. Virol.* **1984**, 2191-2198.

58. (a) Towbin, H.; Staehelin, T.; Gordon, J., *Proc. Natl. Acad. Sci. USA* **1979**, *76*, 4350-4354; (b) Renart, J.; Reiser, J.; Stark, G. R., *Proc. Natl. Acad. Sci. USA* **1979**, *76*, 3116-3120.

59. Results of antiprion activity and densitometric analysis of Western blots were provided

by Charles May III from the Westaway group in the University of Alberta's Centre for Prions and Protein Folding Diseases.

60. (a) Doh-Ura, K.; Iwaki, T.; Caughey, B., *J Virol* **2000**, *74*, 4894-4897; (b) Kobayashi, Y.; Hirata, K.; Tanaka, H.; Yamada, T., *Rinsho Shinkeigaku* **2003**, *43*, 403-408.

61. Results of toxicity test of multimeric compounds were provided by Charles May III from the Westaway group in the University of Alberta's Centre for Prions and Protein Folding Diseases.

CHAPTER 2

STUDIES TOWARDS THE FORMATION OF *CIS-ANTI-CIS* LINEAR TRIQUINANES VIA PYRAN-2-ONE PHOTOCHEMISTRY

2.1 Introduction of Polyquinanes and Linear Triquinanes

The polyquinanes make up an important class of sesquiterpenoids found in nature with a saturated polycyclic hydrocarbon framework.¹ The unique molecular architecture and promising biological activities in some of the members have made them frequent synthetic targets. According to the number of five-membered rings in the structures, polyquinanes can be classified into diquinane, triquinane and tetraquinane (**Figure 2.1**).^{1a} Among them, triquinanes are the most commonly seen carbocyclic framework in all isolated polyquinane natural products. Triquinanes can be further divided into linear triquinanes, angular triquinanes, or triquinanes fused in propellane as in **Figure 2.1**, depending on the connection of the tricyclic skeletons.^{1b}

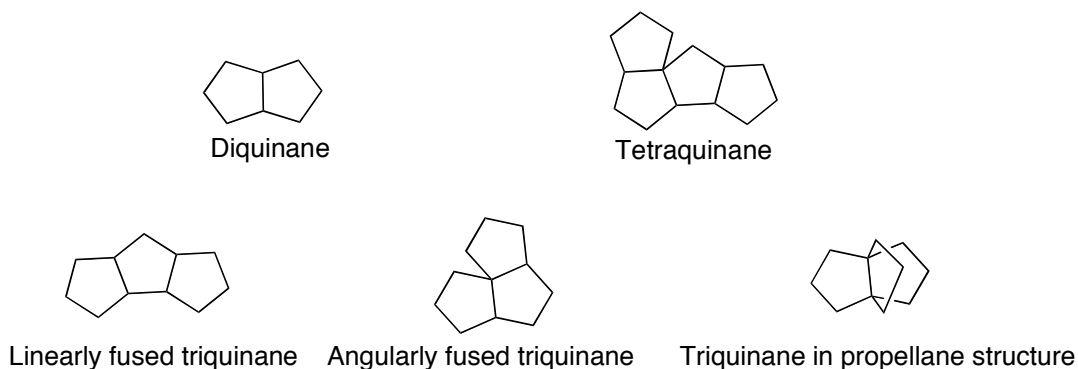


Figure 2.1 Diquinane, tetraquinane and three classes of triquinanes.

In particular, the linear triquinanes are the most abundant ones among various triquinanes isolated from plant,² marine³ and microbial resources.⁴ They are all found to possess the *cis-anti-cis* relative configuration; that is, both ring-fusions are *cis*, but the angular substituents of each ring-fusion are in an *anti* relationship (**Figure 2.2**). This relative stereochemistry is generally considered to be thermodynamically more favored.^{1b} So far, five categories of linear triquinane products have been identified from the natural resources. Each type has a unique fundamental carbocyclic skeleton, and the five types are named as hirsutane type, isohirsutane type, pleurotellane type, ceratopicane type and capnellane type (**Figure 2.3**).^{1b} In contrast, the alternative *cis-syn-cis* relative stereochemistry is not found in any of the naturally occurring triquinanes. They are found to have a potential application to be used as basic building blocks in the synthesis of polyhedral compounds, such as dodecahedrane and peristylane.⁵

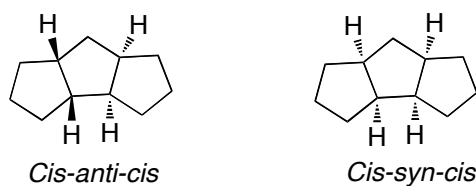


Figure 2.2 Linear triquinanes with natural *cis-anti-cis* and unnatural *cis-syn-cis* relative configuration.

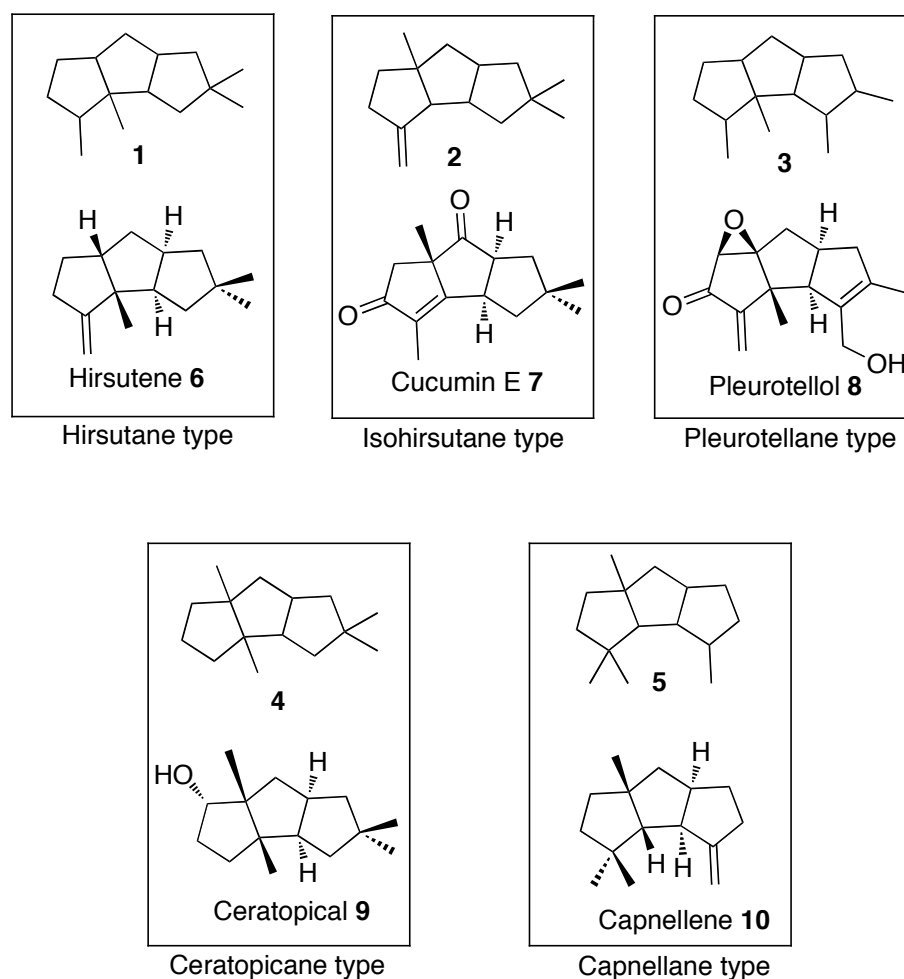


Figure 2.3 Five types of natural linear triquinanes. Their fundamental carbon skeletons **1-5** and the selected examples of natural products **6-10** are listed.

A variety of polyquinane compounds, especially the linear triquinanes, have been discovered to exhibit interesting biological properties. For example, coriolin **11** has both antitumor and antibacterial properties,⁶ and hirsutic acid **12** shows antibiotic activities.^{4b,7} More over, capnellene **13** and capnellanols have the capability to inhibit the growth of microorganisms as well as to prevent larval settlement (**Figure 2.4**).⁸

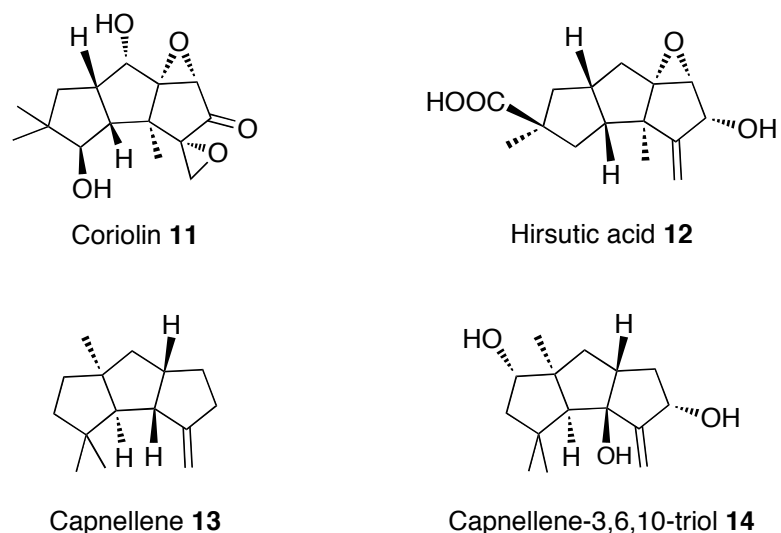
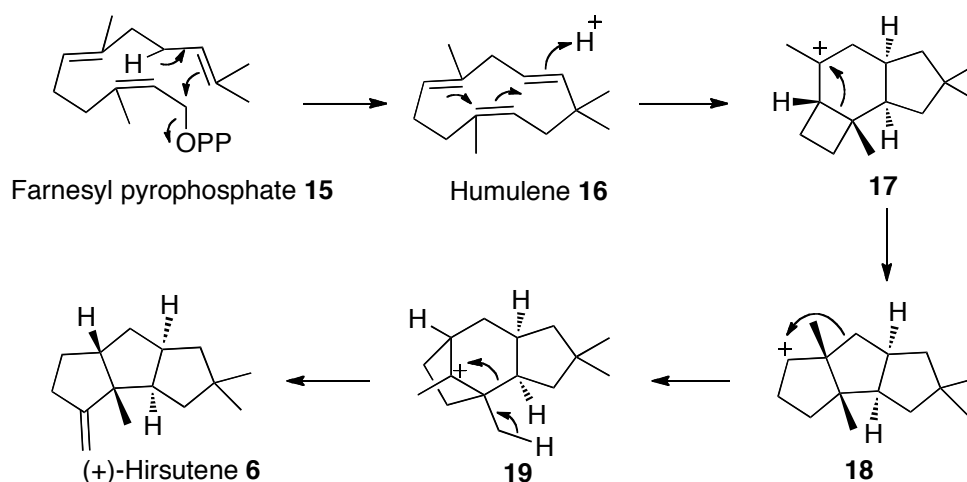


Figure 2.4 Structures of coriolin, hirsutic acid, capnellene and one type of capnellanol.

Among all linear triquinane natural products, hirsutene **6** has been a popular synthetic target molecule to illustrate newly developed methods or strategies in building tricyclic ring systems, due to its comparatively simple structure. Hirsutene is a fungal metabolite isolated from Basidiomycete *Coriolus consors* with *cis-anti-cis* tricyclo [6.3.0.0^{2,6}]-undecane core.^{4e} In addition, hirsutene is presumed to be the biogenetic precursor of other more complexed natural products as well, such as coriolin **11** and hirsutic acid **12**. In the biogenetic pathway, hirsutene is thought to be produced from its precursor farnesyl pyrophosphate **15** via humulene-type **16** and other intermediates **17-19** by a sequence of cationic rearrangements as in **Scheme 2.1**.⁹

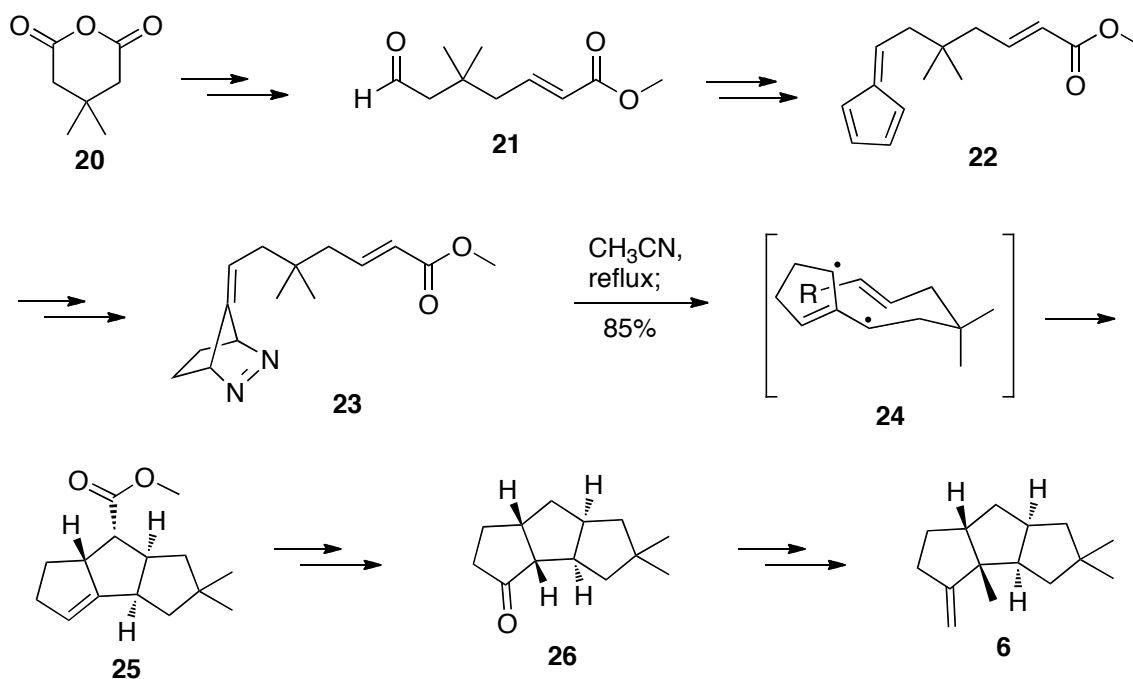


Scheme 2.1 The biosynthetic pathway to form (+)-hirsutene **6**.

2.2 Reported Routes to Build Linear Triquinanes

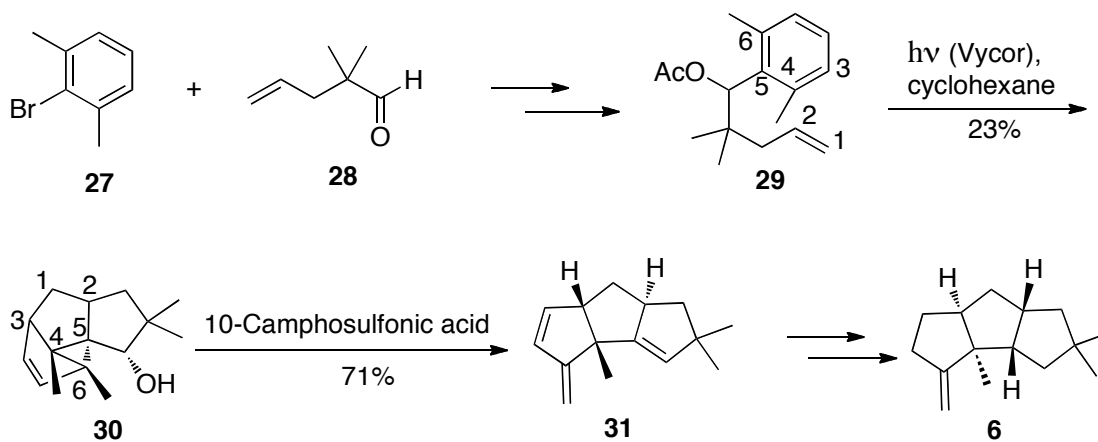
The dense connectivity, contiguous stereogenic centers, and infrequent occurrence of functional groups in the natural linear triquinane products make the synthesis a challenge, and this has drawn extensive attention from the synthetic community to develop more effective and rapid approaches. Many common methods of making five-membered carbocyclic rings have been employed in the synthesis of linear triquinanes, which include aldol condensation,¹⁰ Nazarov cyclization,¹¹ [3+2] cycloaddition,¹² as well as Pauson-Khand reaction¹³ and others. In addition, versatile synthetic methods have been specifically designed and developed from readily available precursors to build the three-ring fused skeletons in a single step. A few approaches reported since 1980s are discussed as below.

Intramolecular 1,3-diyil trapping reaction was first developed by Little and his coworkers, and it was later applied in the synthesis of hirsutene and capnellene in 1981 by the same group.¹⁴ For the synthesis of hirsutene, the precursor **22** was prepared through condensation of cyclopentadiene and aldehyde **21** (**Scheme 2.2**). Subsequent Diels-Alder reaction and selective reduction of the cyclic olefin gave rise to azo-compound **23**. When azo-compound **23** was heated in MeCN, it underwent intramolecular 1,3-diyil reaction to form compound **25** with linear triquinane framework, and further modification led to hirsutene **6**.



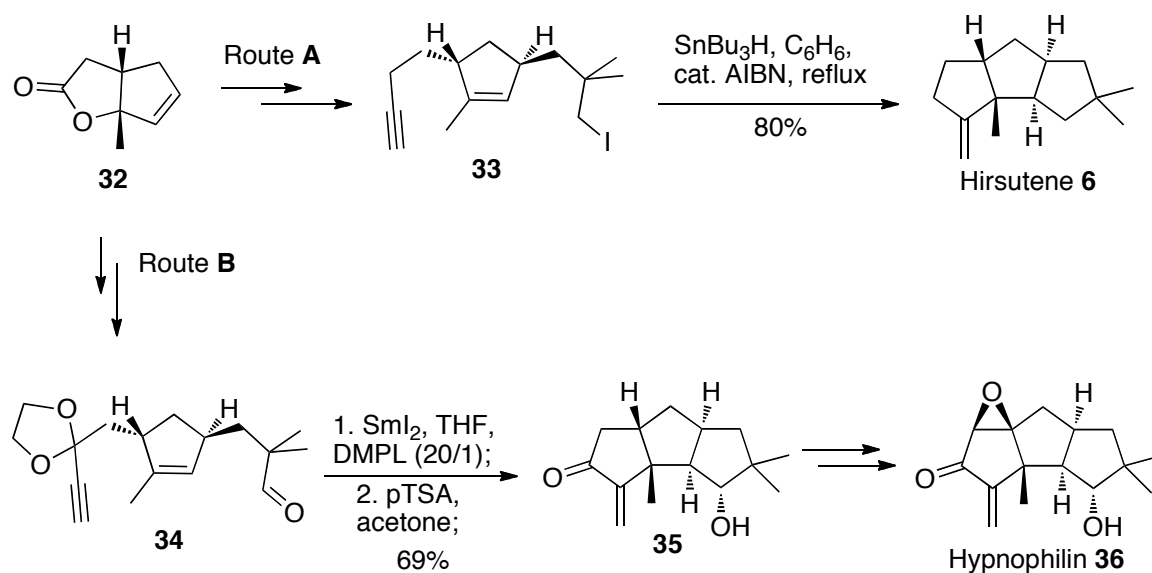
Scheme 2.2 Intramolecular 1,3-diyil trapping reactions to synthesize hirsutene.

Intramolecular photochemical meta-cycloaddition/cyclopropane cleavage was reported by Wender and Howbert in the total synthesis of hirsutene in 1982.¹⁵ Arene-olefin **29** was prepared through condensation of aldehyde **28** and a Grignard-reagent that was derived from bromo-arene **27**. Arene-olefin **29** underwent the key transformation through intramolecular meta-cycloaddition to form strained tetracyclic compound **30** as the major product. Under the acidic condition, the highly strained cyclopropane in **30** was cleaved to form linear triquinane **31**, which was further converted to natural product **6**.



Scheme 2.3 Intramolecular meta-cycloaddition/cyclopropane cleavage pathway.

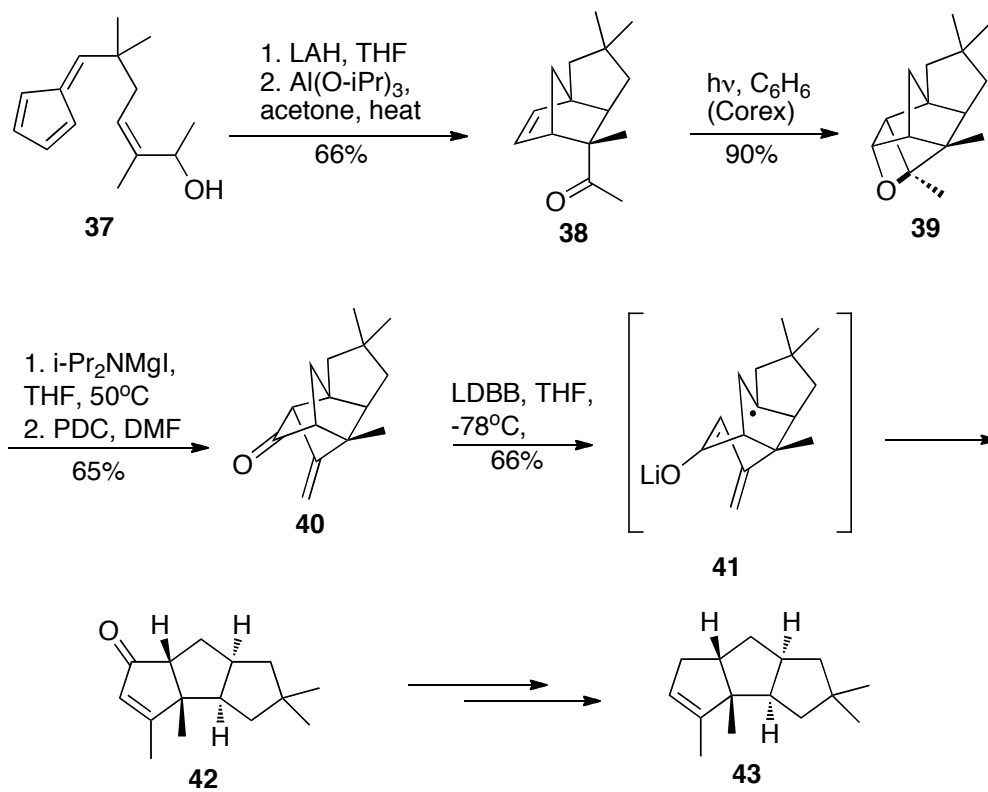
Curran and his coworkers applied radical initiated tandem polyolefinic cyclization in the total synthesis of (+/-) hirsutene in 1985 and (+/-) hypnophilin in 1988.¹⁶ The same starting material, lactone **32**, was used to make two precursors **33** and **34** in a few steps in both routes **A** and **B** as in **Scheme 2.4**. In the key step, Bu_3SnH was used to initiate the radical chain reaction for the formation of hirsutene **6** (Route **A**), while samarium iodide was found to be most effective in triggering the tandem polyolefinic cyclization in the synthesis of the related triquinane hypnophilin **36** (Route **B**).



Scheme 2.4 Radical initiated tandem polyolefinic cyclization pathways.

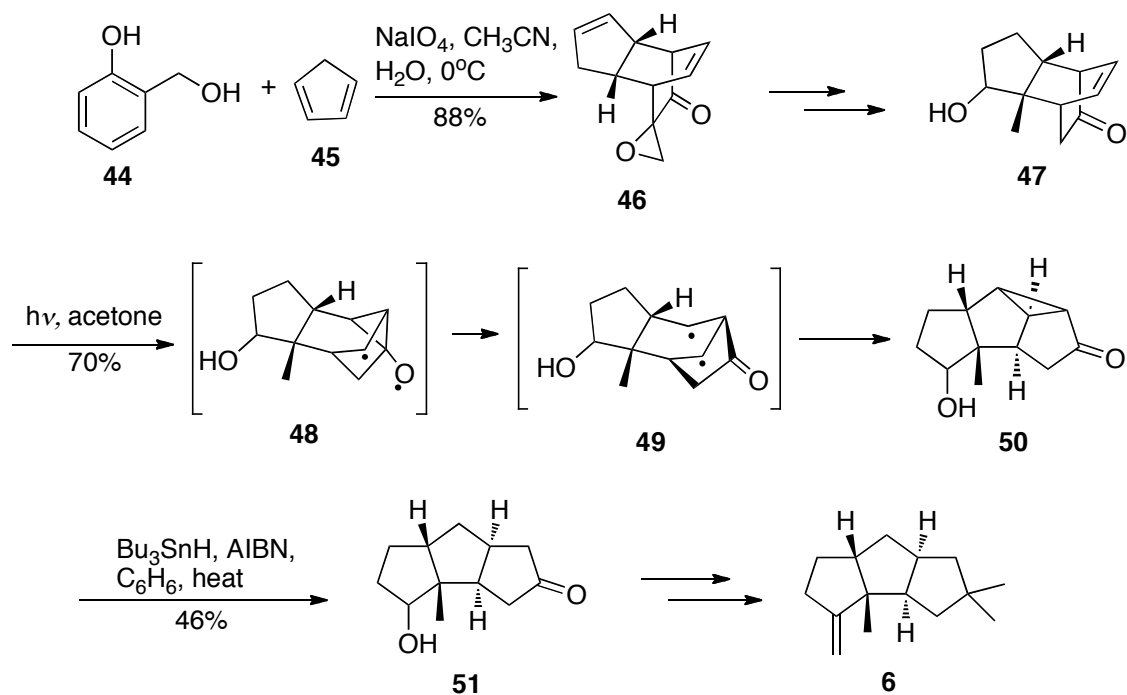
A sequence of Diels-Alder/Paterno-Büchi reaction/reductive fragmentation was reported by Rawal and his co-workers to build diquinanes and triquinanes efficiently,¹⁷ and this pathway was applied in the synthesis of isocomene¹⁸ and endo-hirsutene.¹⁹ In the case of endo-hirsutene, fulvene **37** was reduced by LAH to its related cyclopentadiene, and subsequent oxidation and intra-molecular Diels-Alder reaction gave rise to norbornene **38**. With irradiation, a highly strained cage compound, oxetane **39**, was obtained after Paterno-Büchi reaction. Subsequent cleavage of oxetane **39** under basic conditions and oxidation gave rise to ketone **40**. Reductive fragmentation opened the caged ring system,

and further modifications led to the formation of endo-Hirsutene **43**.



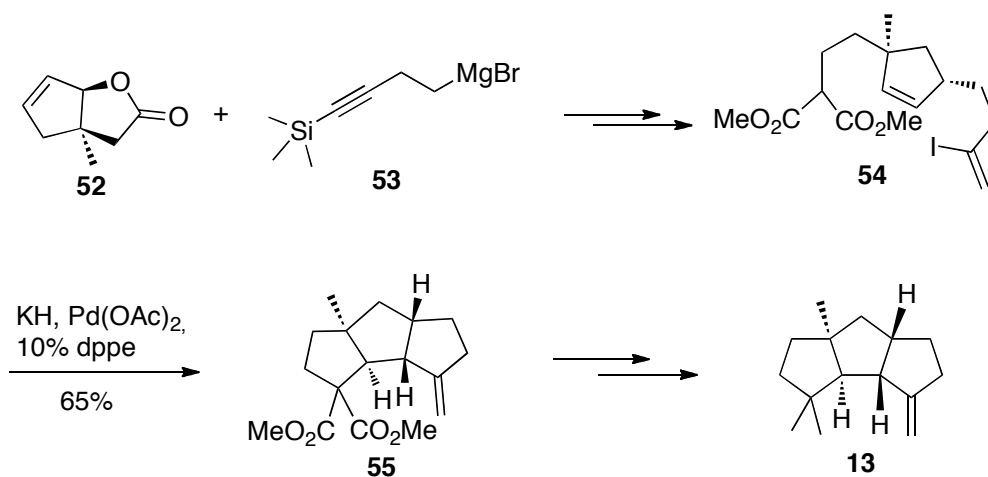
Scheme 2.5 Diels-Alder/Paterno-Büchi reaction/reductive fragmentation pathway.

The Diels-Alder reaction/1,2-acyl shift (oxa-di- π -methane rearrangement)/reductive cleavage sequence was developed by Demuth in 1982,²⁰ and it was later applied in the total synthesis of hirsutene by the Singh group in 2002.²¹ Bridged tetracyclic epoxide **46** was assembled from saligenin **44** and cyclopentadiene **45** in a single pot reaction. Modification of **46** led to tetracyclic compound **47** in a few steps. With UV irradiation of **47**, 1,2-acyl shift occurred to give rise to strained compound **50**. Reductive cleavage of compound **50** and further modifications led to natural product hirsutene **6**.



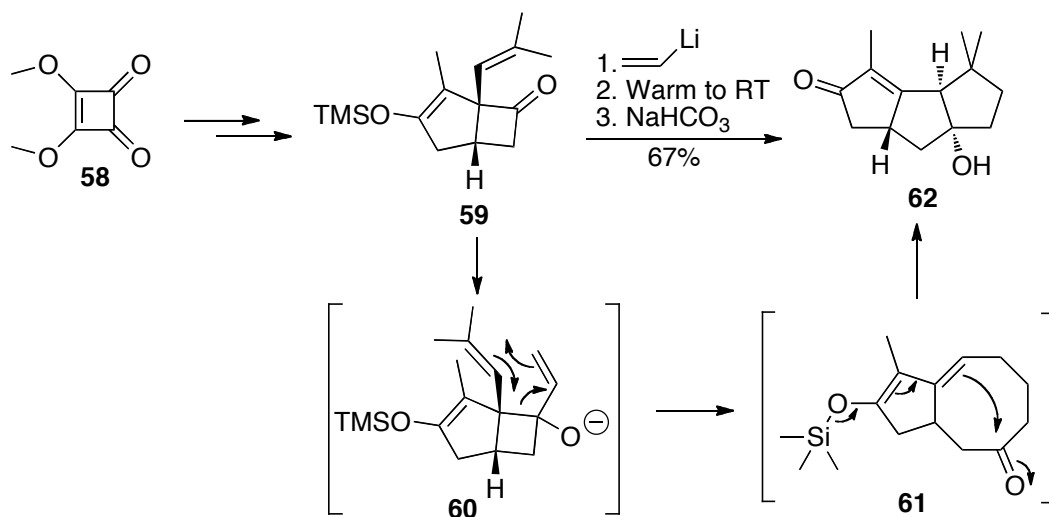
Scheme 2.6 Diels-Alder reaction/1,2-acyl shift/reductive cleavage pathway.

A pathway of palladium catalyzed cyclization was applied by the Balme group in 1994 in the total synthesis of capnellene **13**.²² Precursor **54** was prepared through the addition of Grignard reagent **52** to unsaturated lactone **53** and other steps. With the treatment of KH and palladium catalyst, compound **54** underwent Wacker-type process as elegantly designed to generate linear triquinane **55** in a single step with the expected stereochemistry. Further transformation of **55** gave rise to the natural product, capnellene **13**.



Scheme 2.7 Palladium catalyzed intramolecular cyclopentannation pathway.

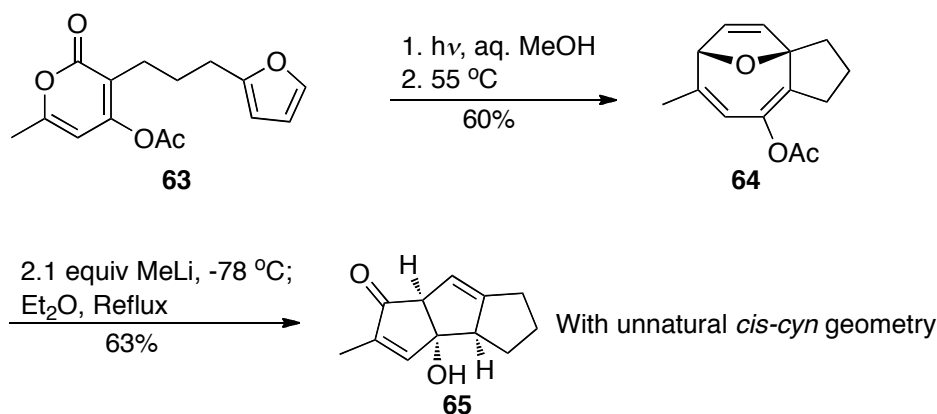
The last approach involved tandem oxy-Cope-transannular reactions, which was developed by the Moore group to synthesize triquinanes as well as other polyquinanes.²³ In the example in **Scheme 2.8**, precursor **59** was prepared in a few steps from dimethyl squarate **58**, and it underwent oxy-Cope-transannular ring closure sequences to form tricyclic product **62** efficiently with natural configuration.



Scheme 2.8 Tandem oxy-Cope-transannular reactions.

2.3 Concise Route to Linear Triquinanes From Pyran-2-ones

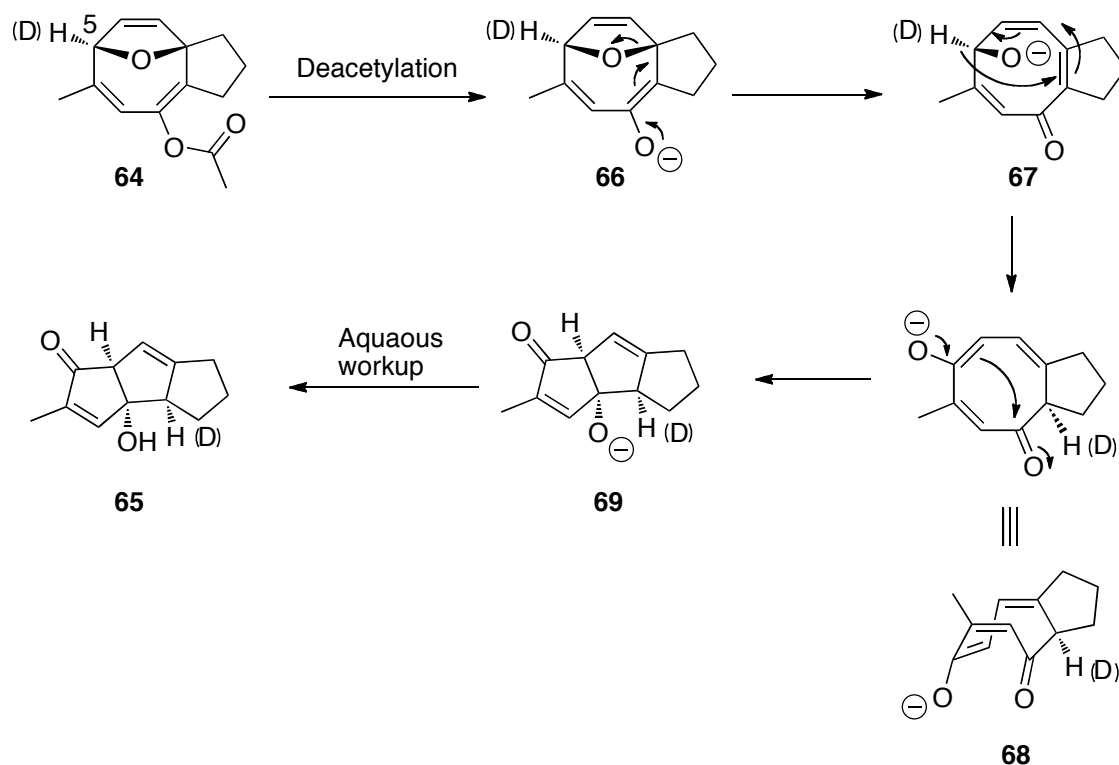
Our group has developed a concise route to build linear triquinanes with unnatural *cis, syn* relative configuration from pyran-2-ones with pendent furan traps.²⁴ As the example in **Scheme 2.9**, Pyran-2-one **63** underwent a sequence of [4+4] cycloaddition reaction and subsequent thermal decarboxylation to produce advanced bicyclic intermediate **64**, which contained a cyclooctatriene ring system.²⁵ When compound **64** was treated with excess methyl lithium, linear triquinane **65** was obtained in a moderate yield. However, the relative configuration of the triquinane **65** is *cis-syn*, which is the unnatural form.



Scheme 2.9 Concise route developed by a previous group member from pyran-2-ones to linear triquinanes with *cis-syn* configuration through a sequence of [4+4] cycloaddition/thermal decarboxylation/MeLi-mediated rearrangement.^{24a}

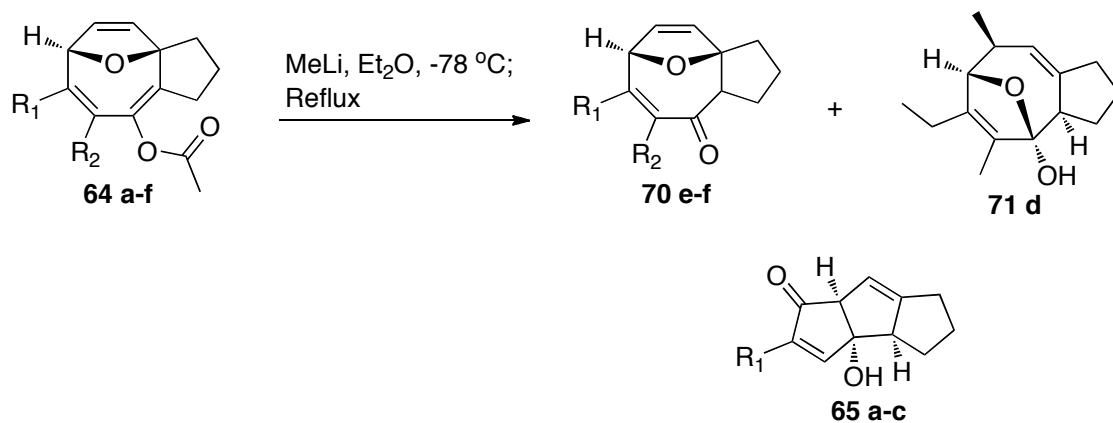
A proposed mechanism is illustrated in **Scheme 2.10** for the unusual formation of the linear triquinane in the last step.^{25c} With the treatment of MeLi, deacetylation occurred to generate intermediate **66**. Subsequent β -elimination cleaved the bridged ether to generate intermediate **67**, and a process of 1,5-hydrogen shift was believed to occur immediately afterwards to get to the stage of intermediate **68**, which underwent transannular aldol addition to furnish the tricyclic ring system after aqueous workup. The

outcome of a deuterium labeling experiment at C-5 position was consistent with the proposed mechanism. The transfer of the deuterium was both regio- and stereo-specific and the yield of *d*-**65** was comparable to that of the unlabelled case under identical reaction conditions.



Scheme 2.10 Proposed mechanism for the formation of linear triquinane.^{24a}

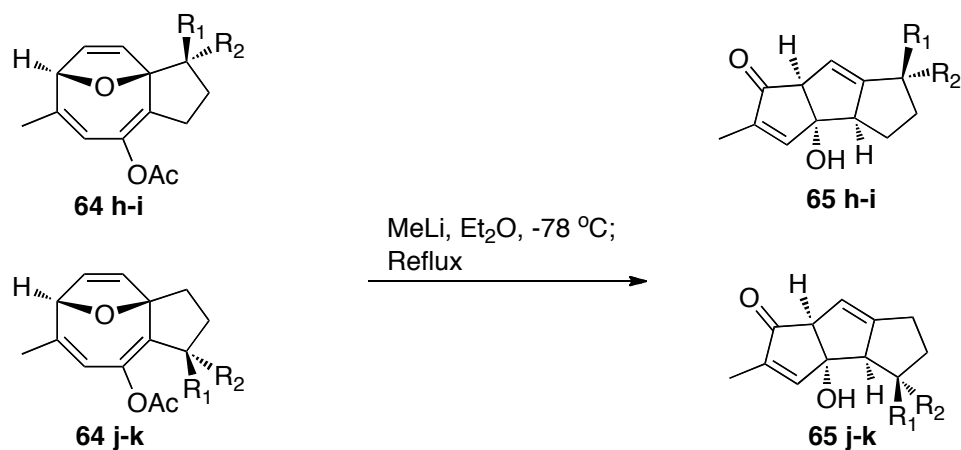
The generality of this reaction was investigated, and it was found that the substitutions at R_1 and R_2 on the cyclooctatriene ring have an important influence upon the generation of the linear triquinanes as in **Table 2.1**. Entry 2 was the only case that has similar yield of linear triquinane as the one in **Scheme 2.9**, while in other cases either enones **70** or hemiketals **71** was isolated as the major product. That indicated that there are competing pathways beside the β -elimination route, which are affected by the substitutions on the cyclooctatriene ring.



Entry	Substrate	R ₁	R ₂	Product	Yield (%)
1	64 a	Me	H	65 a	63
2	64 b	Et	H	65 b	60
3	64 c	Ph	H	65 c	Trace
4	64 d	Et	Me	71 d	67
5	64 e	Me	Me	70 e	90
6	64 f	(CH ₂) ₃		70 f	80

Table 2.1 Scope of MeLi-mediated reaction to form triquinanes.^{24a}

However, the tolerance of substitutions at different positions on the fused cyclopentane rings was quite good, as moderate yields of a single diastereomer of linear triquinane products **65 i-k** were obtained in the four cases in **Table 2.2**.



Entry	Substrate	R ₁	R ₂	Product	Yield (%)
1	64 h	Me	H	65 h	56
2	64 i	H	Me	65 i	68
3	64 j	Me	H	65 j	52
4	64 k	H	Me	65 k	63

Table 2.2 Triquinane formations from branched substrates.^{24a}

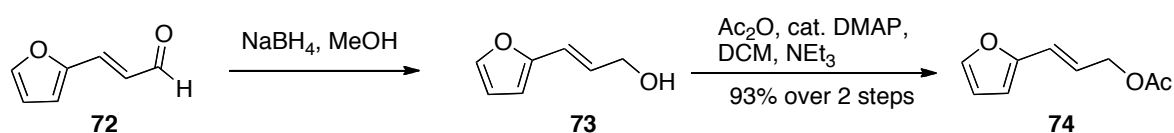
It is therefore desirable to develop a convenient route to invert the configuration of the readily available *cis-cyn* products to *cis-anti-cis* natural form, and thus permit the application of this method in the synthesis of natural products. Conversion of the configuration is the main subject of this chapter.

2.4 Research In The Modification of The Relative Configuration of Unnatural Linear Triquinane

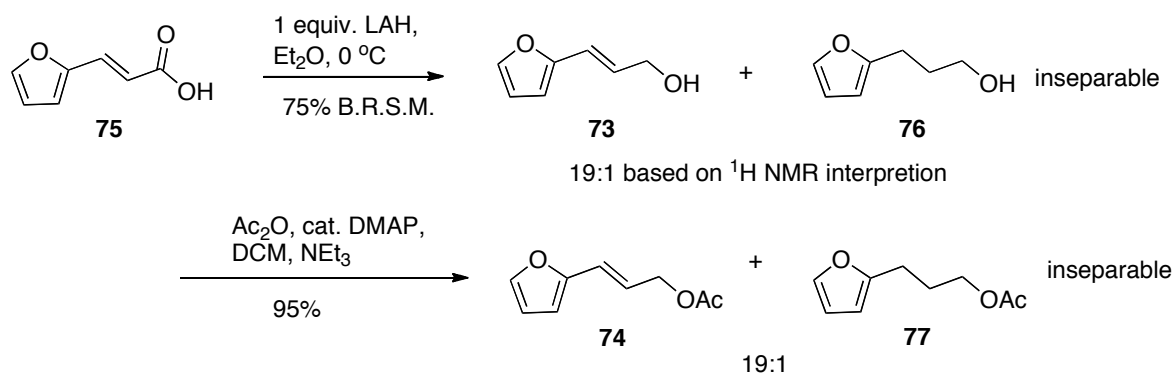
2.4.1 Preparation of the Advanced Intermediate Octatriene 64

Furan **74** was prepared by reduction of its corresponding aldehyde **72** or acid **75** by using NaBH₄ or LAH respectively, followed by hydroxyl group protection (**Scheme**

2.11 and 2.12). However, over-reduction of the conjugated olefin occurred when LAH was used to reduce acid **75**. Furan **76** was identified as a minor by-product by ^1H NMR, and the by-product is inseparable from desired compound **73**. Various equivalent of LAH (0.75 – 2 equiv.) under different temperatures ($-78\text{ }^\circ\text{C}$ - room temperature) were tried to avoid over reduction, but this could not be achieved under any circumstances. Nevertheless, the ratio of the over-reduced product **76** could be optimized to as low as 1:19 compared with the desired product, basing on ^1H NMR interpretation (Scheme 2.12). Another reducing reagent borane (BH_3 in THF) was also tried to reduce acid **75**, but only starting material was recovered. Luckily, it turned out that the existence of the minor by-product **76** does not affect the yield of subsequent Pd-catalyzed coupling reaction.

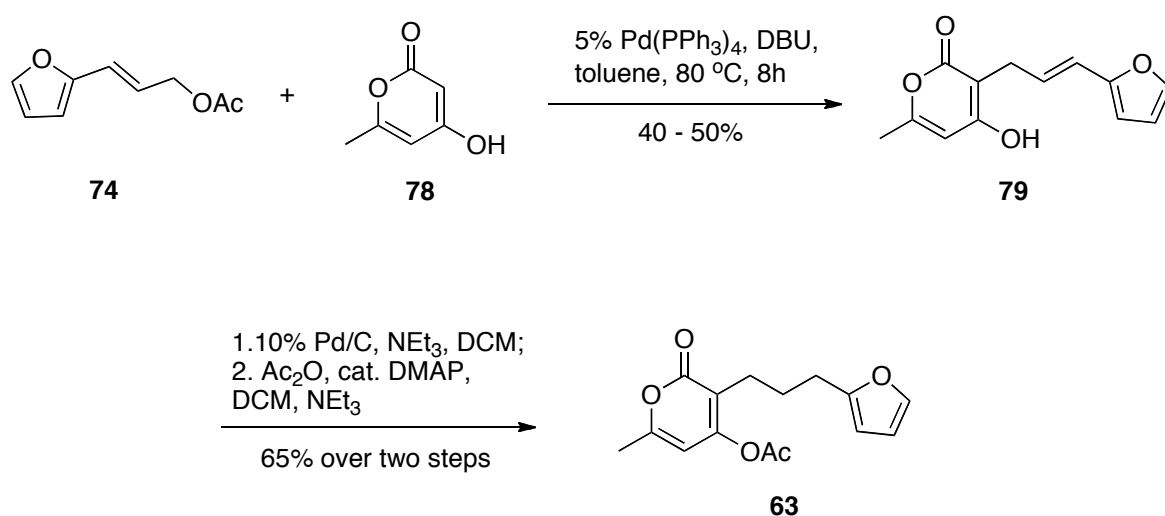


Scheme 2.11 Preparation of furan **74** from aldehyde **72**.



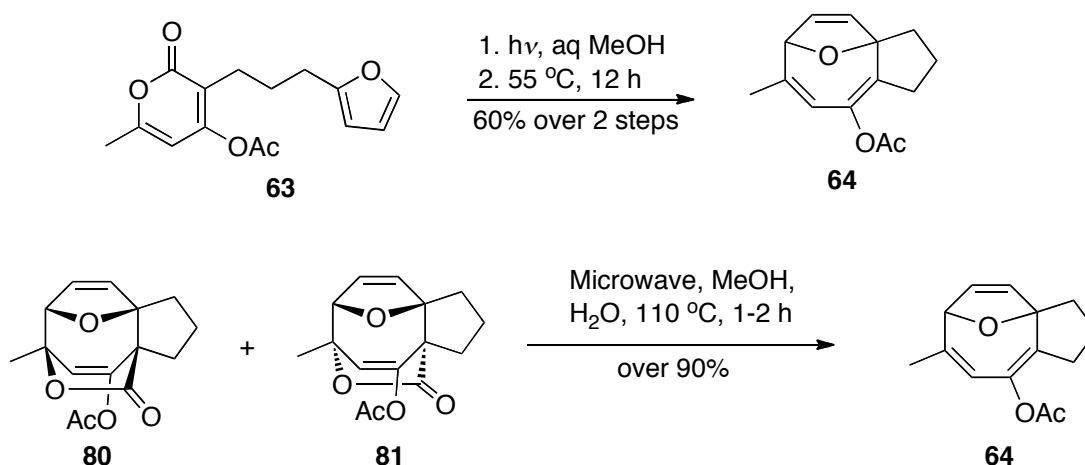
Scheme 2.12 Preparation of furan **74** from acid **75**.

Pyran-2-one **63** with pendent furan was prepared through the step of palladium catalyzed coupling reaction as in Scheme 2.13.²⁶ Coupling of furan **74** and pyranone **78** gave rise to pyran-2-one **79** in moderate yields, and subsequent hydrogenation and protection of hydroxyl group as an acetate led to the key photo-substrate **63**.



Scheme 2.13 Preparation of **63** from furan **74** and pyran **78**.

The advanced intermediate **64** was obtained in a moderate yield in a one-pot reaction of UV irradiation and subsequent overnight heating. An alternative effective pathway to get to **64** was to isolate endo-octadiene **80** and exo-octadiene **81** by flash chromatography after UV irradiation and then treat the mixture of two isomers with microwave and a high temperature (**Scheme 2.14**).



Scheme 2.14 Preparation of cyclooctatriene **64**.

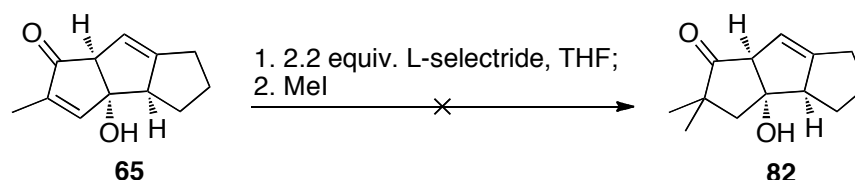
With cyclooctatriene **64** in hand, unnatural linear triquinane **65** could be obtained through MeLi-mediated anionic rearrangement and transannular aldolization in moderate

yields in small-scale reactions (**Scheme 2.9**).

2.4.2 Progress In The Modification of The Configuration of Unnatural Linear Triquinane

Linear triquinane product **65** has the unnatural *cis-syn* configuration of the bridgehead hydrogens and the hydroxyl group. The goal is to modify the configuration of **65** to the natural form, and thus establish a new concise synthetic route to make linear triquinanes with *cis-anti-cis* configuration from pyran-2-ones with pendent furan by the strategy of [4+4] cycloaddition/decarboxylation/MeLi-mediated rearrangement. This strategy might be later applied in the synthesis of natural linear triquinane compounds.

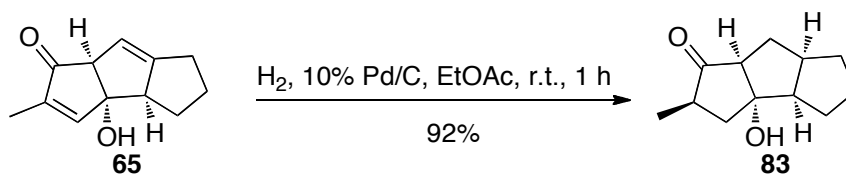
L-selectride was first tried to reduce the cyclic enone as expected and meanwhile set the gem-dimethyl group with the addition of MeI to the reaction mixture (**Scheme 2.15**). However, when the enone **65** in THF was treated with L-selectride under different temperatures, recovered starting material was the main component in all cases.



Temperatures tried for step 1: -78 °C; -23 °C; 0 °C; r.t.

Scheme 2.15 Attempts to reduce enone **65** by L-selectride.

An alternative pathway was tried by hydrogenation of compound **65**. The reaction went smoothly to reduce both carbon-carbon double bonds simultaneously (**Scheme 2.16**). Although two new stereogenic centers were generated in this step, a single diastereomer was produced. The crystal of **83** was obtained and its structure was confirmed by X-ray crystallography to have the *cis-syn-cis* relative configuration (**Figure 2.5**).



Scheme 2.16 Hydrogenation of compound **65**.

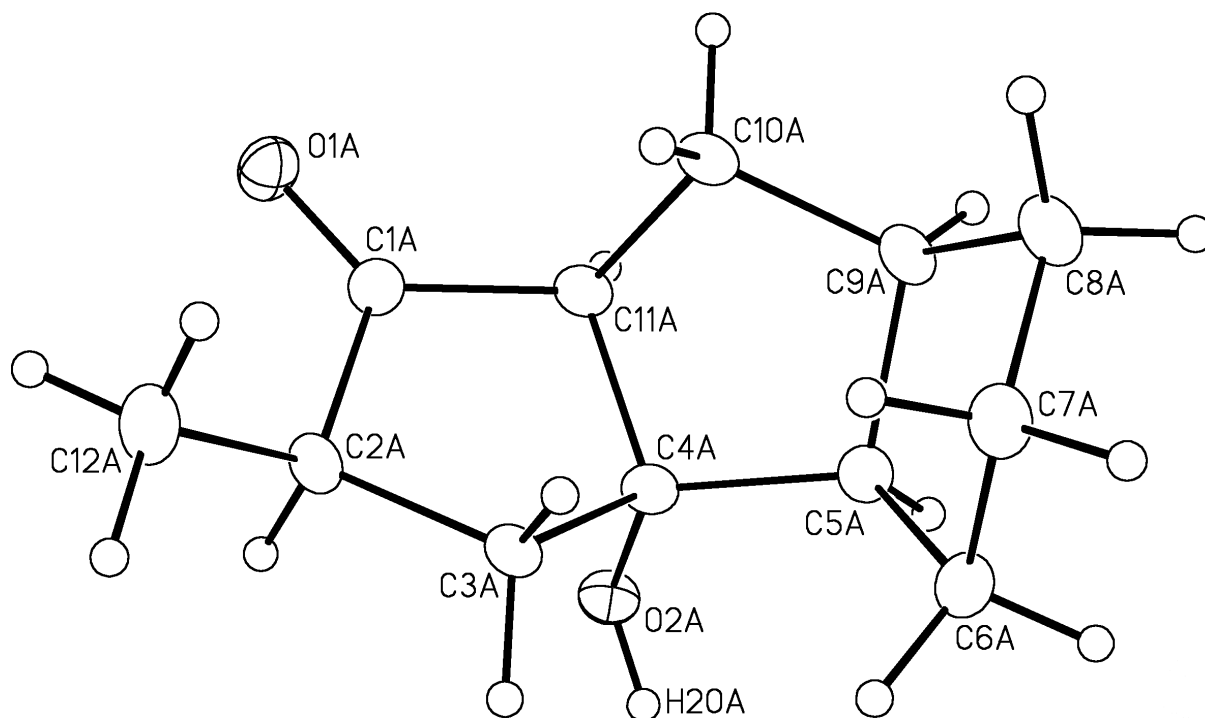
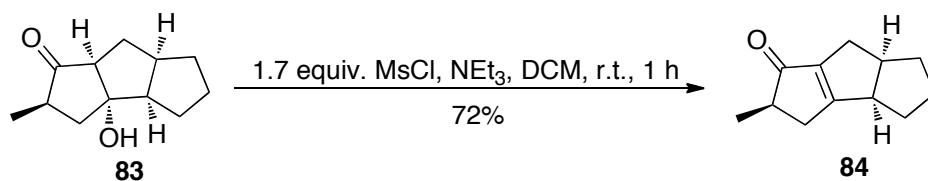


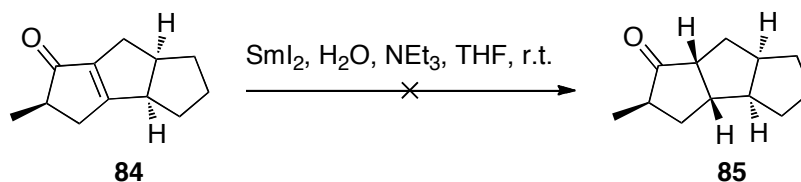
Figure 2.5 X-ray ORTEP representation of **83** at the 20% probability level.

Subsequent dehydration of **83** under basic conditions produced cyclic enone **84** in a decent yield as in **Scheme 2.17**. Two stereogenic centers were removed where a new carbon-carbon double bond was formed. The loss of both bridgehead stereocenters of one of the ring-fusions now presented an opportunity to obtain the alternative *cis-anti-cis* configuration.



Scheme 2.17 Dehydration of compound **83**.

With **84** in hand, it was anticipated that two new stereogenic centers would be set by the reduction of the olefin. Under the right conditions, the product with thermodynamically favored configuration of *cis-anti-cis* would be expected. The SmI_2 -mediated reaction conditions were tried for selective reduction of carbon-carbon double bond in the conjugated system.²⁷ A mixture of H_2O /amine in THF was used as co-solvent because they are able to accelerate the rate of reduction of α,β -unsaturated enone.^{27a, 27c} However, this reaction condition was found to be ineffective in reducing the conjugated double bond since the starting material were recovered in both cases as in **Table 2.3** after more than 1 hour.

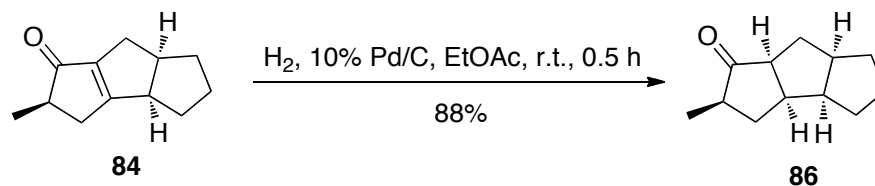


Unit (equivalents)	SmI_2	H_2O	NEt_3
Condition a	2.5	6	5
Condition b	6	60	12

Table 2.3 Attempts to reduce enone **84** with SmI_2 -mediated reaction conditions.

Hydrogenation of the enone **84** gave a single diastereomer **85** with a yield of 88% (**Scheme 2.18**). No correlation between the methyl group and bridgehead hydrogen was detected in the NOE experiment, which might suggest that linear triquinane **85** has the unnatural configuration of *cis-syn-cis*. In addition, the hydrogenation was more likely to

occur from the less hindered side to give the product **86** with the unnatural configuration.



Scheme 2.18 Hydrogenation of compound **84**.

Birch reduction (Li, liq. NH_3) under thermodynamic control is still underway to get to the desired *cis-anti-cis* configuration.

(For further discussion of the conclusions and future directions of this research project, see **Chapter 3**.)

2.5 Experimental Details

2.5.1 General Information

Reactions were conducted in oven-dried (110 °C) or flame-dried glassware under a positive argon atmosphere unless otherwise noted. Transfer of anhydrous solvents, reagents or mixtures was accomplished with oven-dried syringes or *via* cannulae. Solvents were distilled before use: dichloromethane over calcium hydride; tetrahydrofuran and diethyl ether over sodium benzophenone ketyl; toluene over calcium hydride. Thin layer chromatography (TLC) was performed on 0.25 mm thick precoated silica gel plates (Merck Fertigplatten Kieselgel 60F254). Flash chromatography columns were packed with 230-240 mesh silica gel.

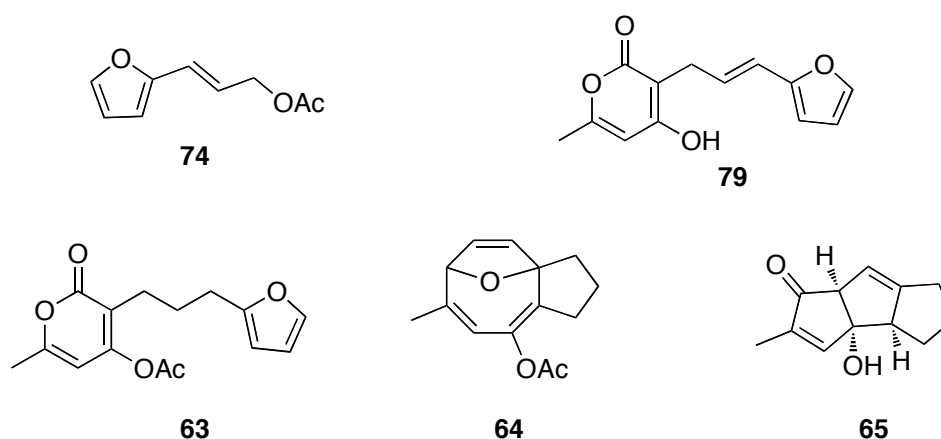
Proton nuclear magnetic resonance spectra (^1H NMR) were recorded at 400 MHz or 500 MHz, and the chemical shifts are reported on the δ scale (ppm) relative to the tetramethylsilane (0 ppm). Coupling constants (J) are reported in Hz. Second order

splitting patterns are indicated. Splitting patterns are designated as s, singlet; d, doublet; t, triplet; q, quartet; m, multiplet; br, broad; dd, doublet of doublets, dt, doublet of triplets; b, broad, etc. Carbon nuclear magnetic resonance spectra (^{13}C NMR) were recorded at 100 MHz or 125 MHz and are reported in ppm relative to the centerline of the triplet from deuteriochloroform at 77.23 ppm. Infrared (IR) spectra were measured with a Magna 750 FT-IR infrared spectrophotometer. Mass spectra were determined on a Kratos Analytical MS-50G spectrometer (EI). Elemental analyses were obtained on a Carlo Erba CHNS-0 EA1108 Elemental Analyzer. X-ray crystallographic experiments were carried out on a Bruker PLATFORM diffractometer / SMART APEX II CCD area detector system with an associated liquid nitrogen based crystal cooling system capable of temperatures ranging from ambient to $-150\text{ }^{\circ}\text{C}$.

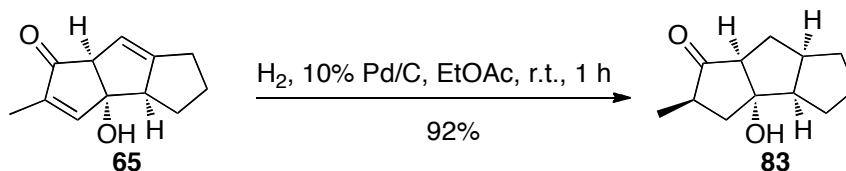
UV irradiation were carried out by using an Ace-Hanovia 450W median pressure quartz, mercury vapor lamp in a quartz water-cooled jacket. Reactions were carried out in a Pyrex round bottom flask under argon after 10 mins of slow stream of argon for deoxygenation before UV irradiation in a light proof enclosure. Microwave heating was carried out in a Biotage Initiator microwave reactor.

All reagents and catalysts were purchased from Aldrich or Sigma or Strem and were used without further purification unless otherwise stated.

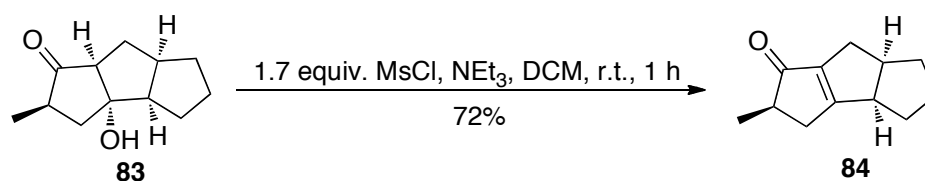
2.5.2 Substrate Synthesis



Preparation of the reported compounds **74**, **79**, **63**, **64** and **65** were carried out by following literature procedures or procedures described in Lei Li's PhD Dissertation.

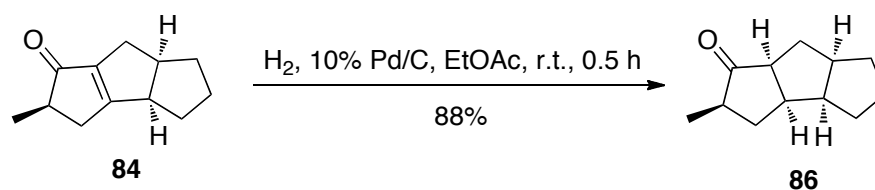


Preparation of 83. 10 mol% Pd/C (35 mg, 0.034 mmol) was added to a solution of **65** (65 mg, 0.34 mmol) in EtOAc (12 mL) in a 25 mL round bottom flask. The reaction was monitored by TLC, and the mixture was stirred under H₂ (balloon pressure) for 1 h until the starting material was completely consumed. The mixture was then filtered over celite and concentrated with rotatory evaporator. Flash chromatography (silica gel, 230-400 mesh, 50% EtOAc/Hexane) of the crude product afforded 60 mg (0.31 mmol, 92%) of the desired **83** as a white solid: m.p. 47-49 °C; R_f = 0.48 (70% EtOAc/Hexane); IR (DCM cast film) 3427, 2951, 2869, 1736 cm⁻¹; ¹H NMR (500 MHz, CDCl₃) δ 2.90-2.80 (m, 1H), 2.79-2.65 (m, 2H), 2.61-2.54 (m, 1H), 2.19-2.08 (m, 2H), 1.73-1.48 (m, 6H), 1.39-1.29 (m, 1H), 1.14 (d, *J* = 4.0 Hz, 3H), 1.11-0.99 (m, 1H) (OH proton was not detected); ¹³C NMR (125 MHz, CDCl₃) δ 219.8, 88.1, 63.1, 55.3, 45.0, 43.8, 40.3, 33.7, 32.2, 26.9, 26.8, 14.6; HRMS (EI) calculated for C₁₂H₁₈O₂ (M⁺) 194.1307, found 194.1308.



Preparation of triquinane 84. MsCl (0.032 mL, 0.41 mmol) was added dropwise to a solution of **83** (46 mg, 0.24 mmol) in 3 mL DCM at the temperature of 0 °C, and NEt₃ (0.16 mL, 1.1 mmol) was added to the solution immediately afterwards. The reaction was

stirred under argon and was monitored by TLC until the complete consumption of the starting material (typically < 1 h). The reaction was then quenched by the addition of 2 mL 10% HCl solution. The two layers were separated and the aqueous layer was extracted with DCM (3x5 mL). The combined organic layers were washed with water (5 mL) and brine (5 mL), dried over MgSO₄ and concentrated to give the crude product as pale yellow oil. Flash chromatography (silica gel, 230-400 mesh, 5:10:1 Et₂O/Hexane/DCM) of the crude product gave 30 mg (0.17 mmol, 88%) of enone **84** as a colorless oil: R_f = 0.40 (5:5:1 Et₂O:Hexane: DCM); IR (CDCl₃ cast film; microscope) 2946, 2864, 1698, 1638 cm⁻¹; ¹H NMR (500 MHz, CDCl₃) δ 3.23-3.10 (m, 2H), 2.76-2.56 (m, 3H), 2.02 (d, *J* = 12.0 Hz, 2H), 1.86-1.73 (m, 2H), 1.60-1.44 (m, 3H), 1.42-1.34 (m, 1H), 1.20 (d, *J* = 8.0 Hz, 3H); ¹³C NMR (125 MHz, CDCl₃) δ 207.2, 186.5, 146.0, 49.1, 46.7, 46.6, 35.3, 33.1, 32.2, 30.0, 26.2, 17.0; HRMS (EI) calculated for C₁₂H₁₆O (M⁺) 176.1201, found 176.1198.



Preparation of triquinane 86. 10 mol% Pd/C (2.0 mg, 0.0018 mmol) was added to a solution of **84** (3.2 mg, 0.018 mmol) in EtOAc (0.5 mL) in a 10 mL round bottom flask. The reaction was monitored by TLC, and the mixture was stirred under H₂ (balloon pressure) for 0.5 h until the starting material was completely consumed. The mixture was then filtered over Celite and concentrated with rotatory evaporator. Flash chromatography (silica gel, 230-400 mesh, 3% EtOAc/Hexane) of the crude product afforded 2.8 mg (0.016 mmol, 88%) of the reduced product **86** as a colorless oil: R_f = 0.31 (5% EtOAc/Hexane); IR (CDCl₃ cast film; microscope) 2960, 2870, 1723 cm⁻¹; ¹H NMR (500 MHz, CDCl₃) δ 2.80-2.60 (m, 3H), 2.38-2.22 (m, 1H), 2.20-2.10 (m, 1H), 2.09-2.00 (m, 1H), 1.73-1.52 (m, 6H), 1.40-1.21 (m, 3H), 1.15 (d, *J* = 8.0 Hz, 3H); ¹³C NMR (125 MHz, CDCl₃) δ 221.6, 55.6, 47.3, 46.2, 46.1, 43.1, 33.8, 32.7, 32.1, 27.9, 27.6, 14.5; HRMS (EI) calculated for C₁₂H₁₈O (M⁺) 178.1357, found 178.1356.

2.6 References and Notes

1. (a) Mehta, G.; Srikrishna, A., *Chem. Rev.* **1997**, *97*, 671-720; (b) Singh, V.; Thomas, B., *Tetrahedron* **1998**, *54*, 3647-3692.
2. (a) Bohlman, F.; Jakupovic, J., *Phytochem.* **1980**, *19* (259-265); (b) Dominguez, K. A.; Cano, C.; France, R.; Villareal, A. M.; Watson, W. H.; Zabel, V., *Phytochem.* **1980**, *19*, 2478; (c) Corbett, R. E.; Lauren, D. R.; Weavers, R. T., *J. Chem. Soc., Perkin. Trans.* **1979**, *1*, 1774-1790; (d) Kaneda, M.; Takahashi, R.; litaka, Y.; Shibata, S., *Tetrahedron Lett.* **1972**, *13*, 4609-4611.
3. (a) Sheikh, Y. M.; Singy, G.; Kaisin, M.; Eggert, H.; Djerassi, C.; Tursch, B.; Daloze, D.; Braekman, J. C., *Tetrahedron* **1976**, *32*, 1171-1178; (b) Kaisin, M.; Sheikh, Y. M.; Durham, L. J.; C., D.; Tursch, B.; Daloze, D.; Braekman, J. C.; Losman, D.; R., K., *Tetrahedron Lett.* **1974**, *75*, 2239-2242; (c) Ayanoglu, E.; Gebreyesus, T.; Beechan, C. M.; Djerassi, C.; Kaisin, M., *Tetrahedron Lett.* **1978**, *19*, 1671-1674.
4. (a) Martin, D. G.; Slomp, G.; Mizensak, S.; Duchamp, D. J.; Chidester, C. G., *Tetrahedron Lett.* **1970**, *11*, 4901-4904; (b) Comer, F. W.; McCapra, F.; Qureshi, I. H.; Scott, A. I., *Tetrahedron* **1967**, *23*, 4761-4768; (c) Shuji, T.; Naganawa, H.; Iinuma, H.; Takita, T.; Maeda, K.; Umezawa, H., *Tetrahedron Lett.* **1971**, *12*, 1955-1958; (d) Nakamura, H.; Takita, T.; Umezawa, H.; Kunishima, M.; Nakayama, Y.; Itaka, Y., *J. Antibiot.* **1974**, *27*, 301-302; (e) Nozoe, S.; Furukawa, J.; Sankawa, U.; Shibata, S., *Tetrahedron Lett.* **1976**, *17*, 195-198; (f) Ranieri, R. L.; Calton, G. J., *Tetrahedron Lett.* **1978**, *19*, 499-502.
5. (a) Eaton, P. E.; Mueller, R. H.; Carlson, G. R.; Cullison, D. A.; Cooper, G. F.; Chou, T. C.; Krebs, E. P., *J. Am. Chem. Soc.* **1977**, *99*, 2751-2767; (b) Eaton, P. E.; Mueller, R. H., *J. Am. Chem. Soc.* **1972**, *94*, 1014-1016; (c) Paquette, L. A.; Balogh, D. W.; Usha, R.; Koontz, D.; Christopher, G. C., *Science* **1981**, *211*, 575-576.
6. (a) Takeuchi, T.; Iinuma, H.; Iwanaga, J.; Takahashi, S.; Takita, T.; Umezawa, H., *J. Antibiot.* **1969**, *22*, 215-217; (b) Tatsuta, K.; Akimoto, K.; Kinoshita, M., *J. Antibiot.* **1980**, *23*, 100-102.
7. Comer, F. W.; Trotter, J., *J. Chem. Soc.* **1966**, *6*, 11-18.

8. (a) Burkholder, P.; Burkholder, L., *Science* **1958**, *127*, 1174-1175; (b) Ciereszko, L. S., *Trans. N.Y. Acad. Sci.* **1962**, *24*, 502-503; (c) Stille, J. R.; Grubbs, R. H., *J. Am. Chem. Soc.* **1986**, *108*, 855-856; (d) Mehta, G.; Murthy, N. A.; Reddy, S. D.; Reddy, V. A., *J. Am. Chem. Soc.* **1986**, *108*, 3443-3452.
9. (a) Feline, T. C.; Mellows, G.; Jones, R. B.; Phillips, L., *J. Chem. Soc., Chem. Commun.* **1974**, *1974*, 63-64; (b) Ohfuné, Y.; Shirahama, H.; Matsumoto, T., *Tetrahedron Lett.* **1976**, *17*, 2795-2796; (c) Misumi, S.; Matsushima, H.; Shirahama, H.; Matsumoto, T., *Chem. Lett.* **1982**, *11*, 855-858.
10. (a) Mehta, G.; Pallavi, K., *Tetrahedron Lett.* **2006**, *47*, 8355-8360; (b) Chandler, C. L.; List, B., *J. Am. Chem. Soc.* **2008**, *130*, 6737-6739.
11. (a) Srikrishna, A.; Dethe, D. H., *Org. Lett.* **2003**, *5*, 2295-2298; (b) Srikrishna, A.; Beeraish, B., *Tetrahedron: Asymmetry* **2008**, *19*, 884-886; (c) Rieder, C. J.; Fradette, R. J.; West, F. G., *Chem. Commun.* **2008**, *13*, 1572-1574.
12. (a) Marino, J. P.; Laborde, E., *J. Am. Chem. Soc.* **1985**, *107*, 734-735; (b) Lee, H.-Y.; Kim, Y., *J. Am. Chem. Soc.* **2003**, *125*, 10156-10157.
13. Veretenov, A. L.; Koltun, D. O.; Smit, W. A.; Strelenko, Y. A., *Tetrahedron Lett.* **1995**, *36*, 4651-4654.
14. (a) Little, R. D.; Muller, G. W., *J. Am. Chem. Soc.* **1981**, *103*, 2744-2749; (b) Little, R. D.; Muller, G. W., *J. Am. Chem. Soc.* **1979**, *101*, 7129-7130; (c) Little, R. D.; Carroll, G. L., *Tetrahedron Lett.* **1981**, *22*, 4389-4392.
15. Wender, P. A.; Howbert, J. J., *Tetrahedron Lett.* **1982**, *23*, 3983-3986.
16. (a) Curran, D. P.; Rakiewicz, D. M., *J. Am. Chem. Soc.* **1985**, *107*, 1448-1449; (b) Fevig, T. L.; Elliott, R. L.; Curran, D. P., *J. Am. Chem. Soc.* **1988**, *110*, 5064-5067.
17. (a) Rawal, V. H.; Dufour, C., *J. Am. Chem. Soc.* **1994**, *116*, 2613-2614; (b) Rawal, V. H.; Dufour, C.; Iwasa, S., *Tetrahedron Lett.* **1995**, *36*, 19-22.
18. Rawal, V. H.; Dufour, C.; Eschbach, A., *J. Chem. Soc., Chem. Commun.* **1994**, *1994*, 1797-1798.
19. Rawal, V. H.; Fabre, A.; Iwasa, S., *Tetrahedron Lett.* **1995**, *36*, 6851-6854.
20. Demuth, M.; Schaffner, K., *Angew. Chem. Int. Ed. Engl.* **1982**, *21*, 820-836.
21. Singh, V.; Vedantham, P.; Sahu, P. K., *Tetrahedron Lett.* **2002**, *43*, 519-522.

22. Balme, G.; Bouyssi, D., *Tetrahedron* **1994**, *50*, 403-414.
23. Santora, V. J.; Moore, H. W., *J. Am. Chem. Soc.* **1995**, *117*, 8486-8487.
24. (a) Li, L.; McDonald, R.; West, F. G., *Org. Lett.* **2008**, *10*, 3733-3736; (b) Li, L. Ph.D. Dissertation, University of Alberta, Edmonton, 2009.
25. (a) West, F. G.; Chase, C. E.; Arif, A. M., *J. Org. Chem.* **1993**, *58*, 3794-3795; (b) Chase, C. E.; Bender, J. A.; West, F. G., *Synlett.* **1996**, 1173-1175; (c) Li, L.; Chase, C. E.; West, F. G., *Chem. Commun.* **2008**, *13*, 4025-4027.
26. Moreno-Manas, M.; Ribas, J.; Virgili, A., *J. Org. Chem.* **1988**, *53*, 5328-5335.
27. (a) Dahlen, A.; Hilmersson, G., *Tetrahedron Lett.* **2002**, *43*, 7197-7200; (b) Dahlen, A.; Hilmersson, G., *Tetrahedron Lett.* **2003**, *44*, 2661-2664; (c) Dahlen, A.; Hilmersson, G., *Chem. Eur. J.* **2003**, *9*, 1123-1128; (d) Girard, P.; Namy, J. L.; Kagan, H. B., *J. Am. Chem. Soc.* **1980**, *102*, 2693-2698.

CHAPTER 3

CONCLUSIONS AND FUTURE PLANS

3.1 Conclusions of the Prion and Triquinane Projects

In this thesis, we first reported a concise and effective synthetic route to synthesize and purify a library of porphyrin-based multimeric fluorescent compounds with anticipated anti-prion activity, and nine such molecules have been synthesized, purified and characterized by using either quinoline or 9-amino-acridine as the binding units. The anti-prion assay results of the six quinoline-linked target molecules have been obtained, but they are unexpectedly ineffective in reducing the amount of PrP^{Sc} *in vitro*, which may suggest that other porphyrin-based multimeric compounds are not likely to have strong anti-prion activity as well. In contrast, three arene-based multimeric compounds prepared by another group member show promising anti-prion activity.

In the second chapter, the studies toward the formation of linear triquinanes with natural *cis-anti-cis* configuration via pyran-2-one photochemistry were discussed. Linear triquinanes with unnatural *cis-syn* configuration were readily available from substituted pyran-2-ones in a concise route of [4+4] photochemistry/thermal decarboxylation/MeLi-mediated rearrangement.¹ Hydrogenation and subsequent dehydration produced an enone. Reduction of the enone presented an opportunity to obtain the natural *cis-anti-cis* configuration. Different reduction conditions were tried, but they were either ineffective in reduction or gave the product with *cis-syn-cis* configuration. Reduction under thermodynamic control (Li, liq. NH₃) is still underway to get to the desired natural configuration.

3.2 Future Directions of The Research Projects

3.2.1 Future Plan of the Prion Project

Since three arene-based trimeric compounds have been identified by the anti-prion assay to have strong capability in reducing the amount of PrP^{Sc} *in vitro* (**Figure 1.19**), it suggests that such compounds with a linker of 1,2-ethanediamine or 1,3-propanediamine can better fix the space of aggregate of PrP^{Sc} and thus bind to them effectively. Therefore, new series of arene-based multimeric molecules can be envisioned by employing different binding units. Some compounds that already show promising anti-prion activity can be selected as the mono-binding units, which may include 2-methylquinoline,² 2-phenylquinazoline,² acridines,²⁻³ and phenothiazine derivatives⁴ (**Figure 3.1**). In particular, fluorescent mono-binding units, 9-amino-acridines, will be of great interests in building arene-based fluorescent multimeric compounds. A fluorescent compound with high affinity towards PrP^{Sc} could represent a major breakthrough, since it would have the potential to both inhibit the propagation of PrP^{Sc} and detect the presence of infectious particles.

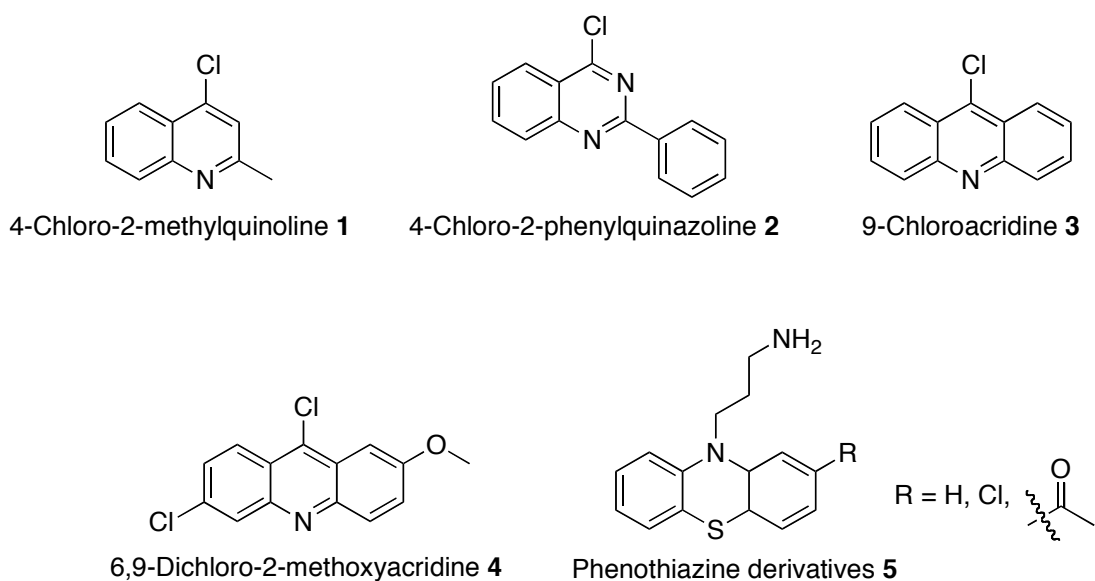


Figure 3.1 Structures of mono-binding units 1-5.

Compounds **6-8** in **Figure 3.2** can be prepared by heating the mixture of **1-4** and diamines as described in **Scheme 1.5**.⁵ Subsequently, the target molecules can be obtained through the amide bond formation of trimesic acid and compounds **5-8** (**Scheme 3.1**).

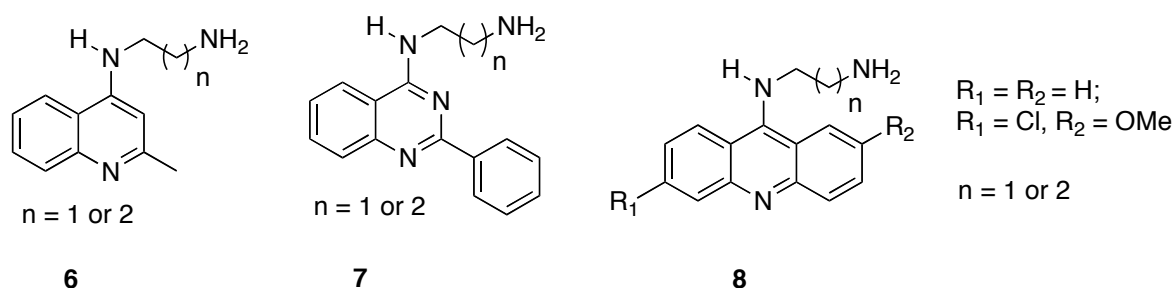
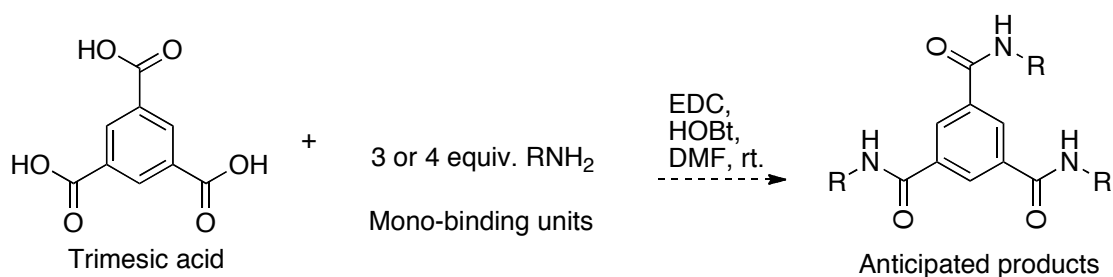
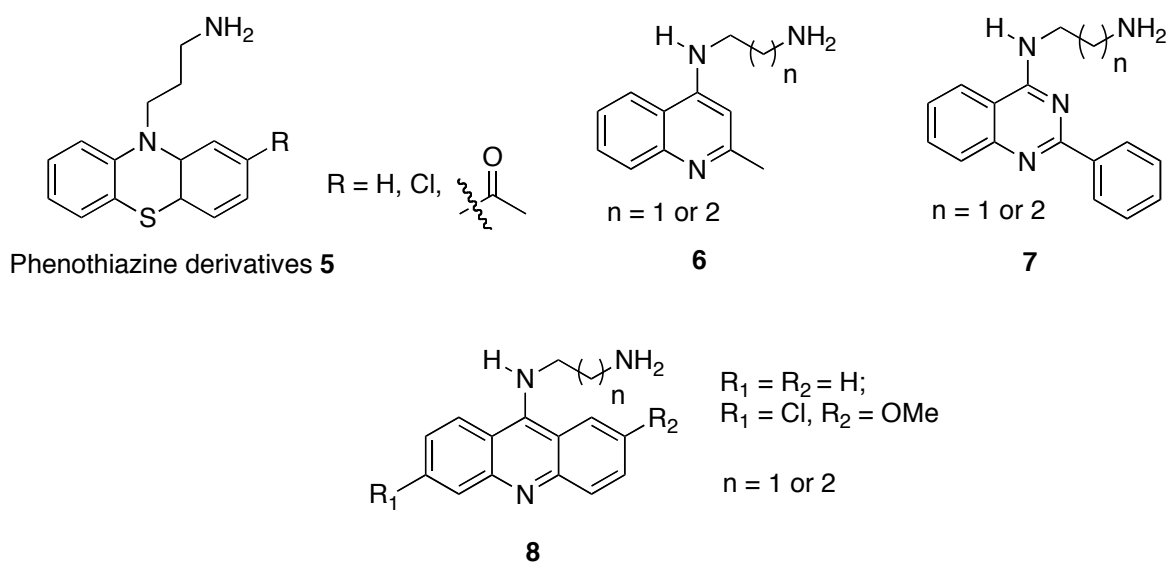


Figure 3.2 Structures of 2-methylquinoline-diamines **1**, 2-phenylquinoxaline-diamine **2**, acridine-diamines **3-4**.



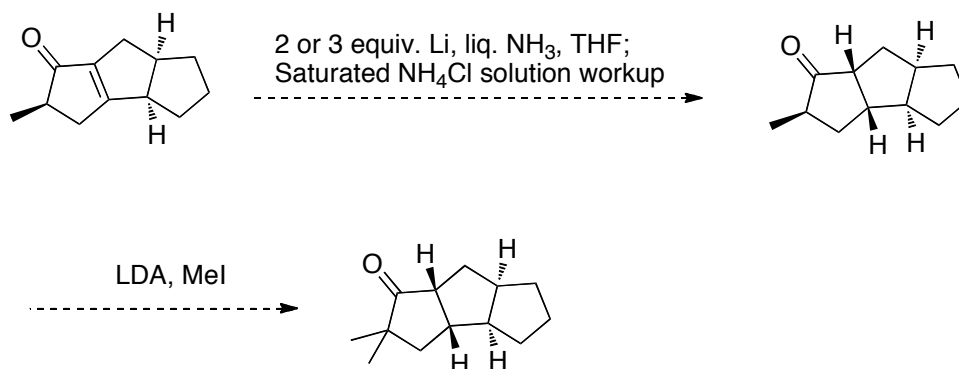
Mono-binding units **5-8**:



Scheme 3.1 Synthesis of arene-based trimesic compounds by using acridine or others as the binding units.

3.2.2 Future Plan of the Triquinane Project

Birch reduction under thermodynamic control may give rise to the product with natural *cis-anti-cis* configuration, and further methylation at α -position will set the gem dimethyl group which is commonly found in natural triquinane compounds (**Scheme 3.2**).



Scheme 3.2 Birch reduction and methylation at α -position.

Once the inversion of configuration strategy is fully developed, this overall route will be applied to one or more linearly fused triquinane natural products. Possible targets include hirsutene, ceratopical and cucumins.

3.3 References

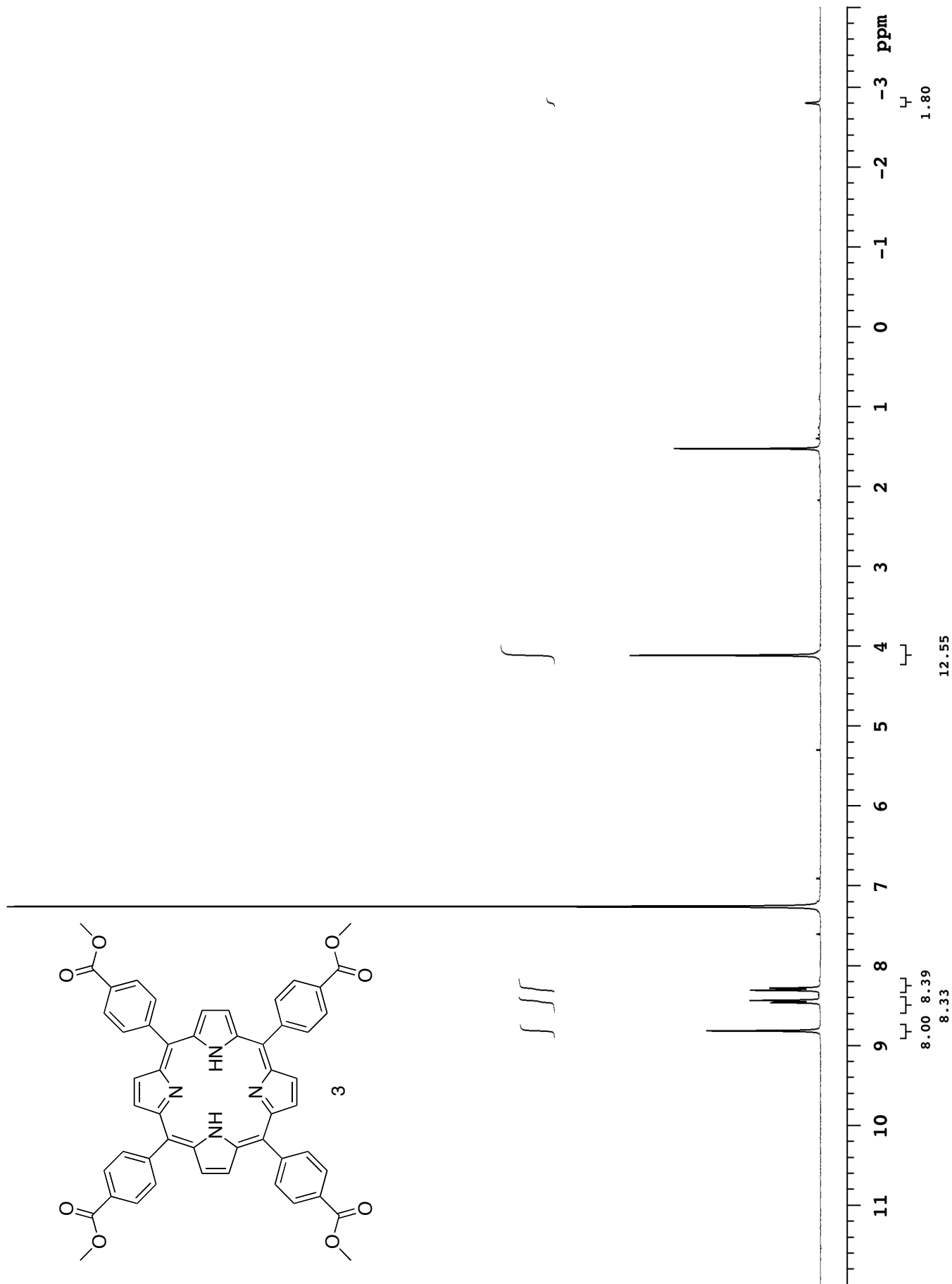
1. Li, L.; McDonald, R.; West, F. G., *Org. Lett.* **2008**, *10*, 3733-3736.
2. Cope, H.; Mutter, R.; Heal, W.; Pascoe, C.; Brown, P.; Pratt, S.; Chen, B., *European Journal of Medicinal Chemistry* **2006**, *41*, 1124-1143.
3. Barret, A.; Tagliavini, F.; Forloni, G.; Bate, C.; Salmons, M.; Colombo, L.; De Luigi, A.; Limido, L.; Suardi, S.; Rossi, G.; Auvre, F.; Adjou, K. T.; Sales, N.; Williams, A.; Lasmezas, C.; Deslys, J. P., *J. Virol.* **2003**, *77*, 8462-8469.
4. Korth, C.; May, B. C. H.; Cohen, F. E.; Prusiner, S. B., *Proc. Natl. Acad. Sci. USA* **2001**, *98*, 9836-9841.

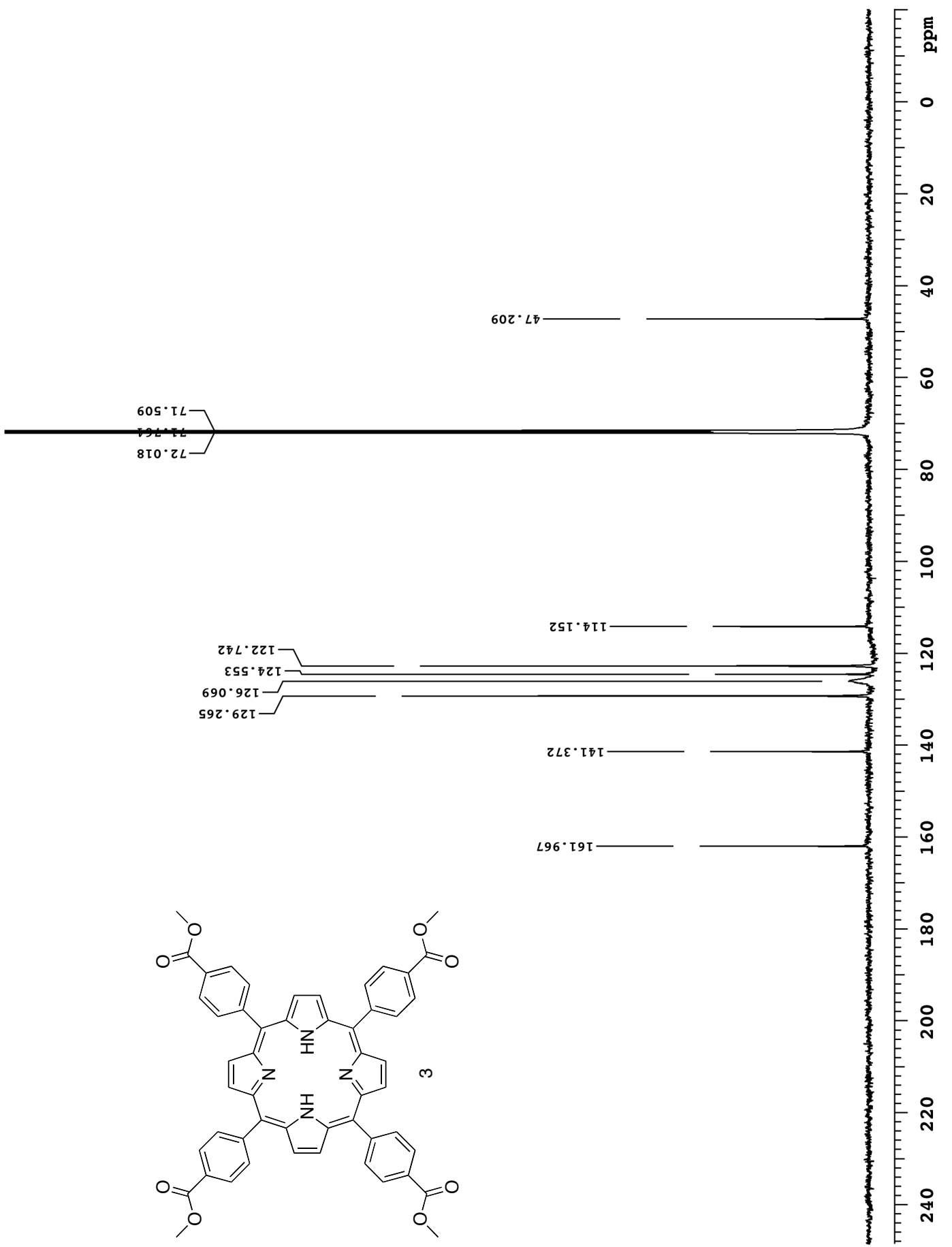
5. Chibale, K.; Haupt, H.; Kendrick, H.; Yardley, V.; Saravanamuthu, A.; Fairlamb, A. H.; Croft, S. L., *Bioorg. Med. Chem. Lett.* **2001**, *11*, 2655-2657.

APPENDIX A
SELECTED NMR SPECTRA FROM CHAPTER 1

Pulse Sequence: s2pul

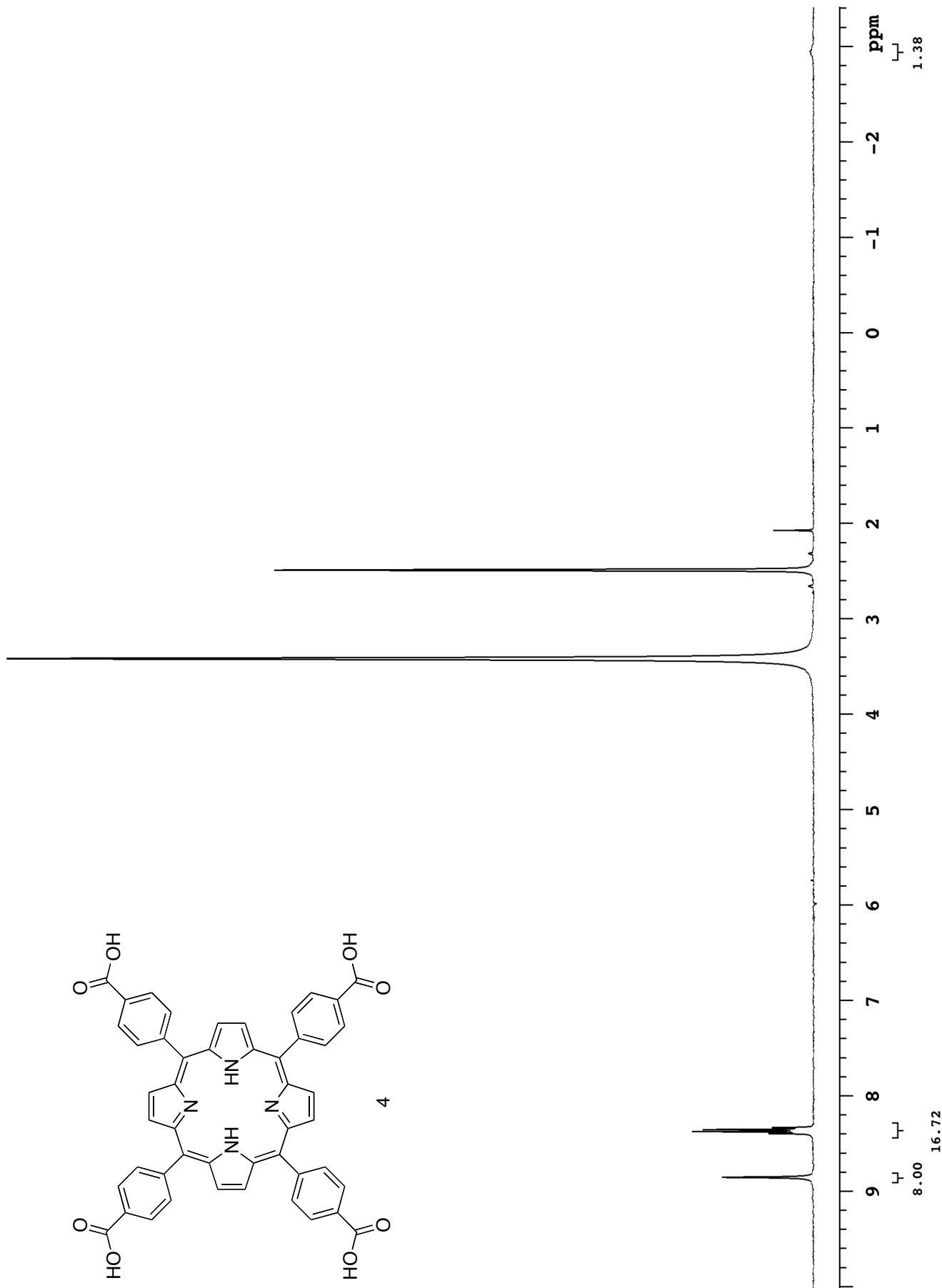
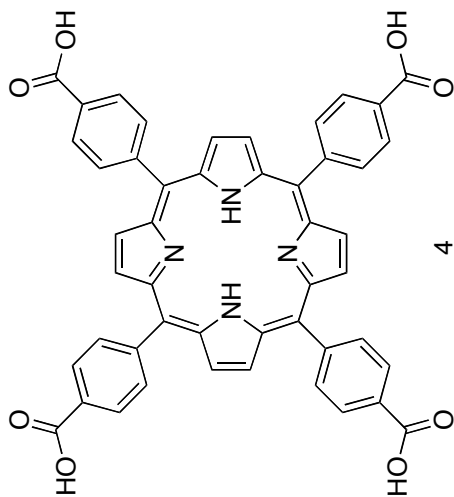
299.971 MHz H1 1D in cdcl3 (ref. to CDCl3 @ 7.26 ppm), temp 27.5 C -> actual temp = 27.0 C, id300 probe

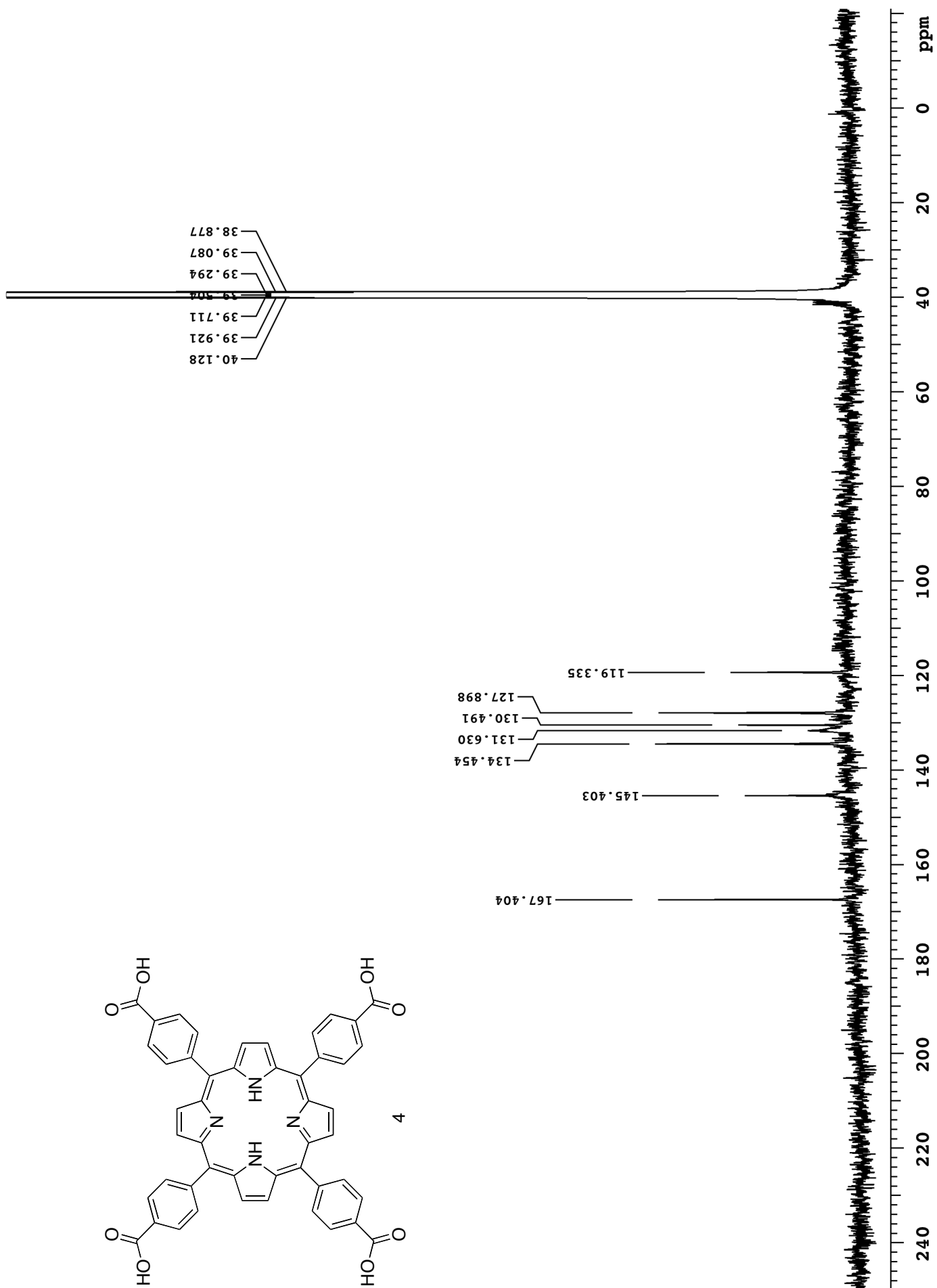




Pulse Sequence: s2pul

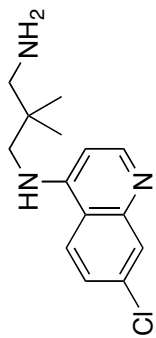
399.796 MHz H1 1D in dms0 (ref. to DMSO @ 2.49 ppm), temp 26.5 C -> actual temp = 27.0 C, autoudb probe



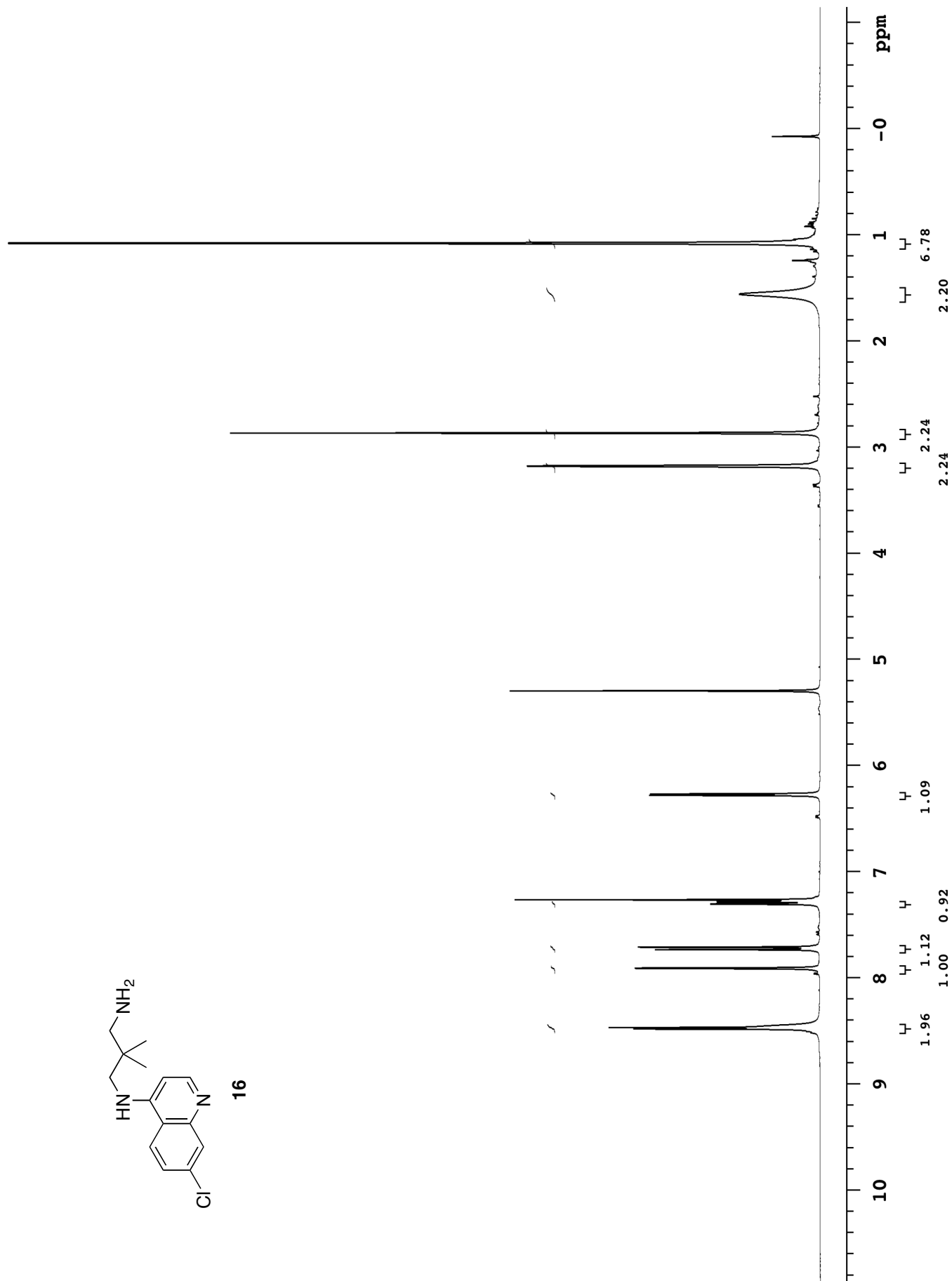


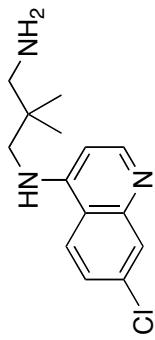
Pulse Sequence: s2pul

399.794 MHz H1 1D in cdcl3 (ref. to CDCl3 @ 7.26 ppm), temp 26.5 C -> actual temp = 27.0 C, autoxdb probe

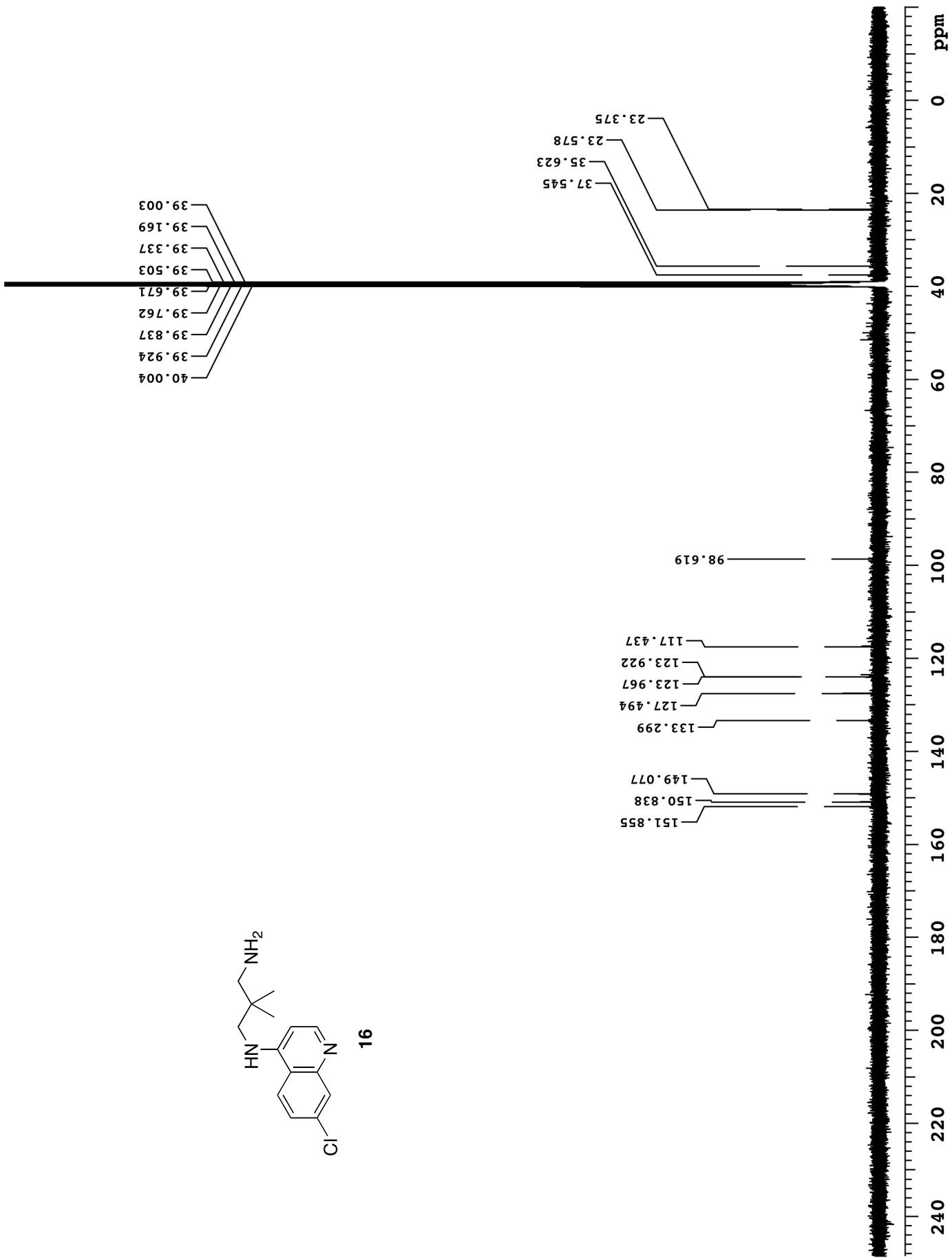


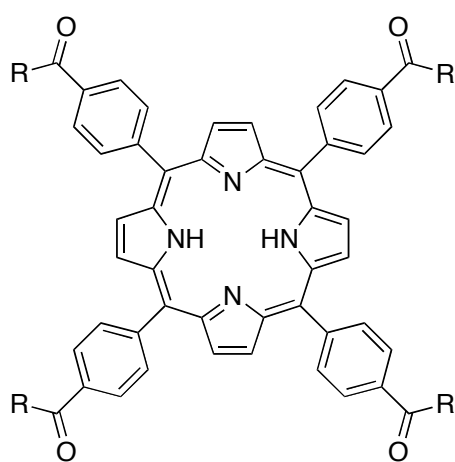
16





16

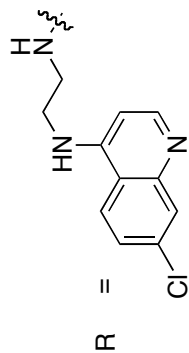




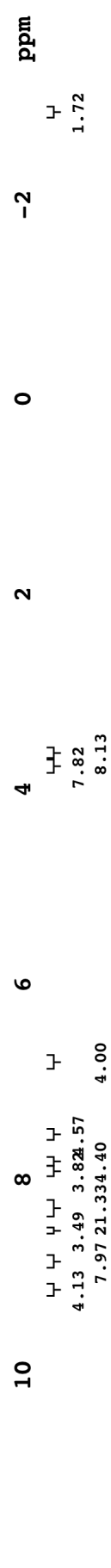
Generalized structure of compound **18-23** and **30-32**

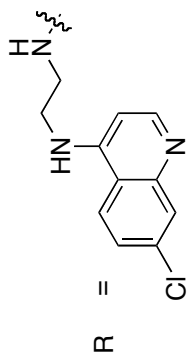
Pulse Sequence: s2pul

399.796 MHz H1 1D in dms0 (ref. to DMSO @ 2.49 ppm), temp 26.5 C -> actual temp = 27.0 C, autoxdb probe

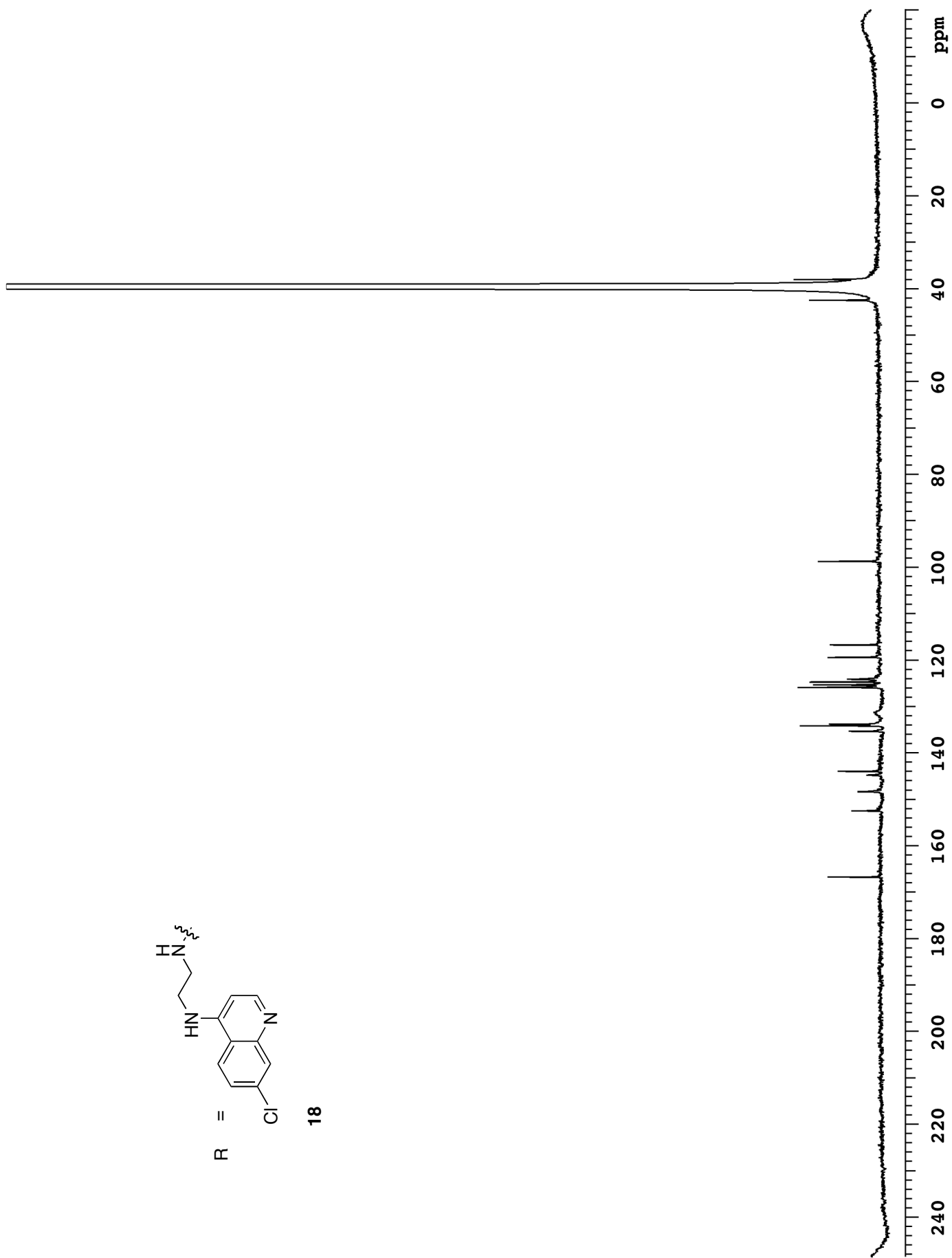


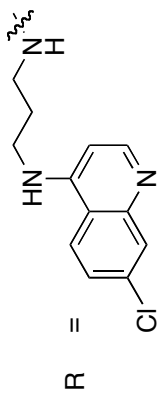
18



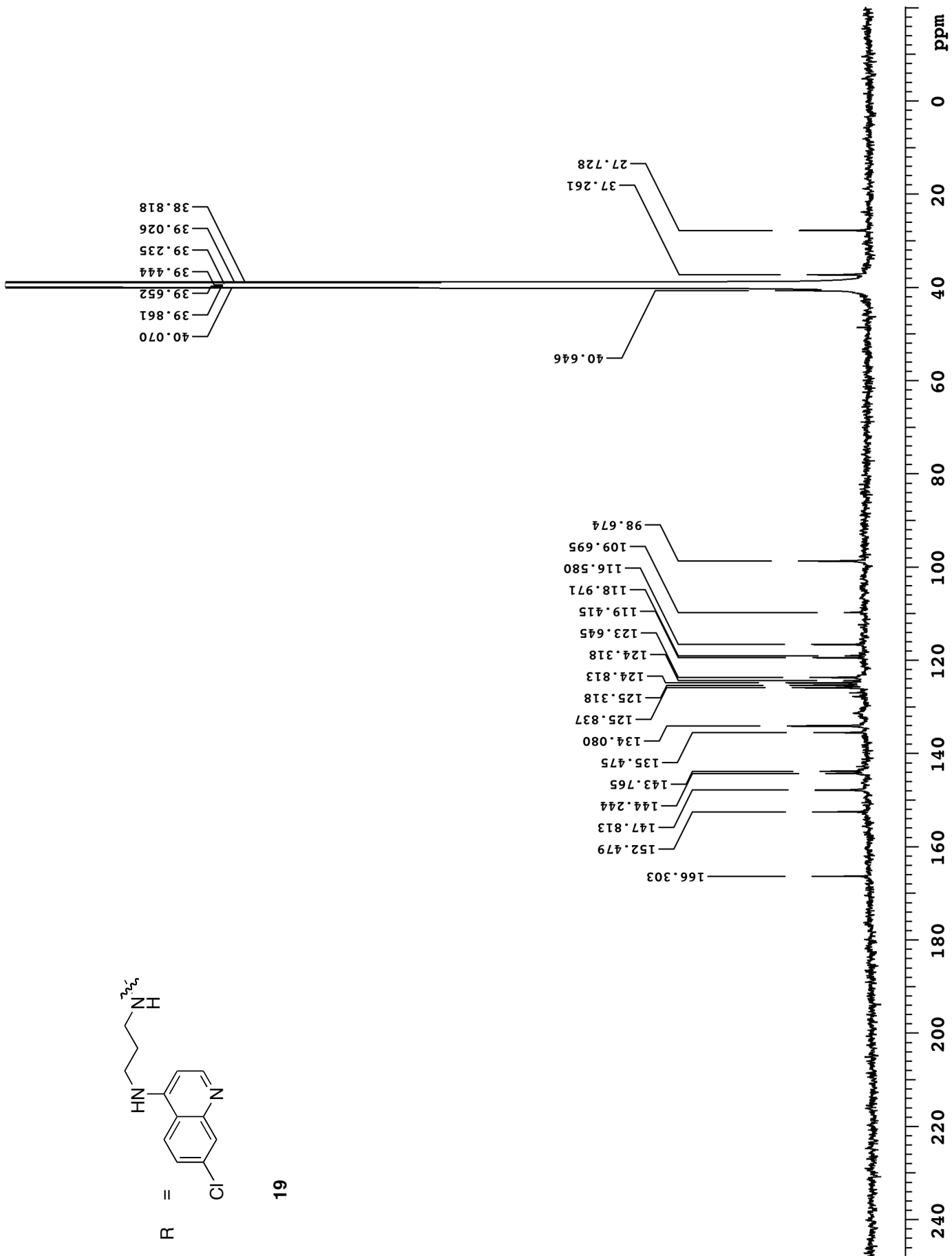


18



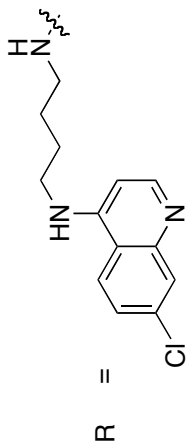


19

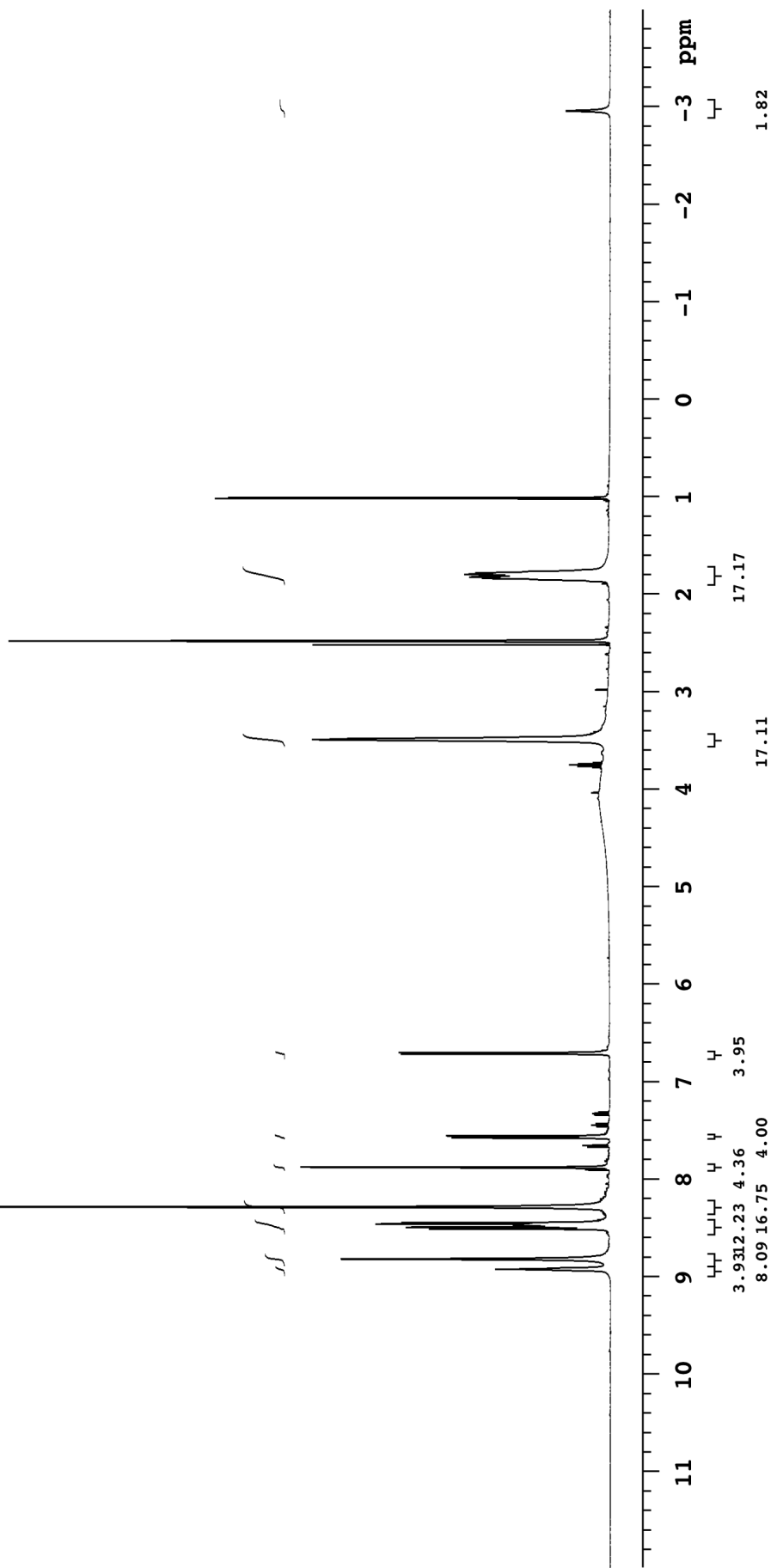


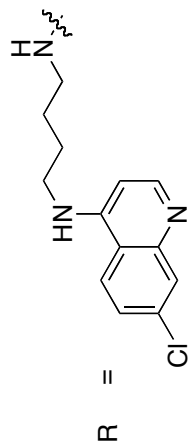
Pulse Sequence: s2pul

498.124 MHz H1 1D in dms0 (ref. to DMSO @ 2.49 ppm), temp 27.2 C -> actual temp = 27.0 C, autotx db probe

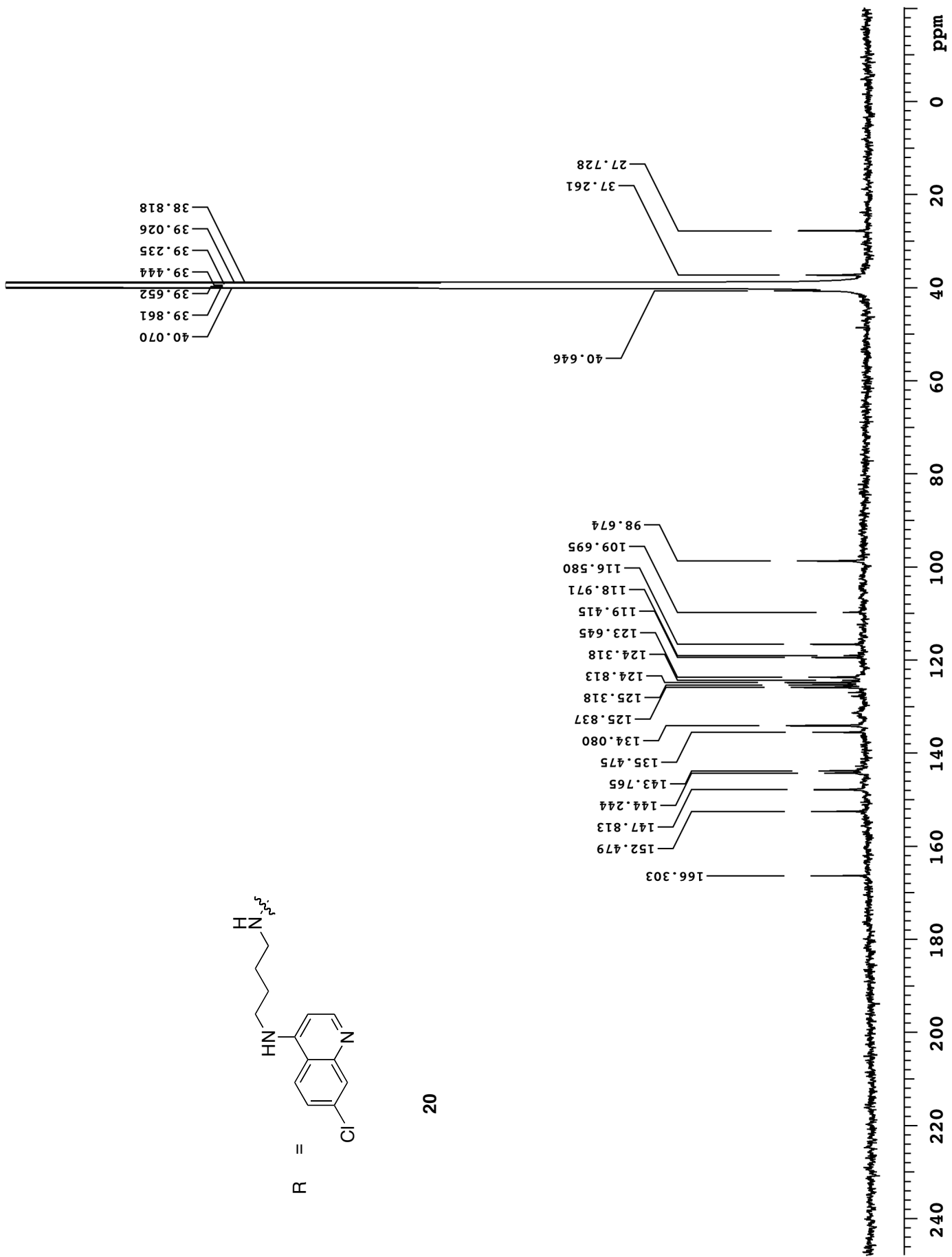


20



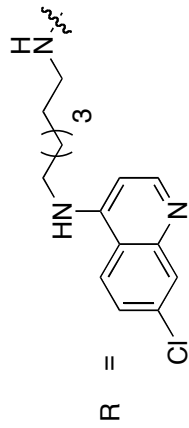


20

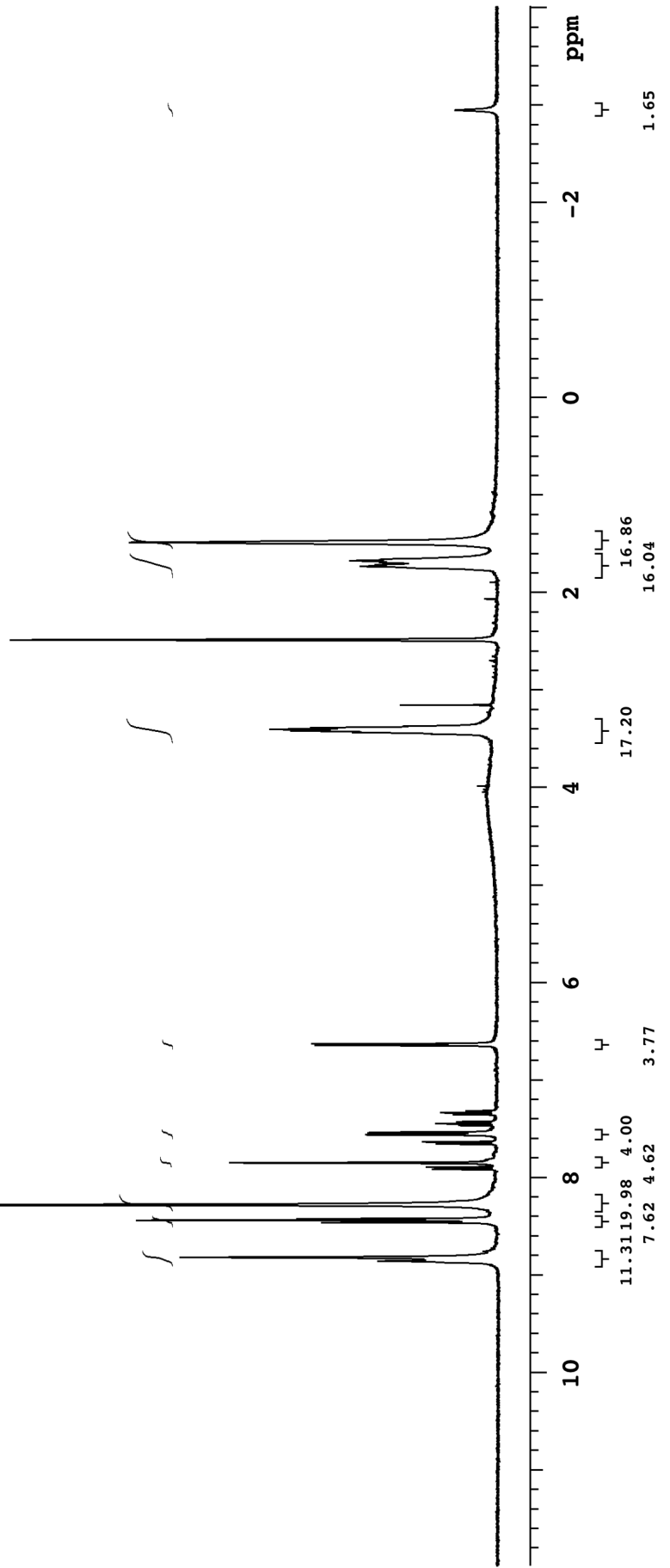


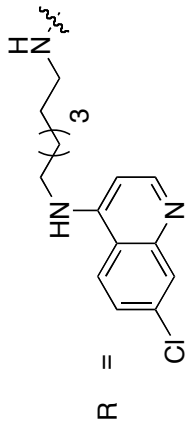
Pulse Sequence: s2pul

399.796 MHz H1 1D in dms0 (ref. to DMSO @ 2.49 ppm), temp 26.5 C -> actual temp = 27.0 C, autotxdb probe

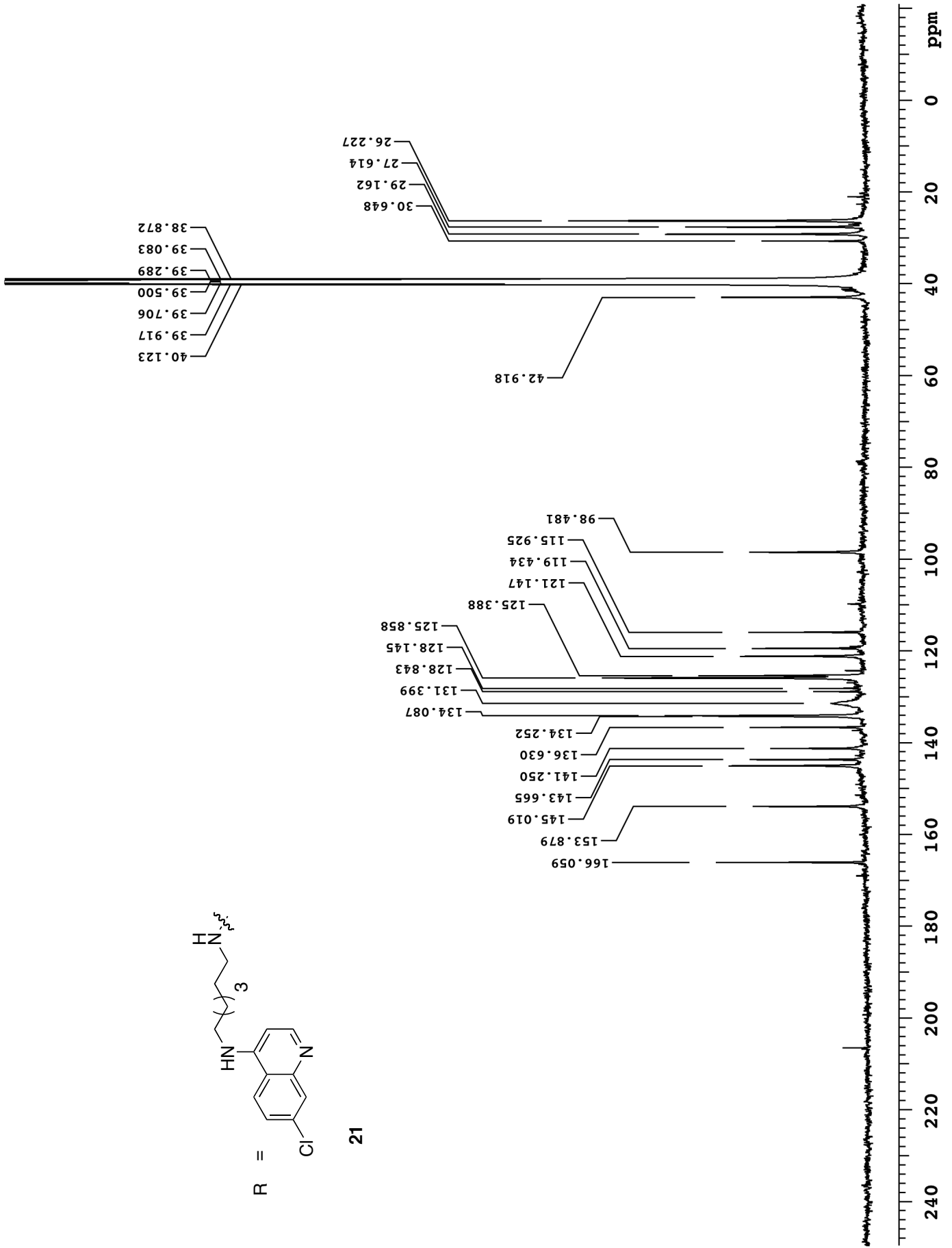


21



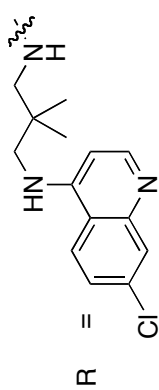


21

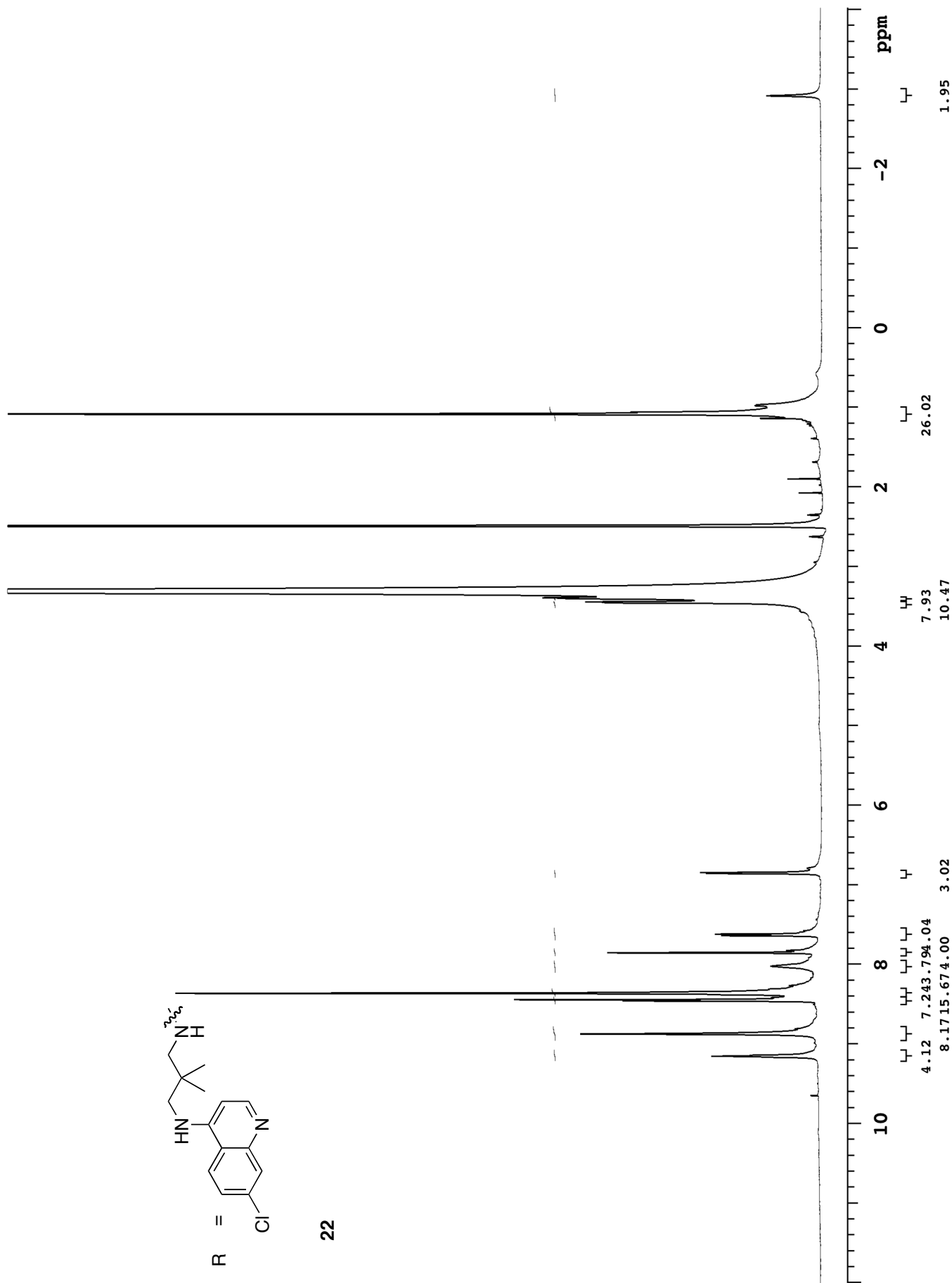


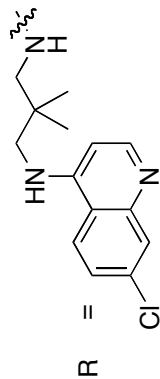
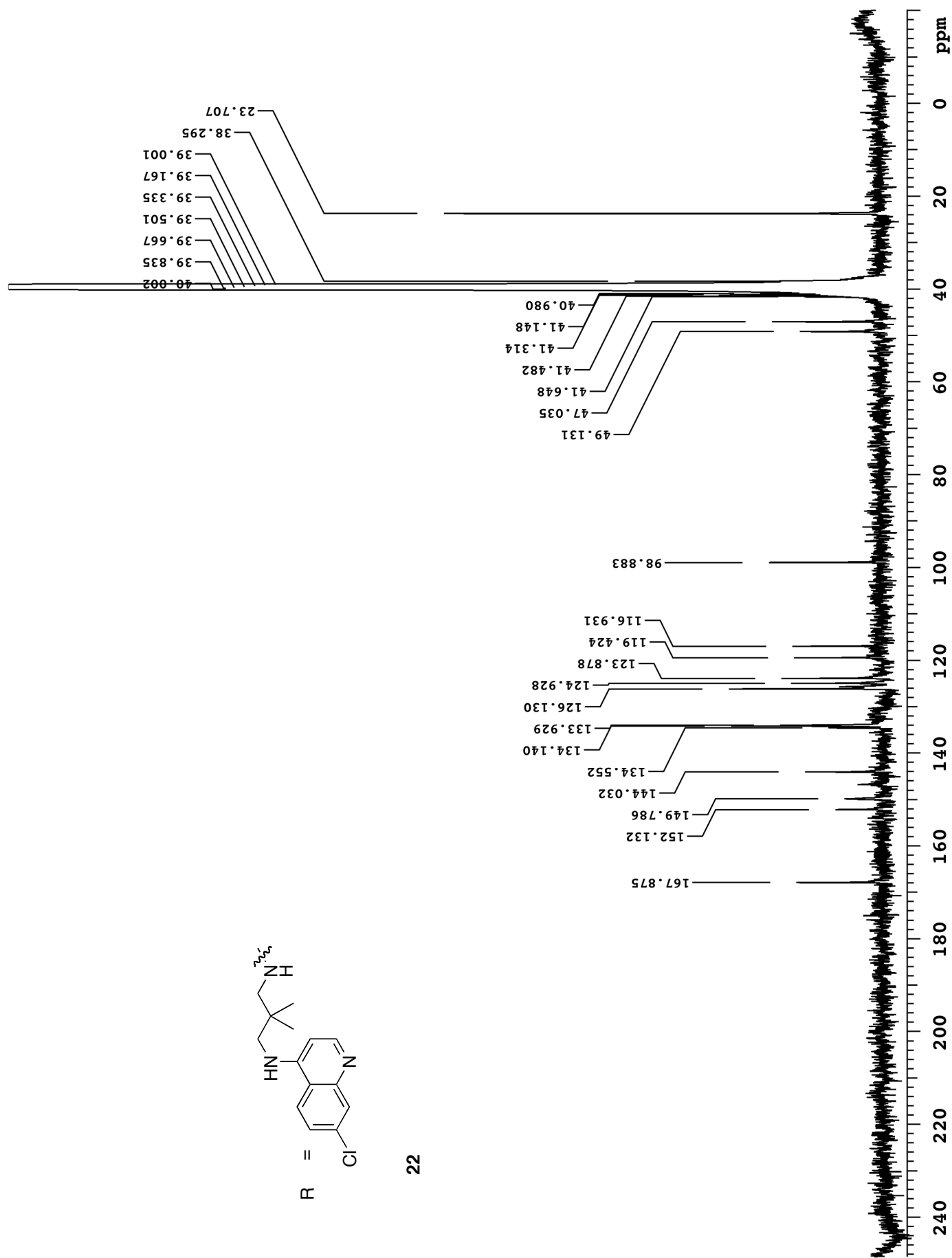
Pulse Sequence: s2pul

499.817 MHz H1 1D in dms0 (ref. to DMSO @ 2.49 ppm), temp 27.7 C -> actual temp = 27.0 C, coldddual probe



22

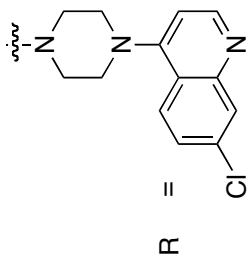




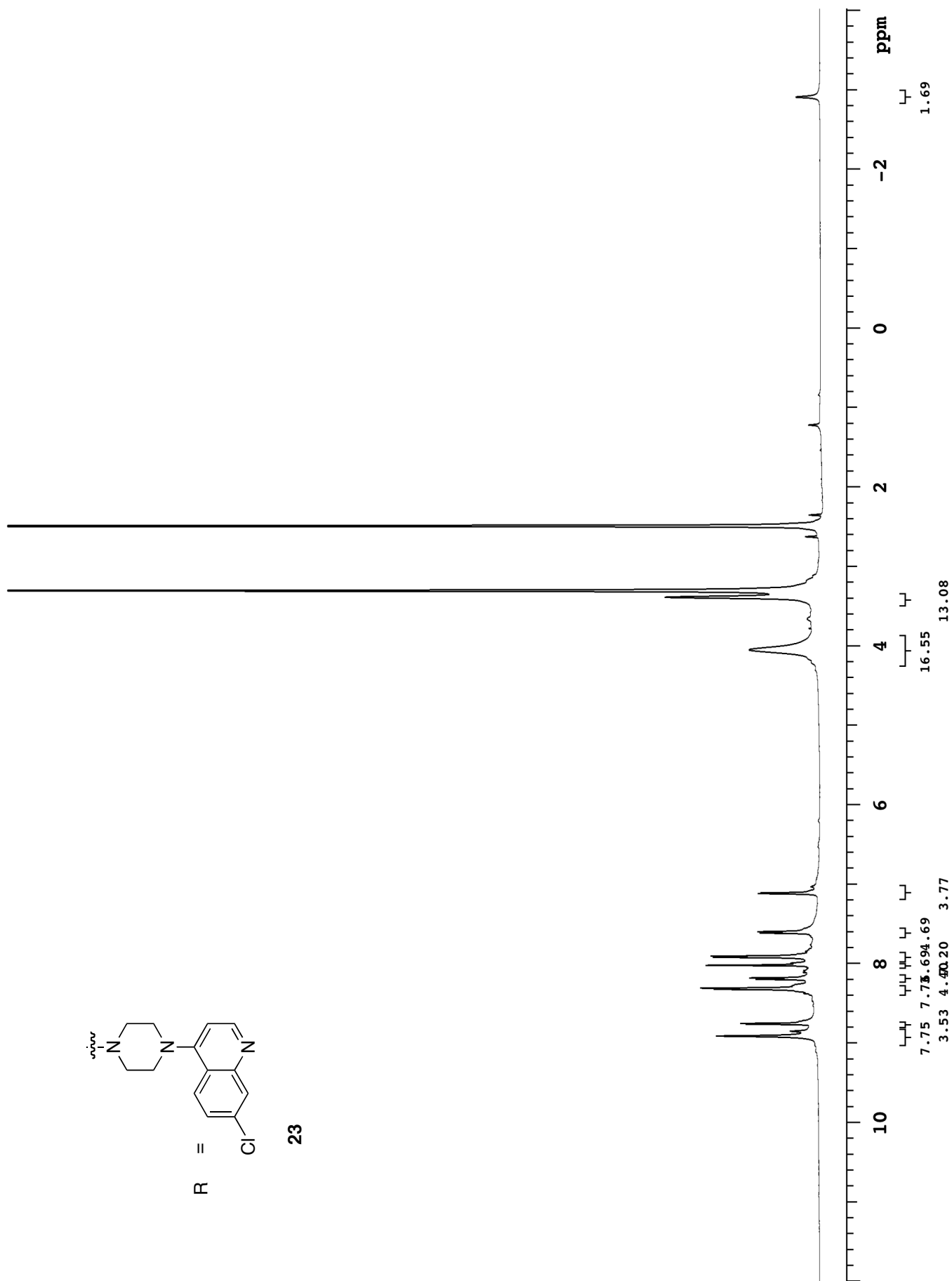
22

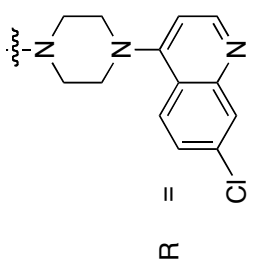
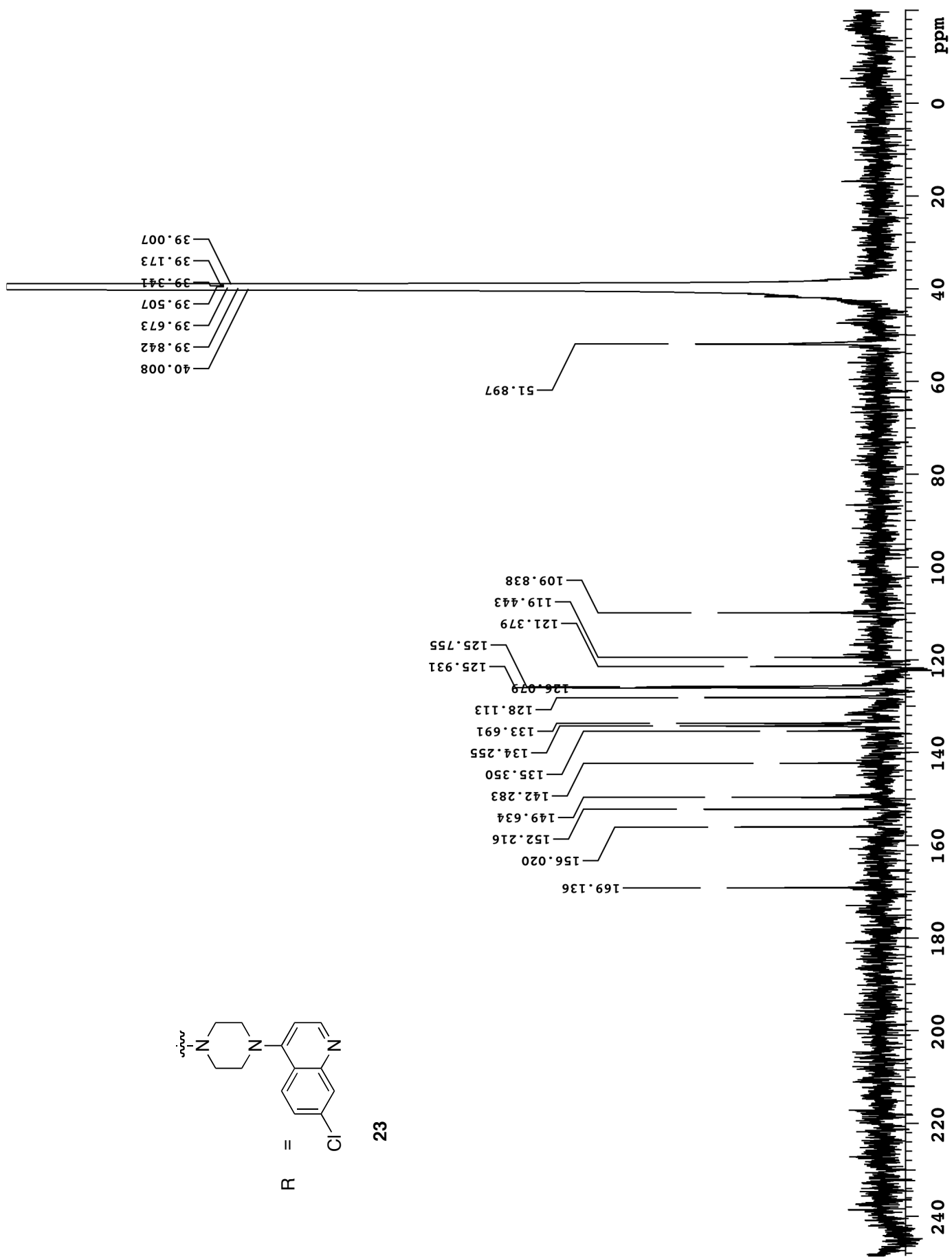
Pulse Sequence: s2pul

499.817 MHz H1 1D in dmso (ref. to DMSO @ 2.49 ppm), temp 27.7 C -> actual temp = 27.0 C, coldcdual probe

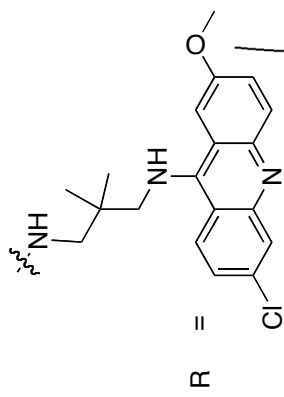


23

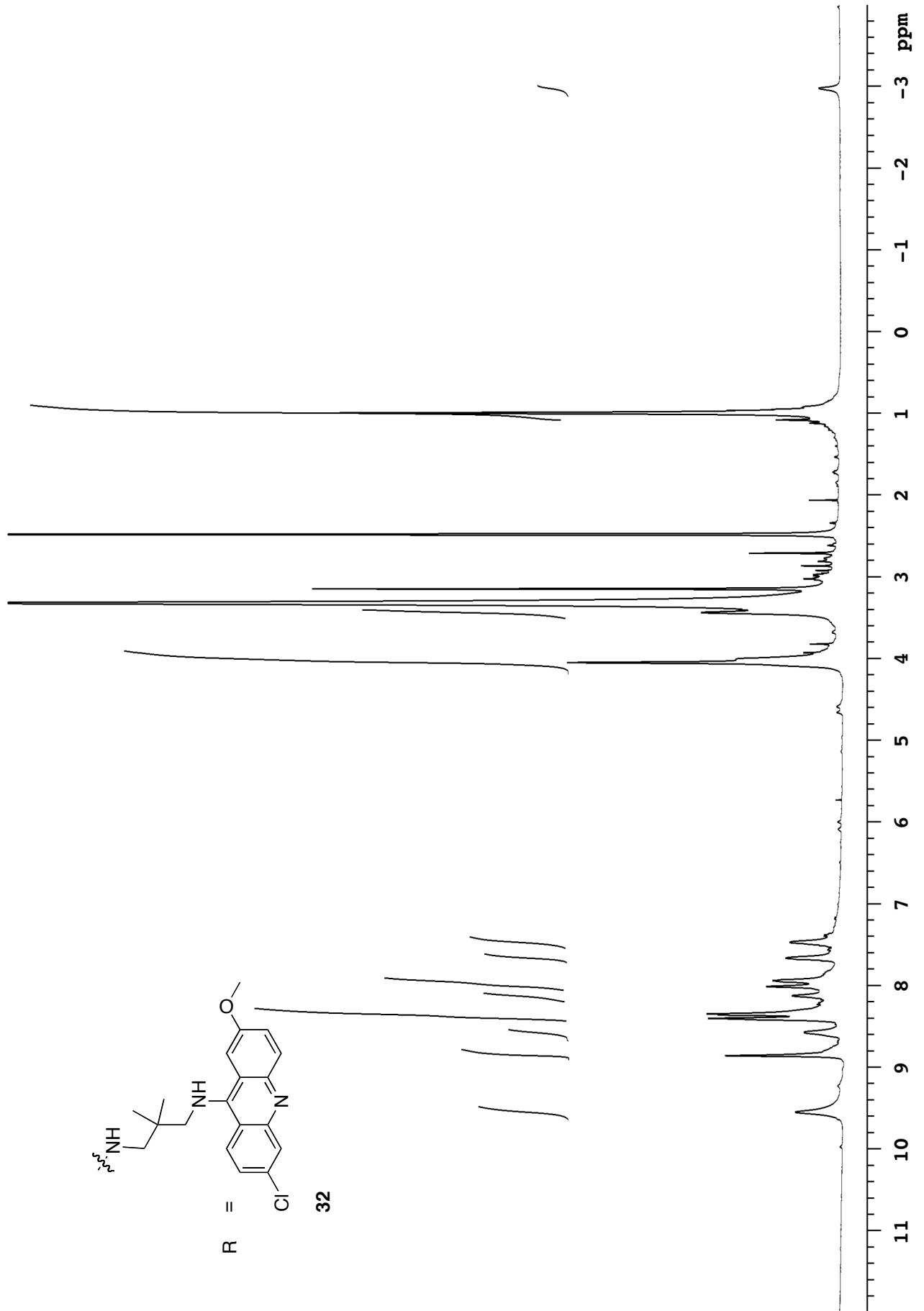


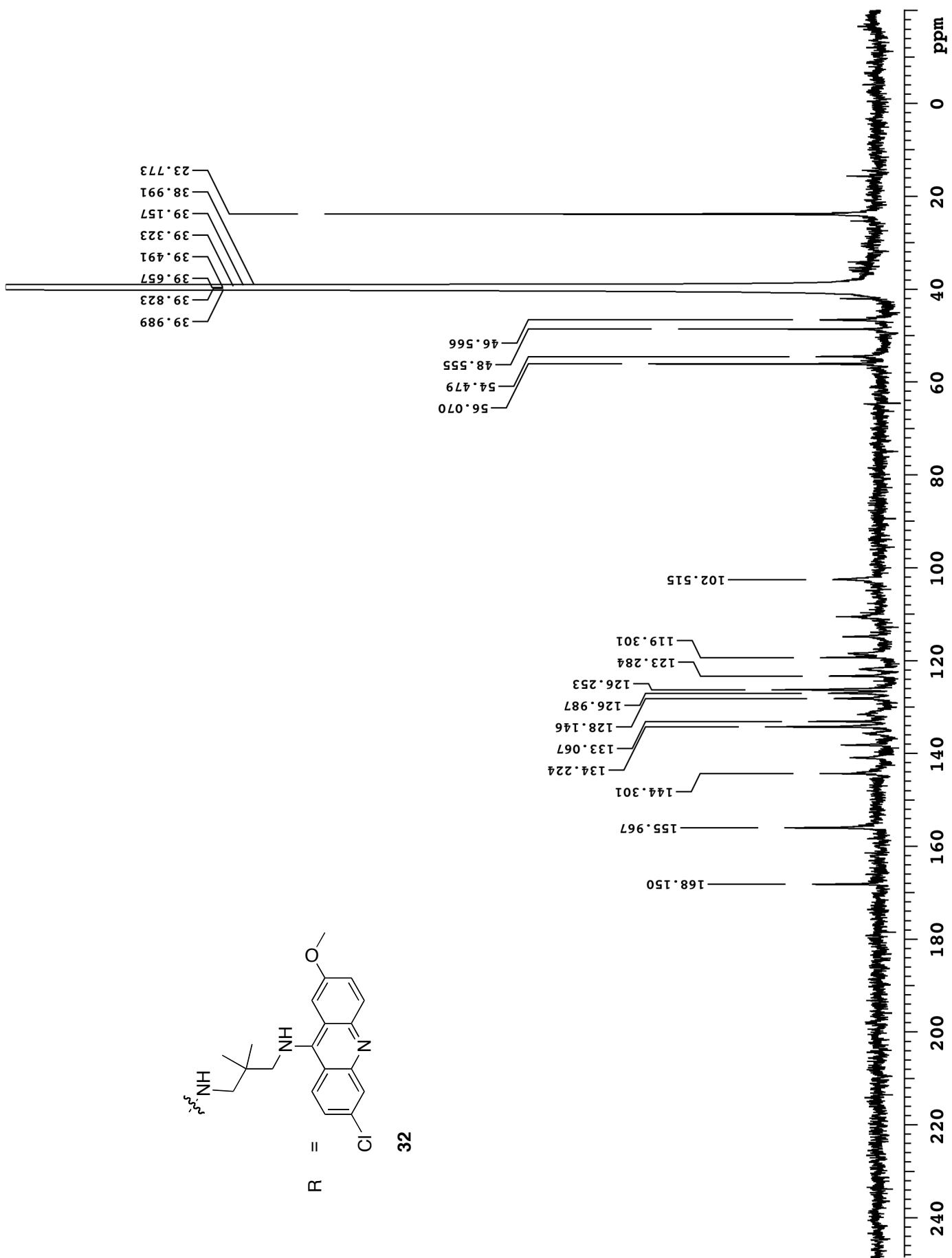


23

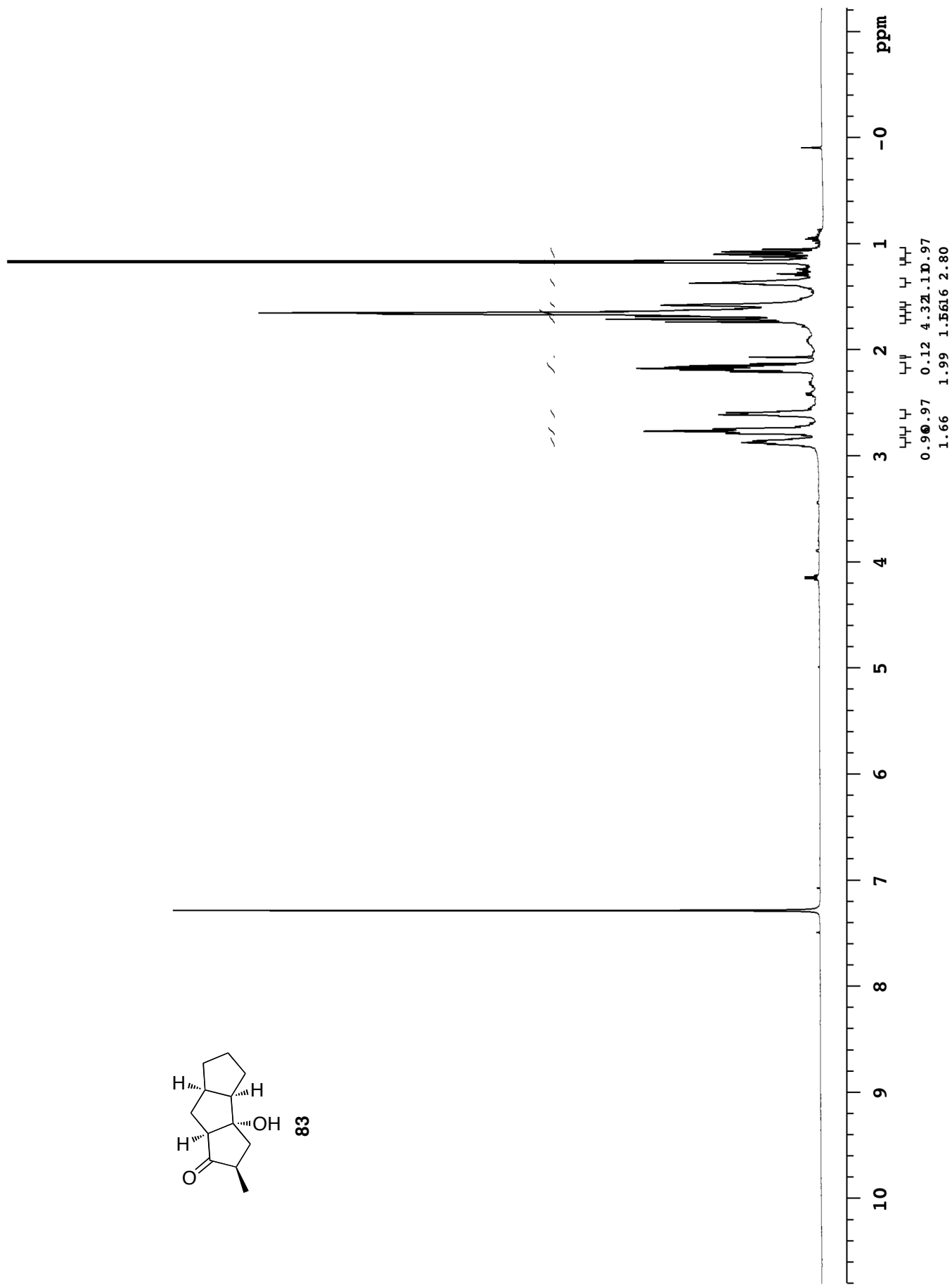
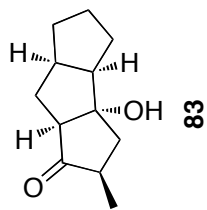


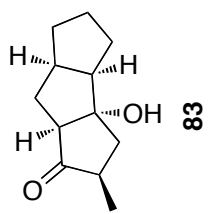
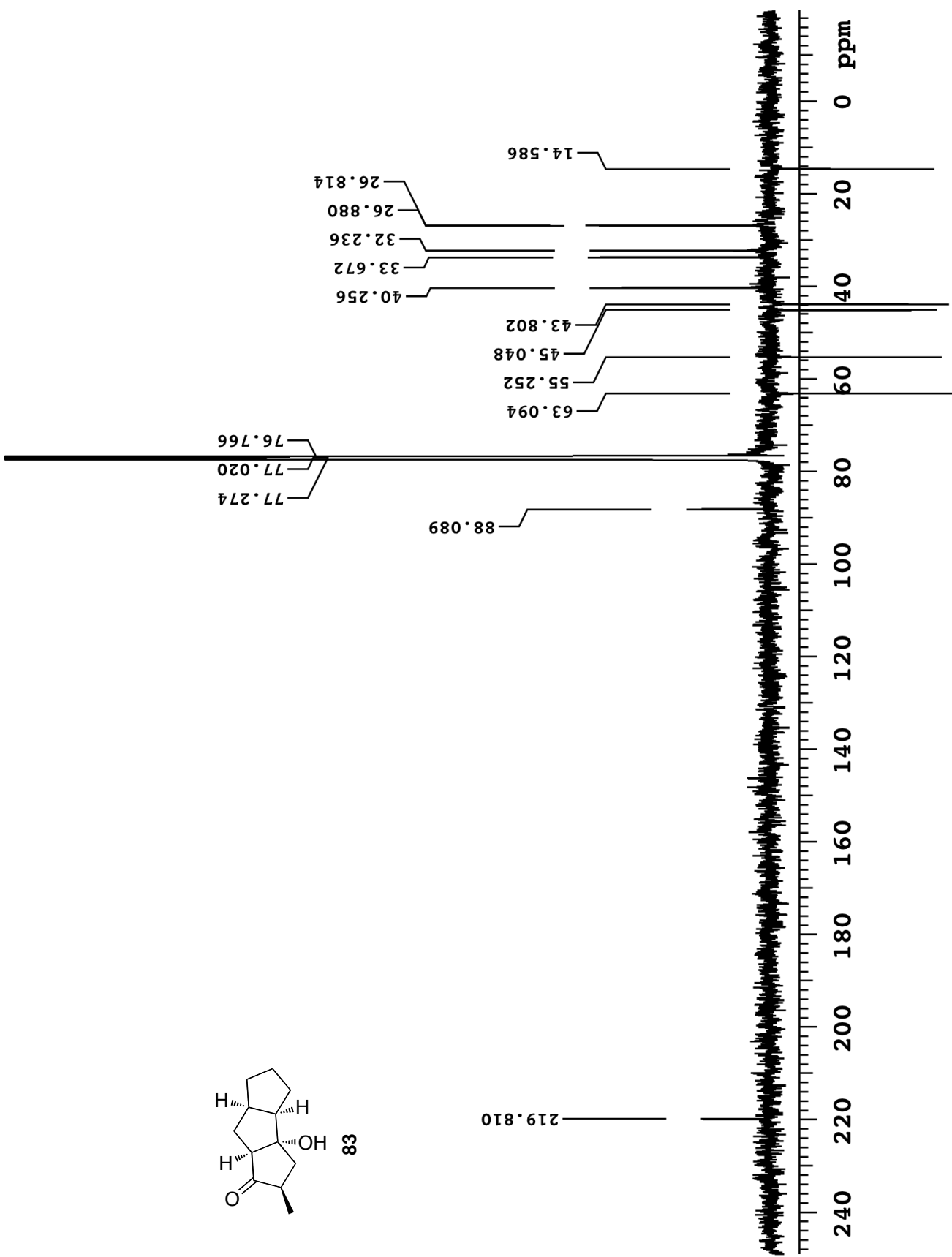
32

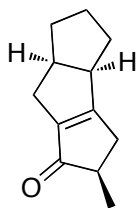




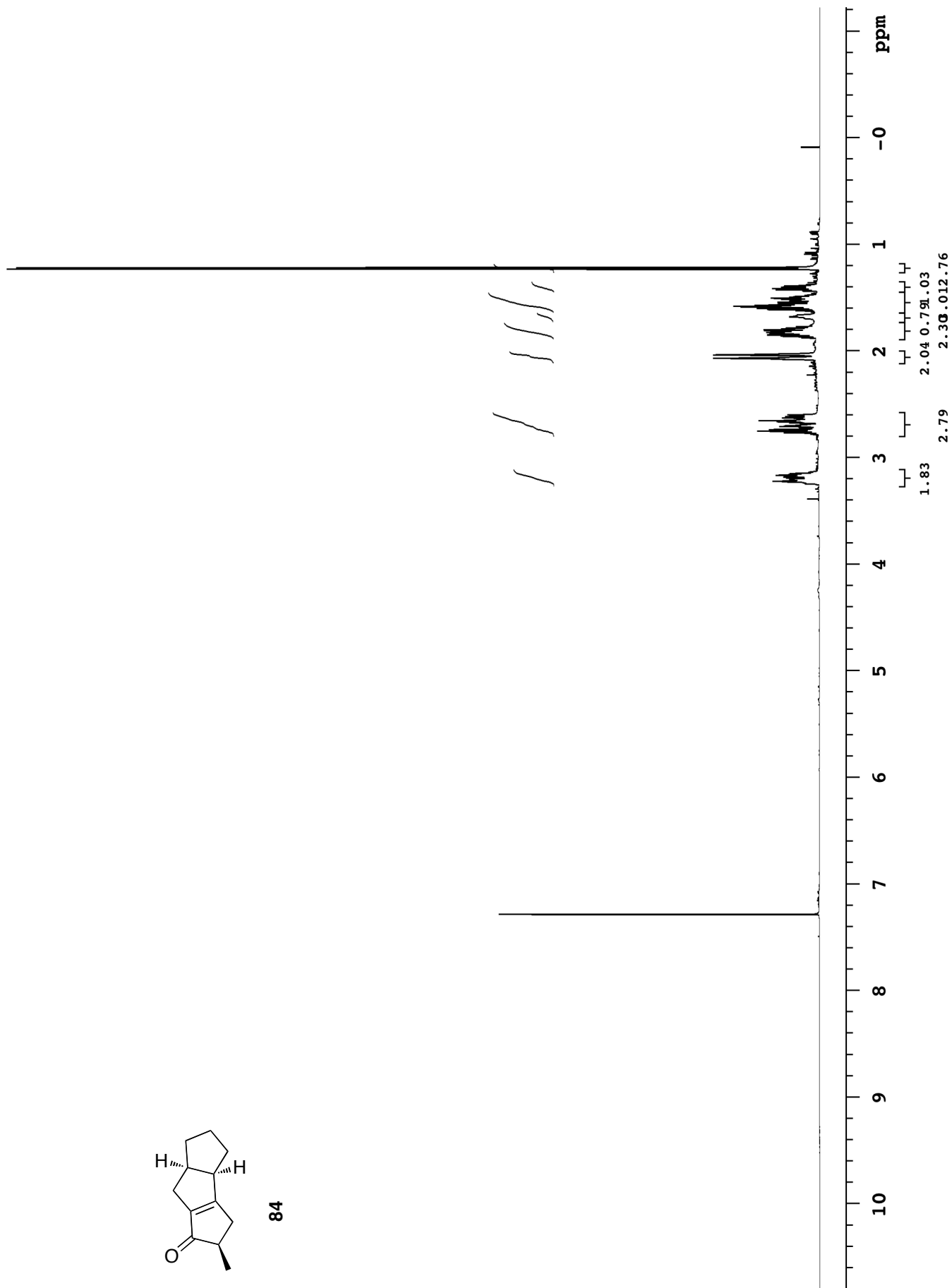
APPENDIX B
SELECTED NMR SPECTRA FROM CHAPTER 2

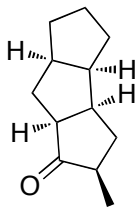




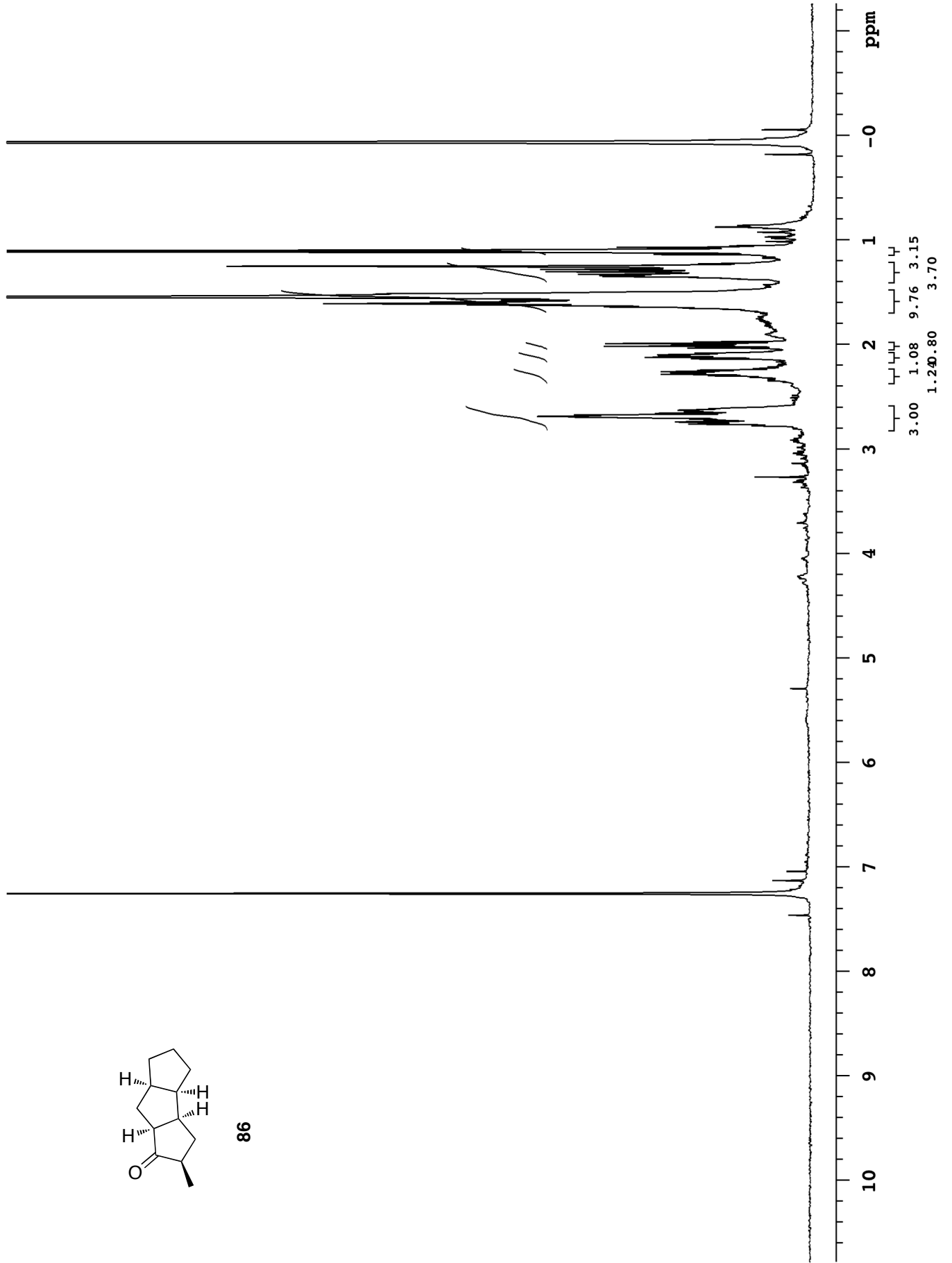


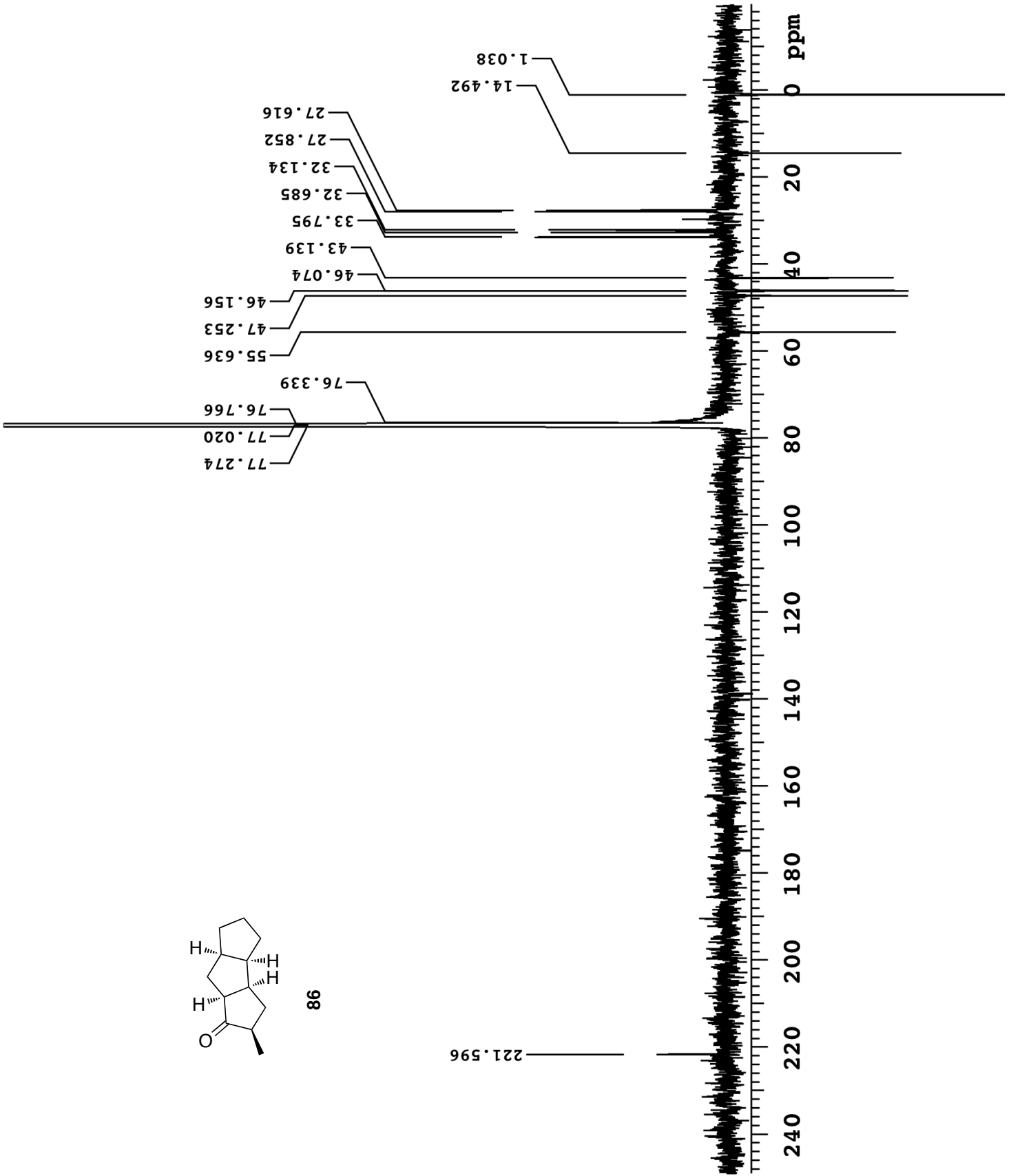
84





86





APPENDIX C

X-RAY CRYSTALLOGRAPHIC DATA TABLES FOR COMPOUND **83**

(CHAPTER 2)

STRUCTURE REPORT

XCL Code: FGW1104

Date: 13 July 2011

Compound: 3a-hydroxy-2-methyldecahydro-1*H*-cyclopenta[*a*]pentalen-1-one

Formula: C₁₂H₁₈O₂

Supervisor: F. G. West

Crystallographer: R. McDonald

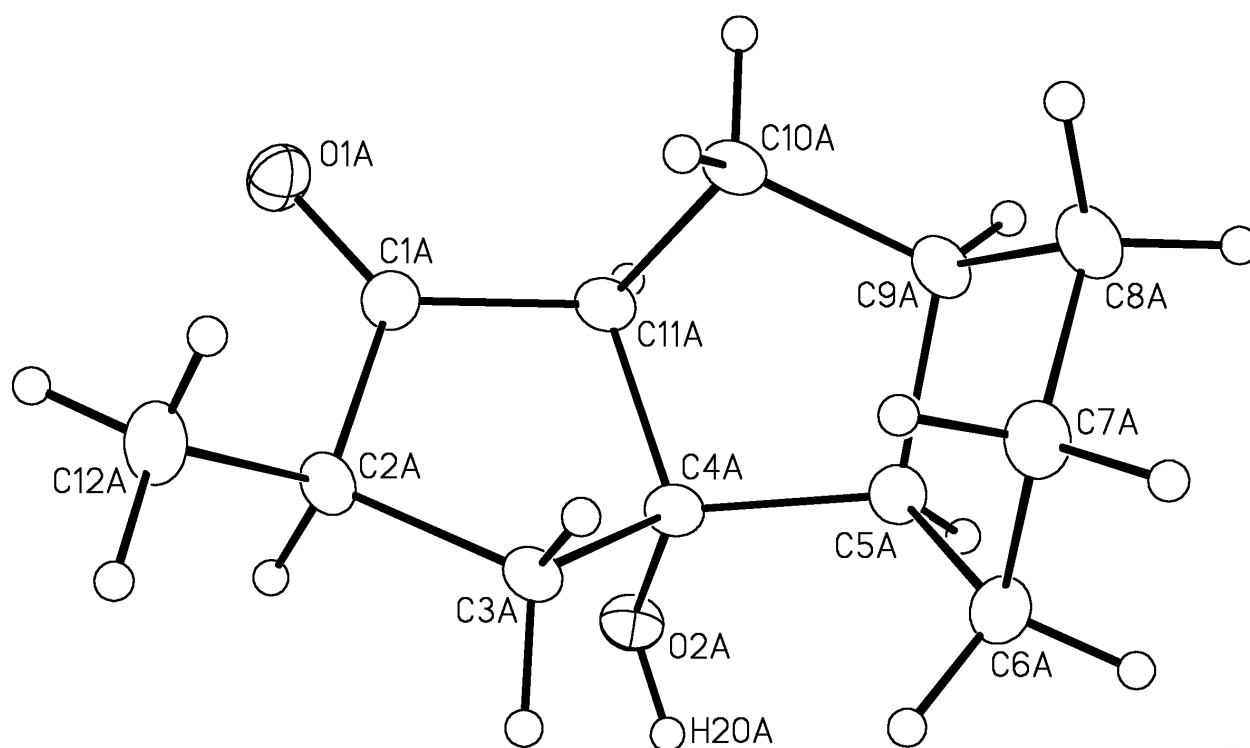
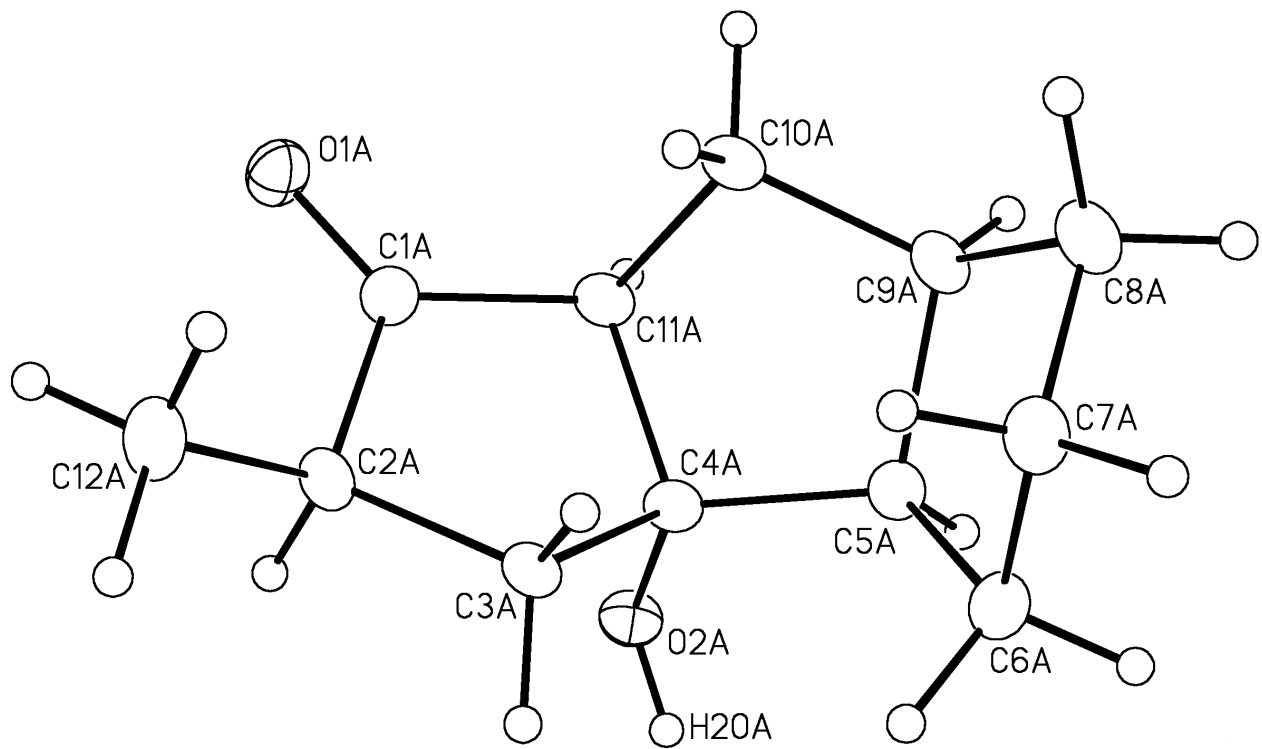
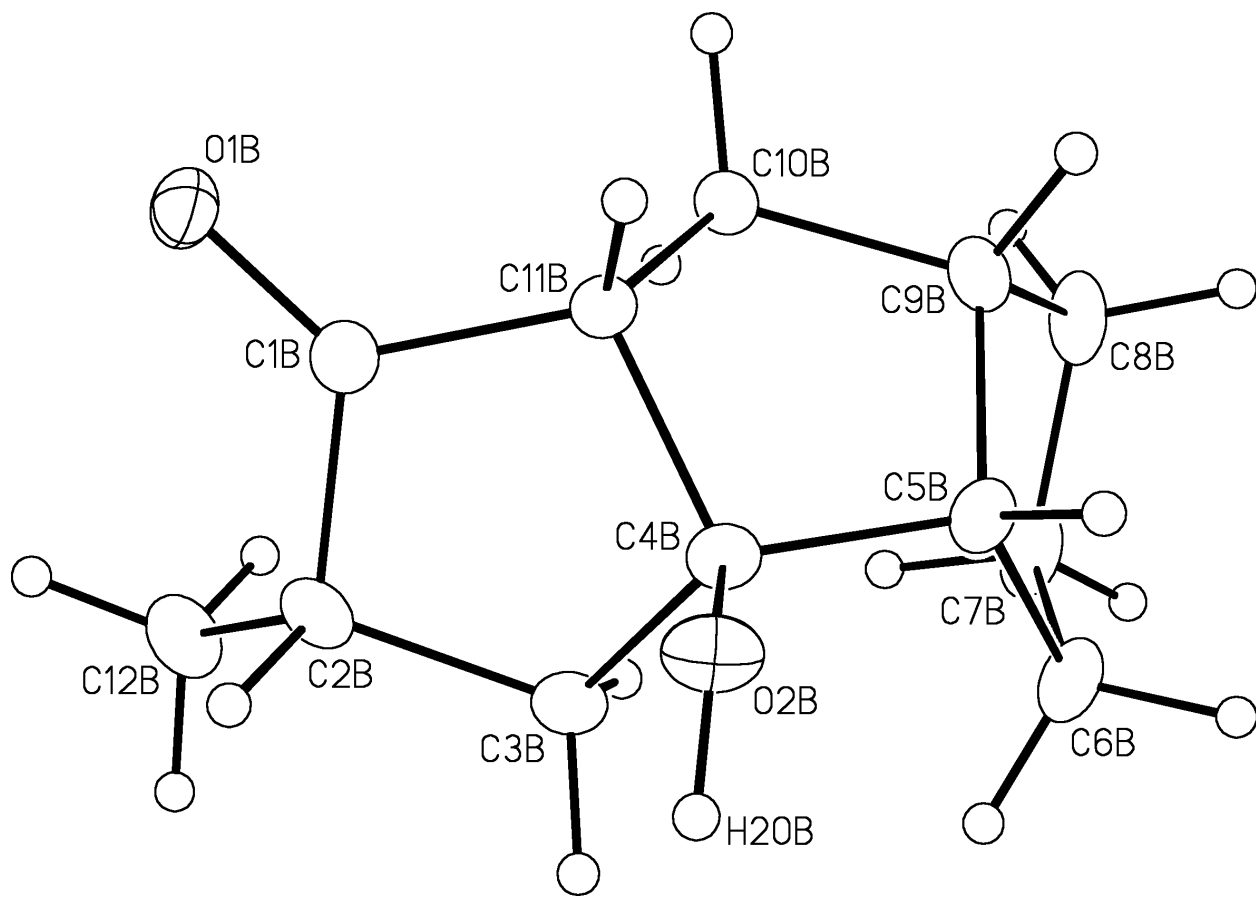
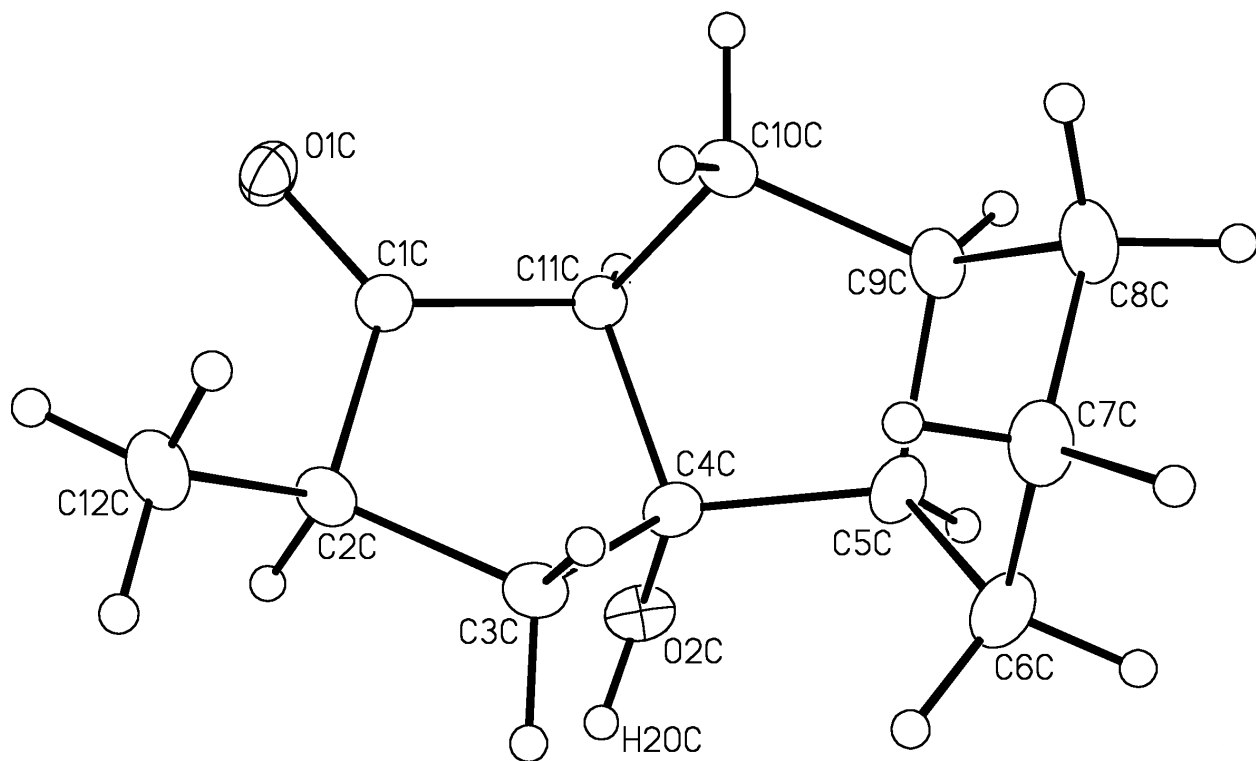


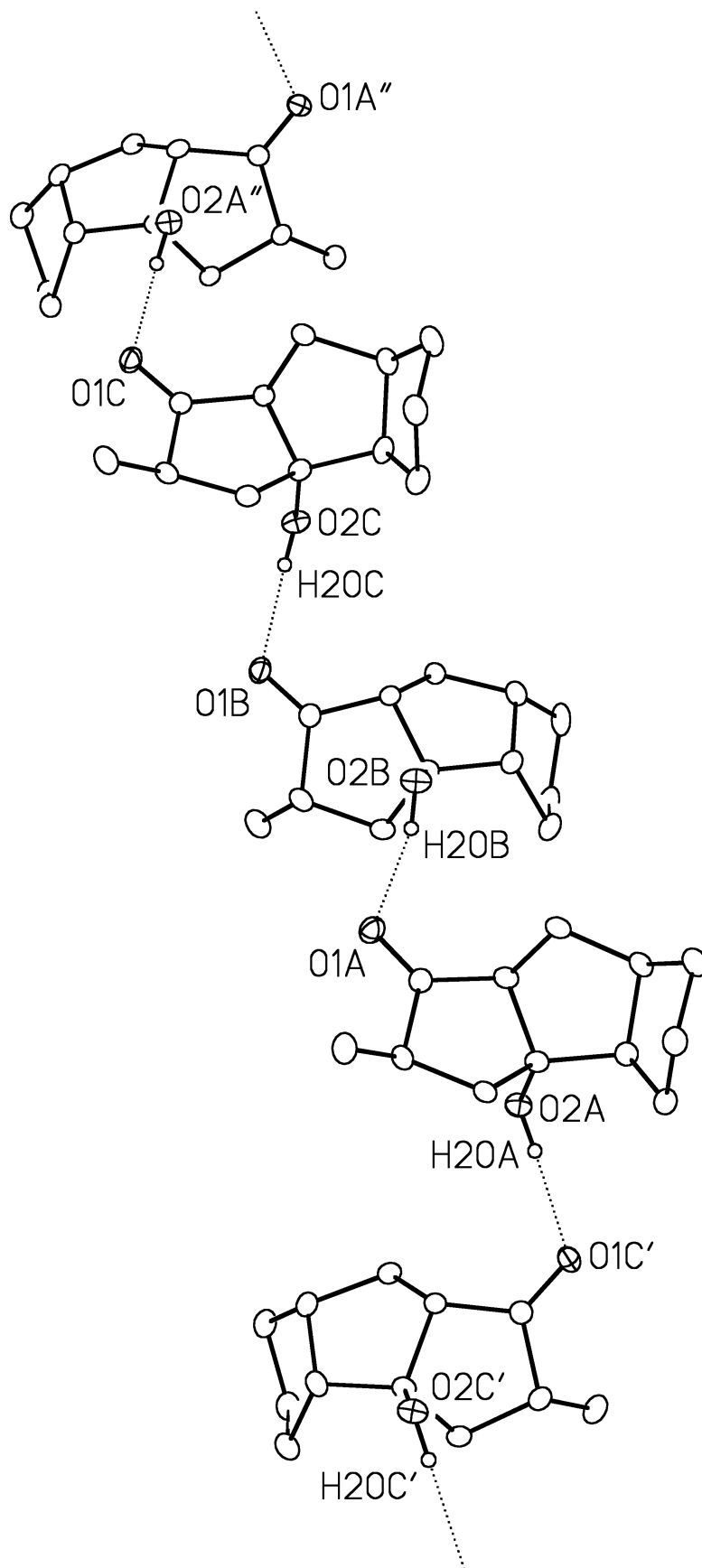
Figure Legends

- Figure 1.** Perspective view of one of the three crystallographically-independent molecules of 3a-hydroxy-2-methyldecahydro-1*H*-cyclopenta[*a*]pentalen-1-one (molecule A) showing the atom labelling scheme. Non-hydrogen atoms are represented by Gaussian ellipsoids at the 20% probability level. Hydrogen atoms are shown with arbitrarily small thermal parameters.
- Figure 2.** View of the second of the three crystallographically-independent molecules of 3a-hydroxy-2-methyldecahydro-1*H*-cyclopenta[*a*]pentalen-1-one (molecule B). Note that this is the enantiomer opposite to molecules A and C; in fact, since this is a centrosymmetric space group, both enantiomers are present in equal abundance.
- Figure 3.** View of the third of the three crystallographically-independent molecules of 3a-hydroxy-2-methyldecahydro-1*H*-cyclopenta[*a*]pentalen-1-one (molecule C).
- Figure 4.** Illustration of hydrogen-bonded interactions between adjacent molecules within the crystal lattice. Primed atoms are related to unprimed ones via the crystallographic symmetry operation $(1-x, -1/2+y, 1/2-z)$. Double-primed atoms are related to unprimed ones via the crystallographic symmetry operation $(1-x, 1/2+y, 1/2-z)$.









List of Tables

- Table 1.** Crystallographic Experimental Details
- Table 2.** Atomic Coordinates and Equivalent Isotropic Displacement Parameters
- Table 3.** Selected Interatomic Distances
- Table 4.** Selected Interatomic Angles
- Table 5.** Hydrogen-Bonded Interactions
- Table 6.** Torsional Angles
- Table 7.** Anisotropic Displacement Parameters
- Table 8.** Derived Atomic Coordinates and Displacement Parameters for Hydrogen Atoms

Table 1. Crystallographic Experimental Details*A. Crystal Data*

formula	C ₁₂ H ₁₈ O ₂
formula weight	194.26
crystal dimensions (mm)	0.37 × 0.16 × 0.06
crystal system	monoclinic
space group	<i>P</i> 2 ₁ / <i>c</i> (No. 14)
unit cell parameters ^a	
<i>a</i> (Å)	9.0349 (5)
<i>b</i> (Å)	32.1439 (16)
<i>c</i> (Å)	11.6359 (6)
β (deg)	109.0391 (7)
<i>V</i> (Å ³)	3194.4 (3)
<i>Z</i>	12
<i>r</i> _{calcd} (g cm ⁻³)	1.212
μ (mm ⁻¹)	0.080

B. Data Collection and Refinement Conditions

diffractometer	Bruker PLATFORM/APEX II CCD ^b
radiation (<i>λ</i> [Å])	graphite-monochromated Mo <i>Kα</i> (0.71073)
temperature (°C)	−100
scan type	<i>ω</i> scans (0.3°) (20 s exposures)
data collection 2 <i>q</i> limit (deg)	50.80
total data collected	22892 (−10 ≤ <i>h</i> ≤ 10, −38 ≤ <i>k</i> ≤ 38, −14 ≤ <i>l</i> ≤ 14)
independent reflections	5877 (<i>R</i> _{int} = 0.0724)
number of observed reflections (<i>NO</i>)	3514 [<i>F</i> _o ² ≥ 2 <i>s</i> (<i>F</i> _o ²)]
structure solution method	direct methods (<i>SHELXD</i> ^c)
refinement method	full-matrix least-squares on <i>F</i> ² (<i>SHELXL</i> −97 ^d)
absorption correction method	Gaussian integration (face-indexed)
range of transmission factors	0.9954–0.9712
data/restraints/parameters	5877 / 0 / 382
goodness-of-fit (<i>S</i>) ^e [all data]	1.025
final <i>R</i> indices ^f	
<i>R</i> ₁ [<i>F</i> _o ² ≥ 2 <i>s</i> (<i>F</i> _o ²)]	0.0516
<i>wR</i> ₂ [all data]	0.1315
largest difference peak and hole	0.156 and −0.185 e Å ⁻³

^aObtained from least-squares refinement of 3421 reflections with 4.76° < 2*q* < 39.20°.

^bPrograms for diffractometer operation, data collection, data reduction and absorption correction were those supplied by Bruker.

(continued)

Table 1. Crystallographic Experimental Details (continued)

^cSchneider, T. R.; Sheldrick, G. M. *Acta Crystallogr.* **2002**, *D58*, 1772-1779.

^dSheldrick, G. M. *Acta Crystallogr.* **2008**, *A64*, 112–122.

^e $S = [Sw(F_o^2 - F_c^2)^2/(n - p)]^{1/2}$ (n = number of data; p = number of parameters varied; $w = [s^2(F_o^2) + (0.0449P)^2 + 1.3669P]^{-1}$ where $P = [\text{Max}(F_o^2, 0) + 2F_c^2]/3$).

^f $R_1 = S||F_o| - |F_c||/S|F_o|$; $wR_2 = [Sw(F_o^2 - F_c^2)^2/Sw(F_o^4)]^{1/2}$.

Table 2. Atomic Coordinates and Equivalent Isotropic Displacement Parameters*(a) molecule A*

Atom	<i>x</i>	<i>y</i>	<i>z</i>	$U_{\text{eq}}, \text{\AA}^2$
O1A	0.4515(2)	0.30938(6)	0.14811(17)	0.0498(5)*
O2A	0.1818(2)	0.22113(5)	0.22994(14)	0.0402(4)*
C1A	0.3587(3)	0.28057(8)	0.1219(2)	0.0349(6)*
C2A	0.3986(3)	0.23709(8)	0.0915(2)	0.0367(6)*
C3A	0.2393(3)	0.21610(7)	0.0402(2)	0.0327(6)*
C4A	0.1374(3)	0.23681(7)	0.1081(2)	0.0315(6)*
C5A	-0.0403(3)	0.23718(7)	0.0436(2)	0.0347(6)*
C6A	-0.1104(3)	0.20550(8)	-0.0601(2)	0.0390(6)*
C7A	-0.1334(3)	0.22926(8)	-0.1780(2)	0.0425(7)*
C8A	-0.1819(3)	0.27268(9)	-0.1501(2)	0.0462(7)*
C9A	-0.0786(3)	0.28081(8)	-0.0179(2)	0.0372(6)*
C10A	0.0799(3)	0.30087(8)	-0.0032(2)	0.0381(6)*
C11A	0.1904(3)	0.28231(7)	0.1157(2)	0.0334(6)*
C12A	0.5026(3)	0.23625(9)	0.0113(3)	0.0535(8)*

(b) molecule B

Atom	<i>x</i>	<i>y</i>	<i>z</i>	$U_{\text{eq}}, \text{\AA}^2$
O1B	0.6753(2)	0.47296(6)	0.37366(17)	0.0479(5)*
O2B	0.3519(2)	0.39188(5)	0.14847(15)	0.0452(5)*
C1B	0.5751(3)	0.44586(8)	0.3523(2)	0.0352(6)*
C2B	0.6036(3)	0.40160(8)	0.3980(2)	0.0386(6)*
C3B	0.4378(3)	0.38346(8)	0.3691(2)	0.0372(6)*
C4B	0.3347(3)	0.40787(7)	0.2591(2)	0.0317(6)*
C5B	0.1610(3)	0.41313(8)	0.2481(2)	0.0356(6)*
C6B	0.0911(3)	0.38304(9)	0.3205(2)	0.0446(7)*
C7B	0.0929(3)	0.40734(9)	0.4342(2)	0.0509(8)*
C8B	0.0572(3)	0.45170(10)	0.3887(3)	0.0540(8)*
C9B	0.1460(3)	0.45725(8)	0.2981(2)	0.0414(7)*
C10B	0.3147(3)	0.47279(8)	0.3547(2)	0.0364(6)*
C11B	0.4046(3)	0.45175(7)	0.2802(2)	0.0311(6)*
C12B	0.7074(3)	0.39864(9)	0.5302(2)	0.0517(8)*

(c) molecule C

Atom	<i>x</i>	<i>y</i>	<i>z</i>	$U_{\text{eq}}, \text{\AA}^2$
O1C	0.9034(2)	0.63806(6)	0.26806(16)	0.0460(5)*
O2C	0.5872(2)	0.55607(5)	0.33578(14)	0.0428(5)*
C1C	0.8022(3)	0.61111(8)	0.2415(2)	0.0334(6)*
C2C	0.8300(3)	0.56658(8)	0.2104(2)	0.0371(6)*
C3C	0.6643(3)	0.54908(7)	0.1542(2)	0.0351(6)*

Table 2. Atomic Coordinates and Displacement Parameters (continued)

Atom	<i>x</i>	<i>y</i>	<i>z</i>	<i>U</i> _{eq} , Å ²
C4C	0.5641(3)	0.57273(7)	0.2166(2)	0.0323(6)*
C5C	0.3882(3)	0.57810(8)	0.1449(2)	0.0374(6)*
C6C	0.3150(3)	0.54894(9)	0.0355(2)	0.0448(7)*
C7C	0.3076(3)	0.57474(9)	-0.0770(2)	0.0467(7)*
C8C	0.2709(3)	0.61845(9)	-0.0434(2)	0.0513(8)*
C9C	0.3693(3)	0.62271(8)	0.0909(2)	0.0404(7)*
C10C	0.5374(3)	0.63838(8)	0.1130(2)	0.0375(6)*
C11C	0.6329(3)	0.61671(7)	0.2310(2)	0.0312(6)*
C12C	0.9380(3)	0.56338(9)	0.1342(3)	0.0515(8)*

Anisotropically-refined atoms are marked with an asterisk (*). The form of the anisotropic displacement parameter is: $\exp[-2\pi^2(h^2a^{*2}U_{11} + k^2b^{*2}U_{22} + l^2c^{*2}U_{33} + 2klb^*c^*U_{23} + 2hla^*c^*U_{13} + 2hka^*b^*U_{12})]$.

Table 3. Selected Interatomic Distances (Å)*(a) molecule A*

Atom1	Atom2	Distance	Atom1	Atom2	Distance
O1A	C1A	1.219(3)	C4A	C11A	1.532(3)
O2A	C4A	1.433(3)	C5A	C6A	1.548(3)
C1A	C2A	1.514(3)	C5A	C9A	1.561(3)
C1A	C11A	1.500(3)	C6A	C7A	1.524(3)
C2A	C3A	1.524(3)	C7A	C8A	1.529(4)
C2A	C12A	1.526(4)	C8A	C9A	1.540(3)
C3A	C4A	1.546(3)	C9A	C10A	1.528(3)
C4A	C5A	1.534(3)	C10A	C11A	1.538(3)

(b) molecule B

Atom1	Atom2	Distance	Atom1	Atom2	Distance
O1B	C1B	1.222(3)	C4B	C11B	1.532(3)
O2B	C4B	1.440(3)	C5B	C6B	1.547(3)
C1B	C2B	1.511(3)	C5B	C9B	1.555(3)
C1B	C11B	1.507(3)	C6B	C7B	1.532(4)
C2B	C3B	1.539(3)	C7B	C8B	1.519(4)
C2B	C12B	1.520(3)	C8B	C9B	1.530(4)
C3B	C4B	1.531(3)	C9B	C10B	1.533(3)
C4B	C5B	1.542(3)	C10B	C11B	1.526(3)

(c) molecule C

Atom1	Atom2	Distance	Atom1	Atom2	Distance
O1C	C1C	1.224(3)	C4C	C11C	1.531(3)
O2C	C4C	1.437(3)	C5C	C6C	1.545(3)
C1C	C2C	1.517(3)	C5C	C9C	1.552(4)
C1C	C11C	1.505(3)	C6C	C7C	1.533(4)
C2C	C3C	1.532(3)	C7C	C8C	1.523(4)
C2C	C12C	1.521(3)	C8C	C9C	1.532(3)
C3C	C4C	1.534(3)	C9C	C10C	1.539(3)
C4C	C5C	1.545(3)	C10C	C11C	1.530(3)

Table 4. Selected Interatomic Angles (deg)*(a) molecule A*

Atom1	Atom2	Atom3	Angle	Atom1	Atom2	Atom3	Angle
O1A	C1A	C2A	124.3(2)	C4A	C5A	C6A	118.2(2)
O1A	C1A	C11A	125.9(2)	C4A	C5A	C9A	105.74(19)
C2A	C1A	C11A	109.7(2)	C6A	C5A	C9A	105.11(19)
C1A	C2A	C3A	103.5(2)	C5A	C6A	C7A	105.9(2)
C1A	C2A	C12A	113.6(2)	C6A	C7A	C8A	103.3(2)
C3A	C2A	C12A	116.4(2)	C7A	C8A	C9A	104.2(2)
C2A	C3A	C4A	104.67(19)	C5A	C9A	C8A	106.1(2)
O2A	C4A	C3A	109.45(19)	C5A	C9A	C10A	105.57(19)
O2A	C4A	C5A	113.41(19)	C8A	C9A	C10A	115.1(2)
O2A	C4A	C11A	107.30(18)	C9A	C10A	C11A	104.2(2)
C3A	C4A	C5A	117.10(19)	C1A	C11A	C4A	105.1(2)
C3A	C4A	C11A	102.33(19)	C1A	C11A	C10A	114.0(2)
C5A	C4A	C11A	106.15(19)	C4A	C11A	C10A	102.67(19)

(b) molecule B

Atom1	Atom2	Atom3	Angle	Atom1	Atom2	Atom3	Angle
O1B	C1B	C2B	124.8(2)	C4B	C5B	C6B	118.2(2)
O1B	C1B	C11B	125.3(2)	C4B	C5B	C9B	106.23(19)
C2B	C1B	C11B	109.9(2)	C6B	C5B	C9B	105.4(2)
C1B	C2B	C3B	103.8(2)	C5B	C6B	C7B	105.1(2)
C1B	C2B	C12B	113.1(2)	C6B	C7B	C8B	103.7(2)
C3B	C2B	C12B	115.7(2)	C7B	C8B	C9B	104.5(2)
C2B	C3B	C4B	105.8(2)	C5B	C9B	C8B	106.3(2)
O2B	C4B	C3B	110.52(19)	C5B	C9B	C10B	105.2(2)
O2B	C4B	C5B	111.63(19)	C8B	C9B	C10B	114.4(2)
O2B	C4B	C11B	108.25(19)	C9B	C10B	C11B	104.5(2)
C3B	C4B	C5B	116.8(2)	C1B	C11B	C4B	105.47(19)
C3B	C4B	C11B	103.36(19)	C1B	C11B	C10B	112.1(2)
C5B	C4B	C11B	105.52(19)	C4B	C11B	C10B	103.37(19)

(c) molecule C

Atom1	Atom2	Atom3	Angle	Atom1	Atom2	Atom3	Angle
O1C	C1C	C2C	124.0(2)	O2C	C4C	C3C	110.44(19)
O1C	C1C	C11C	126.3(2)	O2C	C4C	C5C	111.3(2)
C2C	C1C	C11C	109.7(2)	O2C	C4C	C11C	108.19(18)
C1C	C2C	C3C	103.5(2)	C3C	C4C	C5C	117.50(19)
C1C	C2C	C12C	113.0(2)	C3C	C4C	C11C	103.19(19)
C3C	C2C	C12C	116.7(2)	C5C	C4C	C11C	105.41(19)
C2C	C3C	C4C	105.16(19)	C4C	C5C	C6C	117.7(2)

Table 4. Selected Interatomic Angles (continued)*(c) molecule C*

Atom1	Atom2	Atom3	Angle	Atom1	Atom2	Atom3	Angle
C4C	C5C	C9C	106.21(19)	C5C	C9C	C10C	105.2(2)
C6C	C5C	C9C	105.4(2)	C8C	C9C	C10C	114.3(2)
C5C	C6C	C7C	105.3(2)	C9C	C10C	C11C	103.8(2)
C6C	C7C	C8C	103.4(2)	C1C	C11C	C4C	105.32(19)
C7C	C8C	C9C	104.0(2)	C1C	C11C	C10C	112.8(2)
C5C	C9C	C8C	106.3(2)	C4C	C11C	C10C	103.40(19)

Table 5. Hydrogen-Bonded Interactions

D-H...A	D-H (Å)	H...A (Å)	D...A (Å)	∠D-H...A (deg)	Note
O2A-H2OA...O1C ^a	0.84	1.94	2.781(2)	177.5	^a At 1-x, -1/2+y, 1/2-z.
O2B-H2OB...O1A	0.84	1.99	2.801(3)	162.2	
O2C-H2OC...O1B	0.84	1.95	2.781(3)	169.1	

Table 6. Torsional Angles (deg)*(a) molecule A*

Atom1	Atom2	Atom3	Atom4	Angle	Atom1	Atom2	Atom3	Atom4	Angle
O1A	C1A	C2A	C3A	-168.4(2)	O2A	C4A	C11A	C10A	-156.04(19)
O1A	C1A	C2A	C12A	-41.3(3)	C3A	C4A	C11A	C1A	-30.7(2)
C11A	C1A	C2A	C3A	12.1(3)	C3A	C4A	C11A	C10A	88.8(2)
C11A	C1A	C2A	C12A	139.3(2)	C5A	C4A	C11A	C1A	-154.02(18)
O1A	C1A	C11A	C4A	-167.5(2)	C5A	C4A	C11A	C10A	-34.5(2)
O1A	C1A	C11A	C10A	80.9(3)	C4A	C5A	C6A	C7A	-98.7(2)
C2A	C1A	C11A	C4A	12.0(2)	C9A	C5A	C6A	C7A	18.9(3)
C2A	C1A	C11A	C10A	-99.7(2)	C4A	C5A	C9A	C8A	131.2(2)
C1A	C2A	C3A	C4A	-31.4(2)	C4A	C5A	C9A	C10A	8.6(2)
C12A	C2A	C3A	C4A	-156.7(2)	C6A	C5A	C9A	C8A	5.4(3)
C2A	C3A	C4A	O2A	-74.8(2)	C6A	C5A	C9A	C10A	-117.2(2)
C2A	C3A	C4A	C5A	154.4(2)	C5A	C6A	C7A	C8A	-36.1(3)
C2A	C3A	C4A	C11A	38.8(2)	C6A	C7A	C8A	C9A	39.2(3)
O2A	C4A	C5A	C6A	-109.0(2)	C7A	C8A	C9A	C5A	-27.5(3)
O2A	C4A	C5A	C9A	133.7(2)	C7A	C8A	C9A	C10A	88.8(3)
C3A	C4A	C5A	C6A	20.0(3)	C5A	C9A	C10A	C11A	-30.0(2)
C3A	C4A	C5A	C9A	-97.3(2)	C8A	C9A	C10A	C11A	-146.6(2)
C11A	C4A	C5A	C6A	133.5(2)	C9A	C10A	C11A	C1A	152.9(2)
C11A	C4A	C5A	C9A	16.1(2)	C9A	C10A	C11A	C4A	39.8(2)
O2A	C4A	C11A	C1A	84.4(2)					

(b) molecule B

Atom1	Atom2	Atom3	Atom4	Angle	Atom1	Atom2	Atom3	Atom4	Angle
O1B	C1B	C2B	C3B	168.6(2)	C3B	C4B	C5B	C9B	98.9(2)
O1B	C1B	C2B	C12B	42.5(3)	C11B	C4B	C5B	C6B	-133.3(2)
C11B	C1B	C2B	C3B	-9.5(3)	C11B	C4B	C5B	C9B	-15.3(2)
C11B	C1B	C2B	C12B	-135.7(2)	O2B	C4B	C11B	C1B	-88.8(2)
O1B	C1B	C11B	C4B	169.9(2)	O2B	C4B	C11B	C10B	153.36(19)
O1B	C1B	C11B	C10B	-78.2(3)	C3B	C4B	C11B	C1B	28.5(2)
C2B	C1B	C11B	C4B	-11.9(3)	C3B	C4B	C11B	C10B	-89.4(2)
C2B	C1B	C11B	C10B	99.9(2)	C5B	C4B	C11B	C1B	151.62(19)
C1B	C2B	C3B	C4B	27.5(2)	C5B	C4B	C11B	C10B	33.7(2)
C12B	C2B	C3B	C4B	152.0(2)	C4B	C5B	C6B	C7B	99.3(3)
C2B	C3B	C4B	O2B	80.7(2)	C9B	C5B	C6B	C7B	-19.2(3)
C2B	C3B	C4B	C5B	-150.2(2)	C4B	C5B	C9B	C8B	-130.7(2)
C2B	C3B	C4B	C11B	-34.9(2)	C4B	C5B	C9B	C10B	-9.0(3)
O2B	C4B	C5B	C6B	109.4(2)	C6B	C5B	C9B	C8B	-4.5(3)
O2B	C4B	C5B	C9B	-132.6(2)	C6B	C5B	C9B	C10B	117.2(2)
C3B	C4B	C5B	C6B	-19.1(3)	C5B	C6B	C7B	C8B	35.8(3)

Table 6. Torsional Angles (continued)*(b) molecule B*

Atom1	Atom2	Atom3	Atom4	Angle	Atom1	Atom2	Atom3	Atom4	Angle
C6B	C7B	C8B	C9B	-38.7(3)	C8B	C9B	C10B	C11B	146.2(2)
C7B	C8B	C9B	C5B	26.7(3)	C9B	C10B	C11B	C1B	-152.6(2)
C7B	C8B	C9B	C10B	-89.0(3)	C9B	C10B	C11B	C4B	-39.5(2)
C5B	C9B	C10B	C11B	29.9(2)					

(c) molecule C

Atom1	Atom2	Atom3	Atom4	Angle	Atom1	Atom2	Atom3	Atom4	Angle
O1C	C1C	C2C	C3C	-166.2(2)	O2C	C4C	C11C	C10C	-153.23(19)
O1C	C1C	C2C	C12C	-39.1(3)	C3C	C4C	C11C	C1C	-28.9(2)
C11C	C1C	C2C	C3C	12.2(2)	C3C	C4C	C11C	C10C	89.7(2)
C11C	C1C	C2C	C12C	139.3(2)	C5C	C4C	C11C	C1C	-152.72(18)
O1C	C1C	C11C	C4C	-171.1(2)	C5C	C4C	C11C	C10C	-34.1(2)
O1C	C1C	C11C	C10C	76.8(3)	C4C	C5C	C6C	C7C	-100.1(3)
C2C	C1C	C11C	C4C	10.6(2)	C9C	C5C	C6C	C7C	18.1(3)
C2C	C1C	C11C	C10C	-101.5(2)	C4C	C5C	C9C	C8C	131.9(2)
C1C	C2C	C3C	C4C	-30.3(2)	C4C	C5C	C9C	C10C	10.2(2)
C12C	C2C	C3C	C4C	-155.0(2)	C6C	C5C	C9C	C8C	6.2(3)
C2C	C3C	C4C	O2C	-78.5(2)	C6C	C5C	C9C	C10C	-115.4(2)
C2C	C3C	C4C	C5C	152.4(2)	C5C	C6C	C7C	C8C	-35.7(3)
C2C	C3C	C4C	C11C	37.0(2)	C6C	C7C	C8C	C9C	39.4(3)
O2C	C4C	C5C	C6C	-110.5(2)	C7C	C8C	C9C	C5C	-28.2(3)
O2C	C4C	C5C	C9C	131.7(2)	C7C	C8C	C9C	C10C	87.4(3)
C3C	C4C	C5C	C6C	18.2(3)	C5C	C9C	C10C	C11C	-31.3(2)
C3C	C4C	C5C	C9C	-99.6(2)	C8C	C9C	C10C	C11C	-147.5(2)
C11C	C4C	C5C	C6C	132.4(2)	C9C	C10C	C11C	C1C	153.8(2)
C11C	C4C	C5C	C9C	14.7(2)	C9C	C10C	C11C	C4C	40.5(2)
O2C	C4C	C11C	C1C	88.1(2)					

Table 7. Anisotropic Displacement Parameters (U_{ij} , Å²)

Atom	U_{11}	U_{22}	U_{33}	U_{23}	U_{13}	U_{12}
O1A	0.0478(12)	0.0437(11)	0.0596(13)	-0.0120(10)	0.0198(10)	-0.0074(10)
O2A	0.0503(12)	0.0428(10)	0.0263(9)	0.0059(8)	0.0109(8)	0.0024(9)
C1A	0.0387(16)	0.0387(15)	0.0280(13)	-0.0040(12)	0.0118(11)	-0.0009(13)
C2A	0.0324(15)	0.0391(15)	0.0362(14)	-0.0048(12)	0.0081(12)	0.0056(12)
C3A	0.0359(15)	0.0306(14)	0.0308(13)	0.0004(11)	0.0098(11)	0.0061(11)
C4A	0.0408(16)	0.0325(14)	0.0232(12)	0.0024(10)	0.0131(11)	0.0026(11)
C5A	0.0367(15)	0.0404(15)	0.0307(13)	0.0010(12)	0.0160(11)	0.0014(12)
C6A	0.0370(16)	0.0449(16)	0.0387(15)	-0.0027(12)	0.0173(12)	-0.0032(12)
C7A	0.0400(17)	0.0547(18)	0.0305(14)	-0.0025(12)	0.0084(12)	-0.0010(13)
C8A	0.0423(17)	0.0566(18)	0.0371(15)	0.0058(13)	0.0093(13)	0.0105(14)
C9A	0.0369(16)	0.0417(15)	0.0348(14)	0.0003(12)	0.0143(12)	0.0119(12)
C10A	0.0448(17)	0.0325(14)	0.0384(15)	0.0032(12)	0.0153(12)	0.0086(12)
C11A	0.0438(16)	0.0317(14)	0.0271(13)	-0.0029(11)	0.0148(11)	0.0053(12)
C12A	0.0418(18)	0.0587(19)	0.065(2)	-0.0166(16)	0.0249(15)	-0.0009(15)
O1B	0.0379(11)	0.0496(12)	0.0599(13)	-0.0036(10)	0.0209(10)	-0.0055(10)
O2B	0.0695(14)	0.0398(10)	0.0301(10)	-0.0042(8)	0.0213(9)	0.0032(10)
C1B	0.0376(16)	0.0407(15)	0.0328(14)	-0.0036(12)	0.0191(12)	0.0005(13)
C2B	0.0420(16)	0.0407(15)	0.0337(15)	-0.0003(12)	0.0134(12)	0.0122(13)
C3B	0.0480(17)	0.0323(14)	0.0308(14)	0.0022(11)	0.0123(12)	0.0022(12)
C4B	0.0424(15)	0.0322(14)	0.0229(12)	-0.0005(10)	0.0138(11)	-0.0006(11)
C5B	0.0364(15)	0.0433(15)	0.0253(13)	0.0018(11)	0.0077(11)	-0.0078(12)
C6B	0.0396(16)	0.0593(18)	0.0324(15)	0.0026(13)	0.0083(12)	-0.0169(14)
C7B	0.0388(17)	0.080(2)	0.0363(16)	-0.0048(15)	0.0155(13)	-0.0177(16)
C8B	0.0287(16)	0.081(2)	0.0544(19)	-0.0157(16)	0.0161(14)	-0.0014(15)
C9B	0.0330(16)	0.0479(17)	0.0404(15)	0.0036(13)	0.0080(12)	0.0061(12)
C10B	0.0342(15)	0.0340(14)	0.0426(15)	-0.0016(12)	0.0149(12)	0.0024(12)
C11B	0.0340(15)	0.0304(13)	0.0311(13)	0.0036(11)	0.0135(11)	-0.0011(11)
C12B	0.0494(19)	0.063(2)	0.0397(16)	0.0015(14)	0.0106(14)	0.0149(15)
O1C	0.0368(11)	0.0471(11)	0.0520(12)	-0.0051(9)	0.0117(9)	-0.0084(9)
O2C	0.0623(13)	0.0405(10)	0.0288(10)	-0.0020(8)	0.0191(9)	-0.0055(10)
C1C	0.0371(16)	0.0383(15)	0.0243(13)	0.0016(11)	0.0093(11)	-0.0004(12)
C2C	0.0396(16)	0.0372(15)	0.0335(14)	0.0057(12)	0.0107(12)	0.0083(12)
C3C	0.0445(16)	0.0305(13)	0.0316(14)	-0.0032(11)	0.0141(12)	0.0008(12)
C4C	0.0402(16)	0.0342(14)	0.0239(13)	-0.0033(11)	0.0121(11)	-0.0044(11)
C5C	0.0340(15)	0.0502(16)	0.0311(14)	-0.0122(12)	0.0147(12)	-0.0096(12)
C6C	0.0417(17)	0.0552(17)	0.0373(15)	-0.0155(13)	0.0126(13)	-0.0128(14)
C7C	0.0405(17)	0.0622(19)	0.0318(15)	-0.0116(13)	0.0040(12)	0.0002(14)
C8C	0.0363(17)	0.0614(19)	0.0458(17)	-0.0078(15)	-0.0006(13)	0.0075(14)
C9C	0.0334(15)	0.0461(16)	0.0393(15)	-0.0107(13)	0.0087(12)	0.0057(13)
C10C	0.0411(16)	0.0330(14)	0.0352(14)	-0.0012(11)	0.0079(12)	0.0041(12)

Table 7. Anisotropic Displacement Parameters (continued)

Atom	U_{11}	U_{22}	U_{33}	U_{23}	U_{13}	U_{12}
C11C	0.0345(15)	0.0307(13)	0.0291(13)	-0.0053(10)	0.0113(11)	-0.0005(11)
C12C	0.0446(18)	0.0592(19)	0.0566(18)	0.0056(15)	0.0245(15)	0.0158(15)

The form of the anisotropic displacement parameter is:

$$\exp[-2\pi^2(h^2a^2U_{11} + k^2b^2U_{22} + l^2c^2U_{33} + 2klb^*c^*U_{23} + 2hla^*c^*U_{13} + 2hka^*b^*U_{12})]$$

Table 8. Derived Atomic Coordinates and Displacement Parameters for Hydrogen Atoms

Atom	<i>x</i>	<i>y</i>	<i>z</i>	$U_{\text{eq}}, \text{\AA}^2$
H2OA	0.1537	0.1962	0.2287	0.060
H2A	0.4567	0.2229	0.1697	0.044
H3AA	0.2480	0.1858	0.0558	0.039
H3BA	0.1941	0.2208	-0.0485	0.039
H5A	-0.0946	0.2342	0.1056	0.042
H6AA	-0.0380	0.1818	-0.0532	0.047
H6BA	-0.2117	0.1947	-0.0571	0.047
H7AA	-0.2164	0.2163	-0.2465	0.051
H7BA	-0.0351	0.2303	-0.1981	0.051
H8AA	-0.2943	0.2734	-0.1579	0.055
H8BA	-0.1620	0.2936	-0.2057	0.055
H9A	-0.1373	0.2979	0.0247	0.045
H10A	0.0739	0.3315	0.0028	0.046
H10B	0.1157	0.2938	-0.0727	0.046
H11A	0.1782	0.2965	0.1886	0.040
H12A	0.6017	0.2503	0.0531	0.080
H12B	0.4494	0.2505	-0.0655	0.080
H12C	0.5234	0.2073	-0.0053	0.080
H2OB	0.3661	0.3660	0.1547	0.068
H2B	0.6569	0.3865	0.3474	0.046
H3AB	0.4372	0.3535	0.3496	0.045
H3BB	0.3998	0.3869	0.4392	0.045
H5B	0.0959	0.4119	0.1603	0.043
H6AB	-0.0172	0.3751	0.2720	0.054
H6BB	0.1554	0.3575	0.3430	0.054
H7AB	0.0122	0.3967	0.4673	0.061
H7BB	0.1967	0.4055	0.4981	0.061
H8AB	0.0943	0.4718	0.4565	0.065
H8BB	-0.0567	0.4557	0.3483	0.065
H9B	0.0865	0.4760	0.2303	0.050
H10C	0.3197	0.5034	0.3487	0.044
H10D	0.3577	0.4646	0.4413	0.044
H11B	0.3904	0.4667	0.2019	0.037
H12D	0.8097	0.4110	0.5393	0.078
H12E	0.7213	0.3694	0.5548	0.078
H12F	0.6583	0.4136	0.5816	0.078
H2OC	0.6137	0.5310	0.3376	0.064
H2C	0.8809	0.5515	0.2885	0.044
H3AC	0.6626	0.5188	0.1698	0.042
H3BC	0.6253	0.5539	0.0653	0.042

Table 8. Derived Parameters for Hydrogen Atoms (continued)

Atom	<i>x</i>	<i>y</i>	<i>z</i>	$U_{\text{eq}}, \text{\AA}^2$
H5C	0.3270	0.5758	0.2024	0.045
H6AC	0.3808	0.5239	0.0410	0.054
H6BC	0.2088	0.5401	0.0324	0.054
H7AC	0.4089	0.5740	-0.0927	0.056
H7BC	0.2241	0.5644	-0.1499	0.056
H8AC	0.1580	0.6215	-0.0549	0.062
H8BC	0.3014	0.6396	-0.0934	0.062
H9C	0.3146	0.6410	0.1339	0.048
H10E	0.5750	0.6304	0.0451	0.045
H10F	0.5433	0.6690	0.1225	0.045
H11C	0.6217	0.6310	0.3040	0.037
H12G	1.0400	0.5755	0.1790	0.077
H12H	0.8919	0.5785	0.0577	0.077
H12I	0.9517	0.5341	0.1169	0.077